ABSTRACT

TRUEBLOOD, VERN JONATHAN. A Novel Formation Mechanism of Volatile Organic Compounds over the Remote Marine Regions. (Under the direction of Dr. Nicholas Meskhidze).

The purpose of this work is to obtain an improved understanding of the intricate processes that connect the ocean-biota-atmosphere systems, specifically in terms of trace gas production and environmental exchange. Observations of formaldehyde concentrations over remote marine regions have been out of sync with model estimates since the 1970s, indicating a gap in the knowledge of the hydrocarbon oxidation chain. We hypothesize that a previously undiscovered biotic source of formaldehyde exists over such regions. This paper presents the work undertaken to test that hypothesis. We begin with an introduction explaining the oxidation cycle of hydrocarbons and a history of formaldehyde observations and estimates over the ocean. We also include an in-depth discussion on the sea-surface microlayer, the ubiquitous interface between the atmosphere-ocean systems that houses unique structures of microorganisms and features an enrichment of various types of organic matter. Finally, a description of the aerosol interactions within the marine boundary layer is given, with emphasis upon the sea-surface microlayer as an important source for primary organic aerosols.

We next focus upon the development of a formaldehyde detection method using an active sampling technique followed by thermal desorption and gas chromatograph- mass spectrometer (GC/MS) analysis. Development of a detection method for a reactive and ubiquitous compound like formaldehyde requires an in-depth knowledge of its chemical characteristics as well as a strong understanding of the theory behind GC/MS analysis. A description of GC/MS theory and previous formaldehyde detection methods is therefore reviewed. We then present the experimental setup of our formaldehyde detection method, the validity of our system calibration, and a discussion of the attempts to augment the method for lower detection limits.

Finally, we conclude with an overview of the experimental setup of our aerosol production/aging apparatus, which will be used with our detection technique to test the viability of our hypothesis. A discussion of the theoretical formaldehyde production amount

using our system is then presented. Preliminary calculations indicate our proposed method is unlikely capable of producing enough formaldehyde to close the gap between models and observations. However, numerous uncertainties regarding the yield of HCHO derived from carbon photolysis exist.

Improving the Gap between Model Predictions and Observations of Formaldehyde over the Remote Marine Regions

by
Jonathan Trueblood

A thesis submitted to the Graduate Faculty of
North Carolina State University
in partial fulfillment of the
requirements for the degree of
Master of Science

Marine, Earth, and Atmospheric Science

Raleigh, North Carolina

2013

APPROVED BY:

_____	_____
Dr. Nicholas Meskhidze Committee Chair	Dr. Markus Petters
_____	
Dr. Christopher Osburn	

DEDICATION

To my parents, for teaching me to always put forth my best effort.

To my sister, for inspiring me to learn as much as humanly possible.

To my friends, for their endless support when it got hard.

To my God, for being with me every step.

To my dog.

BIOGRAPHY

Jonathan Trueblood was born in a suburb of St. Louis, Missouri, thereby sealing his fate as a lifelong fan of the St. Louis Cardinals. Growing up, the three most important aspects of Jon's life were his dog, his baseball team, and the weather. During the Great Flood of 1993, Jon obsessed over the skies, fearing the floodwaters would rise to his house, even though he lived nowhere near any of the affected rivers. After graduating from high school, Jon took his love for science and Cardinals baseball to Northwest Iowa where he studied Physics at Dordt College. Unfortunately, he had to leave his dog in St. Louis. While there, he ran cross country and track, played in the Concert Band, participated in a few productions for the theater department, and cooked every now and then for his 5 other roommates.

Jon began studying at North Carolina State University under the guidance of Dr. Meskhidze in the summer of 2011.

ACKNOWLEDGMENTS

So much of my success is owed to the efforts of those around me. I would first like to thank my family and friends for continuing to support and encourage me during these two years. I'd also like to thank my research group members, both current and past. Thanks to Brett Gantt and Matthew Johnson, for taking me under their wing and showing me the ropes to this crazy process called graduate school. Thanks to Kyle Dawson, for being a great office-mate and not throwing me out the window. I'd also like to express gratitude to all of my fellow graduate students who were there to listen, give advice, complain with me, and share thoughts.

I'd also like to thank all the wonderful professors at NCSU, for their commitment to educational excellence. Thank you to my advisor, Dr. Nicholas Meskhidze, for taking a chance on me two years ago, and for teaching me more in the past two years than I've learned in my whole life. A special thank you to my committee members, Dr. Markus Petters and Dr. Christopher Osburn. Their intelligence and experience was crucial during my experimental development and process.

TABLE OF CONTENTS

LIST OF TABLES

LIST OF FIGURES

CHAPTER 1

Formaldehyde and the Hydrocarbon Oxidation Cycle

1.1 Introduction

The chemical composition of the Earth's atmosphere is fundamentally linked to the biological and geological processes that occur at the surface below. As oceans cover nearly 70% of the Earth, the ocean-atmosphere interactions may be some of the most important and yet least understood between two ecospheres. Adding to the complexity of this relationship are the biological organisms found within the ocean, which are thought to have an impact on climatic processes. Proponents of the so-called Gaia hypothesis (Lovelock, 1974) maintain that the Earth itself, consisting of biota, is an evolving and self-regulating system, capable of changing its environment in order to obtain homeostasis. The CLAW hypothesis, inspired by the Gaia hypothesis, states that ocean phytoplankton (e.g., coccolithoporids) have the ability to emit dimethyl sulfide (DMS) gases, which upon oxidation in the atmosphere, form sulfur containing aerosols. These aerosols can in turn affect the incoming solar radiation reaching the Earth's surface through what is called the direct aerosol effect (Charlson et al., 1987).

In addition to the direct effect, aerosols can indirectly influence climate by altering marine cloud properties that play a key role in the regulation of incoming solar radiation. There are two known indirect effects from aerosols: 1) the suppression of precipitation leading to increased cloud lifetimes (Albrecht, 1989) and 2) the brightening of clouds due to

a rise in cloud condensation nuclei concentration (assuming constant liquid water content), also known as the Twomey effect (Twomey, 1977). The magnitude of forcing that such perturbations have on the global climate, as well as the characteristics of additional unknown interactions and feedbacks between the atmosphere and aerosols remains unclear.

Similar to aerosols, the presence of trace gas species is linked to the air quality, chemical composition, oxidative capacity, and radiative budget of the atmosphere. An understanding of the biogeochemical cycling of such gases, as well as their ensuing chemical reactions and transformations is key to attaining a clearer picture of their environmental impacts. In another manifestation of the Gaia hypothesis, photosynthesis by marine phytoplankton converts dissolved CO_2 into organic carbon, leading to a reduction in surface ocean values and a net CO_2 flux into the ocean. As a result, the biological nature of the oceans has historically played a large role in the evolution of atmospheric CO_2 content, and is presently a primary sink for anthropogenically produced CO_2.

After water vapor and CO_2, methane is the third most abundant greenhouse gas in the troposphere (1.8 parts-per-million) and has a much greater climate warming potential than CO_2 on a per molecule basis (Brasseur et al., 1999). The oxidation of methane by hydrogen radical species (i.e. HO_x) is seen as the first step in an intricate chain of reactions known as the hydrocarbon oxidation cycle. The hydrocarbon oxidation cycle and the radicals involved are central to regional tropospheric chemistry and air quality, as they alter the oxidizing capacity of the atmosphere. Complicating attempts to understand the cycling of methane is the oxidation of additional nonmethane hydrocarbons (NMHC), which are released from a variety of anthropogenic and biogenic sources (Brasseur et al., 1999). While a large percentage of NMHC emissions *stem* from terrestrial vegetation, a smaller fraction is known to occur as a result biological activity in the ocean. The high reactivity of NMHCs as well as the extreme variability of their concentrations in both time and space makes the diagnosis of their impacts on hydrocarbon cycling a difficult task.

Formaldehyde (HCHO) is an important and ubiquitous intermediate reaction product in the global atmospheric hydrocarbon oxidation cycle (Kormann et al., 2003). In the absence of heterogeneous losses, nearly every methane molecule in the atmosphere is eventually

converted to formaldehyde (Brasseur et al., 1999). HCHO is a major immediate source for the global budgets of carbon monoxide (CO) and molecular hydrogen (H_2), as all of its reaction channels eventually leads to their production (Arlander et al., 1995). Additionally, photolysis of HCHO and other carbonyl compounds is the second major source of hydrogen radical species, behind the reaction of excited oxygen atoms with water vapor. Finally, HCHO can affect the acidity of the atmosphere, as its heterogeneous aqueous reaction is a known source of formic acid. In these ways, formaldehyde is an important compound as it drives both the trace gas chemistry of the marine atmosphere and influences the aerosol interactions in the marine boundary layer (MBL). It is clear that the complex physical relationships between marine organisms, gas emissions, aerosols, clouds, and radiative forcing have important implications for the current and future climate. Therefore, a better understanding of the cycling of organic carbon from the ocean, as well as its role in trace gas formation, aerosol generation, and cloud interactions is warranted.

1.2 The Oxidation of Hydrocarbons

To gain a better appreciation for formaldehyde's role in the tropospheric chemistry of remote regions, a closer look at the cycling of relevant hydrocarbons in such areas is needed. The overall photo-oxidation sequence for a hydrocarbon can be described according to Brasseur et al. (1999). Atmospheric reactions involving hydrocarbons begin with oxidation by a strong oxidizer such as the hydroxyl radical (OH), ozone (O_3), or the nitrate radical (NO_3) (Brasseur et al., 1999).

Within a millisecond, resulting carbon-centered radicals attach to oxygen, forming organic peroxy radicals (RO_2). The lifetime of peroxy radicals is on the range of a few seconds, with subsequent reactions involving either one of two nitrogen oxides (NO_x) or another peroxy radical (including the inorganic analogue, HO_2). The two reaction paths represent a critical fork in the hydrocarbon oxidation cycle (Brasseur et al., 1999). In environments with sufficient NO_x concentrations (>30 parts-per trillion), peroxy radical chemistry is driven by reactions with NO:

$$RO_2 + NO \rightarrow RO^{\cdot} + NO_2$$

Completion of this reaction results in extremely active alkoxy radicals (RO), with the conversion of NO to NO_2 eventually acting as an importance source of ozone (Brasseur et al., 1999). A number of other reactions involving the NO radical exist, most leading to the formation of relatively inert organic nitrates ($RONO_2$):

$$RO_2 + NO + M \rightarrow RONO_2 + M$$

where M is any third molecular body. Finally, peroxy radicals can react with NO_2 to form complex species known as peroxynitrates (e.g. peroxyacetylnitrate), which can act as significant reservoirs for reactive nitrogen and may play a role in its long-range transport (Brasseur et al., 1999).

Alternatively, in low NO_x environments, peroxy radical reactions involve either HO_2 or other organic peroxy radicals (RO_2). Reaction products of the peroxy radicals with other organic peroxy radicals vary, and can result in non-radical formation (i.e., ketones, alcohol, and organic acids) or the formation of alkoxy radicals (RO). Furthermore, in environments with exceptionally high hydrocarbon concentrations, these reactions can have a significant effect on the total radical concentration, and therefore the oxidizing capacity of the atmosphere (Brasseur et al., 1999).

The formation of RO indicates a highly reactive portion of the hydrocarbon oxidation cycle. Thermal decomposition, reaction with O_2, and isomerization are the three competing pathways. While the fate of alkoxy radicals is a major point of uncertainty in the overall oxidation scheme, they are of key importance (Brasseur et al., 1999). The products of RO reactions yield a range of partially oxidized species, including aldehydes, ketones, alcohols, and organic acids. Most of these compounds react with OH, but can also react with ozone, NO_3, and sunlight. The final products from these reactions include CO_2, H_2O, CO, and odd hydrogen radicals, all of which are important contributors to the cycling of other hydrocarbons.

The complex tropospheric chemistry of hydrocarbons implies a highly sensitive system of reaction pathways, with relative contributions from each pathway determined by only small changes in species' concentrations and environmental conditions. Radical products from such reactions can further alter the system by increasing or decreasing the

oxidative ability of the atmosphere. For these reasons, a better understanding of the sources and sinks of such gases, as well as their lifetimes and ensuing transformations is necessary.

1.3 The Sources and Sinks of Formaldehyde

1.3.1 Sources

The production of formaldehyde in remote marine regions is primarily driven by the photochemical breakdown of methane and non-methane hydrocarbons (Carlier et al., 1986). In the northern hemisphere, methane is the most abundant hydrocarbon in the clean troposphere with an average mixing ratio of 1.65 parts-per million volume (ppmv) (Lowe and Schmidt, 1983). While the entire methane oxidation scheme is quite complicated, the methane cycling as it relates to the production of formaldehyde can be simplified as follows (Levy, 1971):

$$CH_4 + OH \rightarrow CH_3 + H_2O$$

$$CH_3 + O_2 + M \rightarrow CH_3O_2 + M$$

$$CH_3O_2 + NO \rightarrow NO_2 + CH_3O$$

$$CH_3O + O_2 \rightarrow HCHO + HO_2$$

However, in regions with low NO concentrations, such as over the ocean, this formation pathway competes with two other reaction channels, one involving the methylperoxy radical (CH_3O_2) and HO_2 to form methylhydroperoxide (CH_3O_2H):

$$CH_3O_2 + HO_2 \rightarrow CH_3O_2H + O_2$$

and the other involving two-self reactions of CH_3O_2, which yield HCHO and methanol (CH_3OH):

$$CH_3O_2 + CH_3O_2 \rightarrow 2CH_3O + O_2$$

$$CH_3O_2 + CH_3O_2 \rightarrow HCHO + CH_3OH + O_2$$

Methylhydroxperide and methanol eventually break down further to produce HCHO. However, due to their long lifetimes, they are not efficient sources as they are subject to removal by dry deposition (Arlander, 1995). Using measurements of daytime NO mixing ratios in remote marine regions, Weller et al., (2000) concluded that ~17% of HCHO is produced through the NO pathway. Such findings are supported by the high but variable

CH_3O_2H/HCHO ratio of about 0.9. Logan et al. (1981) estimated that the HCHO yield from methane might be lowered by up to 50% when an efficient heterogeneous loss process of CH_3O_2H on aerosols is assumed.

While NMHCs are much less abundant in the atmosphere, they are known to react more rapidly with OH than methane. This has led to the speculation that in certain scenarios, the production of HCHO from NMHCs may be as important as the methane oxidation mechanism (Hanst et al., 1980). However, measurements of NMHCs over marine regions are relatively scarce. Furthermore, due to the short lifetimes of NMHCs (on the order of ~1 hour), their potential impact as a source of HCHO is constrained to areas near their emission. These considerations, in accordance with uncertainties in NO_x concentrations, make the relative contributions of the various hydrocarbon oxidation pathways difficult to assess.

Additional sources of HCHO in continental regions are direct emissions from incomplete fossil fuel combustion, biomass burning, industrial processing, and emissions from vegetation (Kormann et al, 2003). As our work is focused on the remote marine regions, these mechanisms are not considered in this thesis.

1.3.2 Sinks

The average photochemical lifetime of HCHO near the surface in the sunlit atmosphere is around four hours and decreases with altitude (Lowe and Schmidt, 1983). Major photochemical losses in the remote atmosphere involve photolysis and reaction with OH (Arlander, 1995). The photolytic pathway proceeds through two channels: a molecular channel producing H_2 and CO:

$$HCHO + h\nu \rightarrow H_2 + CO$$

and a radical channel, resulting in the formation of two HO_2 radicals and one molecule of CO:

$$HCHO + h\nu + 2O_2 \rightarrow CO + 2HO_2$$

The reaction of HCHO with OH results in the production of one HO_2 radical, thereby contributing no overall influence on the HO_x budget:

$$HCHO + OH \rightarrow HCO + H_2O$$

$$HCO + O_2 \rightarrow HO_2 + CO$$

Dry deposition and rain are considered to be only minor sinks for HCHO. It is therefore generally accepted that the main process for HCHO loss is photochemical destruction, dependent upon OH radical concentration and photon flux (Lowe and Schmidt, 1983). As evidenced by the reactivity of formaldehyde as well as its tendency to produce reactive hydroxyl radicals, gaining a better understanding of its sources and sinks is key to the elucidation of the hydrocarbon oxidation cycle over remote marine regions.

Measurements and model estimates of formaldehyde concentrations over the ocean have long been in disagreement with one another. Recent studies show a discrepancy of up to a factor of five between models and observations. As proposed mechanisms for HCHO production remain to be insufficient to explain such large discrepancies, the role of marine regions in the creation of HCHO continues to be one of the largest sources of uncertainty in current global chemistry-transport models. The purpose of this study is to create a viable formaldehyde detection method that can be used in-line with a marine aerosol generation/reaction chamber. Using the detection method and the aerosol chamber, future experiments can be conducted to test the contribution of primary marine organic aerosols to the formaldehyde budget over remote marine regions.

CHAPTER 2

Observations and Estimates of Formaldehyde over Remote Marine Regions

2.1 Introduction

Various in-situ and remote sensing studies of atmospheric HCHO content have been carried out over the past several decades. Direct comparison of results is difficult due to temporal and spatial differences, as well as the diverse range of detection methods employed. Nonetheless, general trends in results have been observed. Perhaps most obvious is the fact that marine regions typically exhibit lower HCHO mixing ratios than the polluted continental regions. The characteristic daily average over the ocean ranges between 100-600 pptv, quite low compared to a polluted area such as Los Angeles, which can reach concentrations of 70 ppbv. Despite the overall lower concentrations of formaldehyde in pristine environments, isolated hotspots have been reported (~1600 pptv). Attempts to explain these anomalies through the use of global chemical transport models have largely fallen short, indicating a lack of understanding in hydrocarbon chemistry over the oceans. An overview of recent in-situ and remote sensing measurements is now presented, as well as a review of the attempts by chemical transport models to replicate observed concentrations.

2.2 In-Situ Measurements

While many direct measurements of HCHO concentration in polluted regions (defined as air masses containing ~50,000 particles/cm^3) have been reported, relatively few studies in pristine marine air environments (air masses containing ~1,500 particles/cm^3) have been published. The first report of clean marine air HCHO content was presented by Hadamczik (1947), who found mixing ratios at the Baltic Sea coast ranging from 500-2000 pptv. Since then, most in situ studies over marine regions have resulted in values that are within the range of Hadamczik's findings (Table 2.0).

Table 2.0 Overview of selected HCHO measurement and modeling study comparisons.

Location	Obs. (pptv)	Model (pptv)	Reference
NH Pacific	400 ± 200	180	Zafirou, 1980
NH Pacific	140 ± 70[1]	300	Heikes, 1992
NH Pacific	183 ± 93[2]	215	Zhou, 1996
SH/NH Pacific	300[3]	200[3]	Singh, 2001
SH Pacific	350-450	200	Ayers
NH/SH Pacific	700[4]	400[4]	Arlander et al., 1990
SH Indian	200 ± 70	224	Wagner, 2002
SH Indian	100-200	n/a	Arlander et al., 1990
NH Atlantic	200	270	Lowe and Schmidt, 1983
NH Atlantic	110	410	Jacob et al., 1996
NH Atlantic	470 ± 200	n/a	Harris et al., 1992
NH Atlantic	580 ± 160[5]	330[5]	Weller et al., 2000
Mediterranean	1500	1050	Ladstätter-Weiβenmayer, 2003
Mediterranean	1107[6]	900[6]	Kormann et al., 2003
NH Atlantic	50-270[7]	40-70[7]	Jaegle et al., 2000

[1]Measured air was from the free troposphere
[2]Average of 4 seasons. Spring value was 25% higher than Heikes (1992)
[3]Model/observation comparison from flight path at 0-30° S 165-100° W
[4]Model/observation comparison at 15° N
[5] Model/observation comparison at 28° N-24° N
[6] Model/observation comparison in marine boundary layer. Model under estimate reached a factor of 8 in free troposphere
[7] Model/observation comparison at 8-10 km height

2.2.1 Pacific and Indian Oceans

The earliest attempts to quantify formaldehyde content in remote regions of the Pacific Ocean were carried out by Zafirou et al. (1980). Experiments took place in the central equatorial Pacific from June-August 1979 as part of the Northern Hemispheric Wet Season Experiment. Using a freezeout preconcentration method, Zafirou calculated average gas phase concentrations of HCHO at 400 ± 200 pptv.

As part of the Mauna Loa Observatory Photochemistry Experiment (MLOPEX I) (May 1-June 4 1988), concentrations of various hydrocarbons were measured at the Mauna Loa Observatory (MLO) in Hawaii (19° N, 155° W) at an elevation of 3.4 kilometers on a northward facing slope (Heikes, 1992). Sampled air had generally not been in contact with continental landmasses for at least 5 days, and was therefore a good indicator of remote free troposphere marine air (Mackay et al., 1996). The average formaldehyde mixing ratio was 140 ± 70 pptv (Heikes, 1992).

A second set of measurements at MLO was conducted during the yearlong MLOPEX II study, which occurred from September 1991-August 1992 (Zhou et al., 1996). Average daily HCHO values were 196 ± 108, 149 ± 61, 178 ± 101, and 211 ± 104 pptv for fall, winter, spring, and summer, respectively. The seasonal variation of HCHO concentrations was attributed to the differences in the average height of the synoptic regimes during summer and winter. As the average depth of the MBL was higher during the summer, the downslope flow of free tropospheric air to the measurement site was less common. Conversely, the shallow MBL during the winter allowed the addition of free troposphere air during nighttime cooling. The spring value of 178 pptv was 25% greater than the value presented by Heikes (1992) during MLOPEX I. While the authors do not speculate on the reasons behind the discrepancies between the results from MLOPEX I and II, it is possible that differences in measurement techniques could be to blame. Both studies performed at MLO exhibited a strong diurnal tendency, likely due to a change in air masses caused by local air circulation patterns.

An airborne experiment (NASA/PEM-Tropics B) using DC-8 and P-3B aircraft provided an opportunity for the detailed examination of formaldehyde and other oxygenated

organic compounds in the remote troposphere of the Southern Hemisphere. A total of 18 flights over the Pacific Ocean from 35° N to 35° S and 90° W to 150° E were performed from March-April of 1999. Mixing ratios of formaldehyde were nearly identical in the north and south tropical regions, with values ranging from 70-300 pptv (Singh, 2001).

Ayers et al. (1997) presented measured values of HCHO at the Australian Baseline Station at Cape Grim (40° S 144° E) from November-December 1993. Detection was carried out by sampling air through a Teflon line in which HCHO was stripped by deionized water. The aqueous formaldehyde concentration from the diffusion scrubber was then measured using fast flow injection analysis. Hourly measurements showed a diurnal cycle, with daily HCHO averages ranging from 300-450 pptv.

Arlander et al. (1990) found much higher concentrations of HCHO than previous studies reported while on board the SAGA II cruise in the Pacific Ocean. The North-South transect took place from May through early June 1987 and stretched from Kamchatka Peninsula to Wellington, New Zealand. Measurements indicated an HCHO maximum at the equator (~800 pptv), and a second maximum at 20N (~700pptv), with relatively lower values in the Southern Hemisphere (figure 2.0). The authors hypothesized the main source of formaldehyde was from methane oxidation, with local maxima (such as at 20° N) attributed to ozone-alkene reactions. Furthermore, results indicated a diurnal pattern consistent with photochemical production being the primary source.

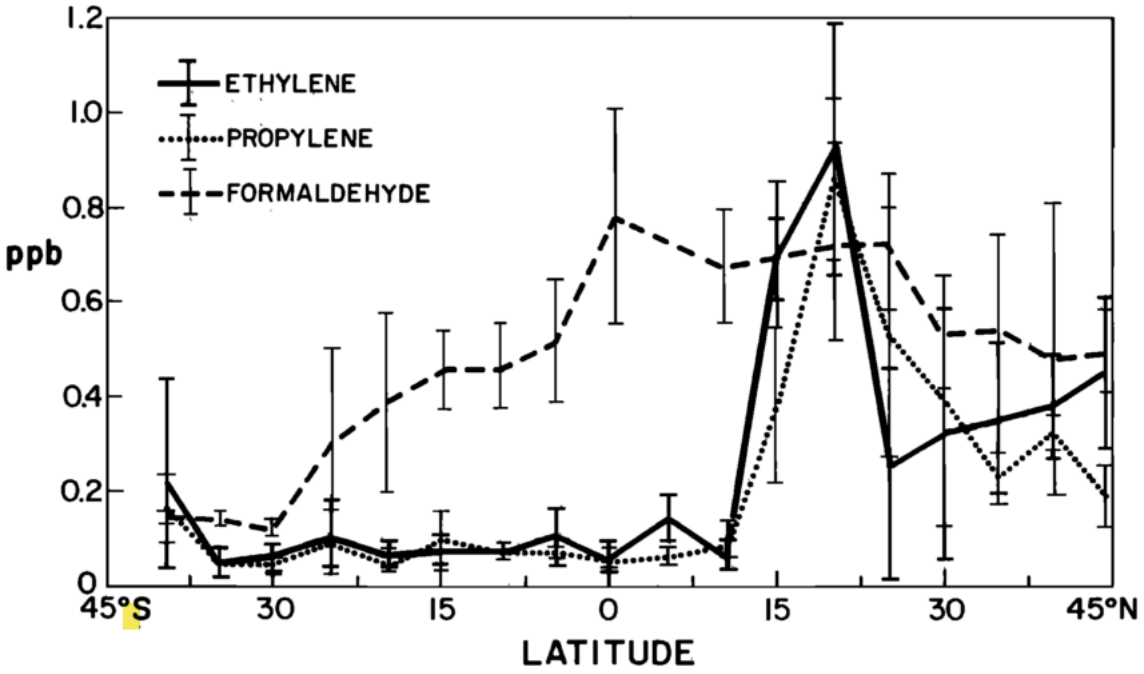

Figure 2.0 Plot of ethylene, propylene, and formaldehyde versus latitude during the SAGA II cruise in the Pacific Ocean. Note the lower HCHO concentrations in the Southern Hemisphere and the two peaks at the equator and ~20° N. (Image from Arlander et al., 1990)

Fewer studies have taken place in the Indian Ocean. Observations aboard the Ronald H. Brown aircraft occurred from February-March, 1999 as part of the Indian Ocean Experiment (INDOEX) (Wagner et al., 2002). Using a tunable diode laser absorption spectrometer set to an absorption line at 1766.32 cm^{-1}, Wagner found that HCHO concentrations in the Southern Indian Ocean averaged 200 ± 70 pptv. As part of the aforementioned SAGA II cruise, measurements of formaldehyde mixing ratios were also taken from 30° S to 7° N in the Indian Ocean along 90° E, with concentrations between 100-200 pptv with only slight diel variations (Arlander et al., 1990). Generally, mean HCHO concentrations in the Indian Ocean are similar to those found in the Pacific regions.

2.2.2 Atlantic Ocean

Lowe and Schmidt (1983) presented measurements taken during a North-South transect of the Atlantic Ocean and at coastal regions in Ireland. A total of 36 air samples were collected at the Irish coastline site. Subsequent analyses indicated an average of 200 pptv for HCHO. Back trajectory calculations confirmed that the air had an origin from the clean marine boundary layer. The authors speculated that particulate organic matter (particles with a diameter greater than 1 μm) originating from sea foam could have led to increased mixing ratios on several days; a hypothesis corroborated by Neitzert and Seiler (1981), who also found evidence of a biogenic contribution to HCHO on South African cliffs.

Measurements were also conducted during a cruise of the F/S Meteor as it crossed the Atlantic Ocean (54° N to 35° S) from October – November, 1980. A total of 151 samples indicated an average of 200 pptv, with slightly higher values in the Northern Hemisphere. Results also suggested that North Atlantic mid-latitudes were more variable than tropical regions.

Jacob et al., (1996) reported aircraft data from the Transport and Atmospheric Chemistry Near the Equator-Atlantic (TRACE-A) study during fall of 1992 over the tropical South Atlantic Basin. The purpose of TRACE-A was to measure ozone and its precursors in hopes of deriving an augmented chemical budget for ozone. Measured compounds included ozone, CO, NO, HCHO, and various other hydrocarbons. Results showed an average of 110 pptv (ranging between 40-250 pptv) for HCHO in the first 4 km of the marine boundary layer, decreasing with height to <40 pptv at 12 km. These values were lower than those found during Lowe and Schmidt's study of the South Atlantic in 1983 (~200pptv).

Measurements of NO_2, HCHO, and H_2O_2 between 40° N and 17° N in the Atlantic Ocean were made aboard the RV Polarstern during the fall of 1988. Harris et al. (1992) presented data from mid infrared absorption spectroscopy using tunable diode lasers (TDLAS). The TDLAS data was averaged over sampling periods of one hour, with mean mixing ratios of 470 pptv ± 200. Similarly, organic peroxides, H_2O_2, and formaldehyde were measured in the mid-Atlantic (48° N-35° S) during the October-November 1996 RV Polarstern cruise (Weller et al., 2000). Twenty-minute averages showed a broad maximum of

600-1200 pptv in the tropical Atlantic, with minima occurring in the inter-tropical convergence zone (ITCZ) (a trend seen in all studies, likely due to washout). Values north and south of the equator ranged between 200-600 pptv. Weller's results were well above those presented by Lowe and Schmidt (1983) (~200pptv), and TRACE-A measurements (50-230 pptv) (Heikes et al., 1996), but agreed well with results from the RV Polarstern cruise (470 pptv ± 200) (Harris et al., 1992), and TROPOZ II measurements over the tropics (600-1000pptv)(Arlander et al., 1995).

2.3 Remotely Sensed Data

Remotely sensed and in situ measurements have revealed remarkably high HCHO mixing ratios over the Mediterranean Sea (up to 1500pptv) (Lelieveld et al., 2002). Average HCHO concentrations in the MBL of the Mediterranean are found to be at least 3X higher than those observed in the Atlantic, Pacific, or Indian Oceans (Lelieveld et al., 2002). This is believed to be attributed to the advection of pollution from eastern and western Europe (Kormann, 2003).

The Global Ozone Monitoring Experiment (GOME) satellite can be used to calculate vertical columns of HCHO. GOME is a nadir-scanning double-monochromator that measures the sunlight scattered from the Earth's atmosphere and/or reflected by the surface in the wavelength region of 240 to 790 nm at a spectral resolution of 0.17 to 0.33 nm (Ladstätter-Weiβenmayer et al., 2003). Vertical columns of HCHO made from measurements of backscattered UV absorption are produced in two steps: (1) slant columns are fitted in the 336-356 nm wavelength region, with a mean column fitting uncertainty of $4x10^{15}$ mol/cm^2 and (2) vertical columns are calculated from fitted slant columns using an air-mass factor formulation (Palmer et al., 2007). Calibration is achieved using a Pt/Cr/Ne hollow cathode gas discharge lamp. Validation of GOME data products is carried out by comparing results to ground-based measurements (Burrows et al., 1998).

Above the Mediterranean region, GOME satellite retrieved HCHO vertical columns averaged during July and August 2001 were $6.4x10^{15}$ molecules cm^{-2} (Ladstätter-Weiβenmayer et al., 2003). Additionally, monthly averaged HCHO vertical columns from

GOME for 1996-2002 showed a strong correlation to seasonal cycles, with mean monthly summertime values between $4x10^{15}$ and $8x10^{15}$ molecules cm^{-2} (Ladstätter-Weiβenmayer et al., 2007). Sabolis et al. (2011) used air mass factor (AMF) corrected Ozone Monitoring Instrument (OMI) retrievals of HCHO columns over the Mediterranean Sea to highlight the distinct seasonal and spatial trends of HCHO over marine regions. Analysis of the data revealed the HCHO peak typically appeared during the warmer seasons and was confined to regions over water (Figure 2.1). A discussion on the possible reasons for the Mediterranean's high HCHO concentrations can be found at the end of this chapter.

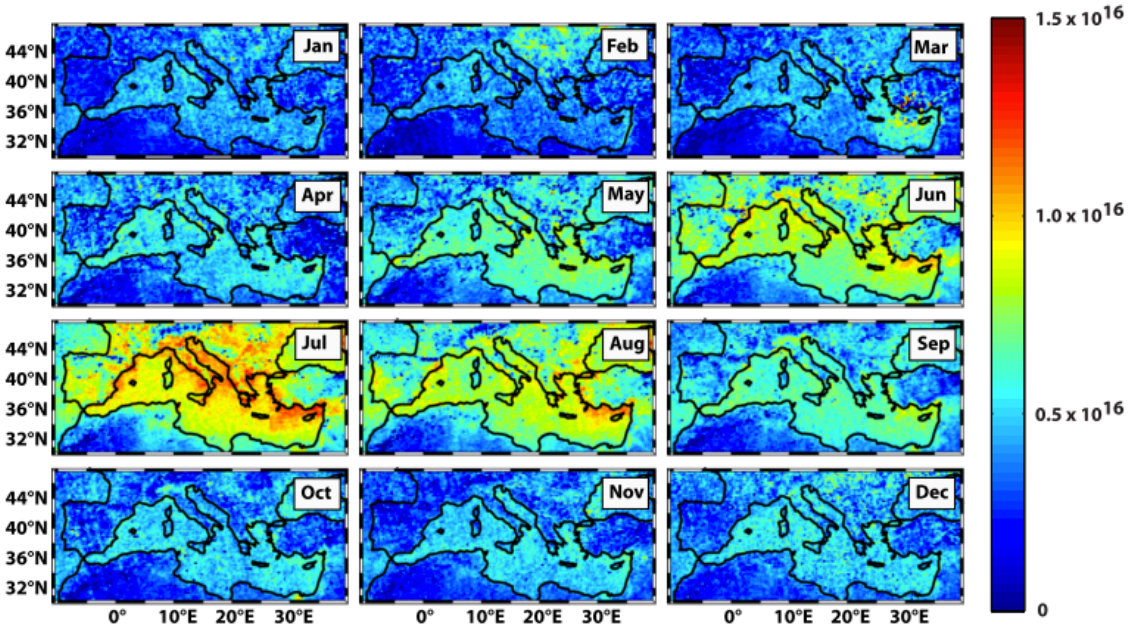

Figure 2.1 Recalculated monthly averaged retrieved HCHO vertical columns from 2005 to 2007 in units of molecules cm^{-2} using correct AMF values. Worth noting are the seasonal and spatial trends. Formaldehyde tends to be concentrated over the marine regions, with highest values occurring during the summer months.

2.4 Chemical Models

Despite the relatively uncomplicated chemistry of the marine background troposphere in comparison with polluted continental regions, chemical modeling studies continue to exhibit large discrepancies from observed formaldehyde concentrations. Computed values of HCHO distributions in the clean troposphere are difficult to compare because of the different assumptions used to generate such models. Interestingly, early studies point towards an over prediction of models with little observable diurnal cycling (Zhou et al., 1996; Jacob et al., 1996). More recent studies, however, have indicated that measured HCHO concentrations are under predicted and exhibit strong diurnal fluctuations (Jaegle et al., 2000; Weller et al., 2000; Ayers et al., 1997).

2.4.1 Mediterranean Sea

Ladstätter-Weiβenmayer et al. (2003) used the Model of Atmospheric Transport and Chemistry (MATCH-MPIC) to compare 3-D photochemistry-transport model results with in-situ airborne and GOME retrievals of HCHO. While remotely sensed and in-situ data were in fairly good agreement, there was considerable underestimation of the model in relation to both measurement techniques (i.e., 30% for in situ and 17% for GOME). The authors speculated that errors in the model could be attributed to an underestimation in emissions of NMHCs. To test this hypothesis, Sabolis (2011) used a simple calculation to estimate the amount of isoprene (the most abundant NMHC over the remote ocean) needed to explain the summertime maxima of HCHO over the Mediterranean Sea. Following the Palmer et al. (2003), HCHO vertical columns were calculated as:

$$HCHO = S * E_{iso} + B$$

Where S is the linear slope corresponding to the HCHO yield from isoprene, E_{iso} is the emission rate, and B the background concentration. Results showed that isoprene emission rates two to three orders of magnitude higher than what was present would be required to explain the summertime maxima in HCHO over the Mediterranean.

Kormann et al. (2003) also used the MATCH-MPIC 3-D global chemistry transport model based on methane and NMHC chemistry in an attempt to model observed values of HCHO from the MINOS campaign. Measured concentrations in the marine boundary layer (1107 pptv) were underestimated by ~200 pptv. At altitudes between 6-12 km HCHO observations (340 ± 150 pptv) were underestimated by as much as 300-400 pptv (a factor of 8). Sensitivity studies indicated that the measurement-model disagreement could not be resolved based on known chemistry and emissions. The authors speculated that relatively long-lived NMHCs from polluted regions might be responsible for the observation-model discrepancies. Indeed, in the upper troposphere, the mean mixing ratio of HCHO showed a dependency on the air mass origin, with low concentrations correlating with West Atlantic air masses and high concentrations coming from Indian monsoon region origins.

2.4.2 Indian Ocean

Wagner et al. (2002) investigated the formaldehyde budget in the MBL over the southern Indian Ocean using a standard photochemical box model based on the Master Chemical Mechanism. When constrained by CH_4 and NMHCs, the model predicted a daily mean concentration of 224 pptv, an over prediction of 12%. When NMHC oxidation was ignored and only methane oxidation was considered, the model predicted an HCHO concentration of 200 pptv (~10% under prediction).

2.4.3 Pacific Ocean

Zafirou et al. (1980) used a steady state calculation driven by the tropospheric methane oxidation chain coupled with photolysis and OH reaction as sinks to approximate the concentration of HCHO over equatorial Pacific regions. This simple estimate produced a mean mixing ratio of 180 pptv, roughly 1.2 standard deviations below the observed average of 400 pptv. Using a simple box model calculation constrained by experimentally determined concentrations of CH_3O_2H, Zhou et al. (1996) modeled formaldehyde concentrations in free troposphere air at the Mauna Loa observatory. Similar to Zafirou et al. (1980), HCHO production was driven using only the methane oxidation chain. However, in contrast to

Zafirou's findings, calculated values for winter and fall (~140 pptv) were on average 20% greater than observations, while spring and summer predictions (~215 pptv) were nearly 50% higher than observations.

Observed values at Cape Grim between mid November and mid December 1993 were 50% higher than expected (~200pptv) when using a box model based on conventional understanding of low NO_x photochemistry (Ayers et al., 1997). As a means of explaining model under predictions, Ayers proposed that the reaction between HO_2 and CH_3O_2 may not proceed with 100% efficiency to CH_3O_2H radical, but may also produce formaldehyde through the following reaction:

$$CH_3O_2 + HO_2 \rightarrow HCHO + H_2O + O_2$$

However, the conditions necessary for such a reaction are not likely under normal atmospheric conditions (Lightfoot et al., 1992), thereby disqualifying the proposed reaction as a possible explanation for the enhanced observed values.

Mixing ratios of formaldehyde and other NMHCs observed over the Pacific during NASA/PAM-Tropics B were compared with results from the Harvard Global Model (Singh et al., 2001). The robust model included 80 chemical species to represent ozone-NO_x hydrocarbon chemistry. While modeled formaldehyde concentrations were generally accurate, under estimates on the order of 40% were present (Singh et al., 2001). The authors posited that photochemical degradation of dissolved organic matter present in the surface oceans could act as an important source of formaldehyde and other oxygenated hydrocarbons (Singh, 2001).

2.4.4 Atlantic Ocean

Over predictions of HCHO in the Atlantic Ocean were common in early studies. Lowe and Schmidt (1983) compared 131 observations across the mid Atlantic with theoretical profiles of latitudinal HCHO distribution in October and November using a two-dimensional model from the Atomic Energy Research Establishment. The observed mixing ratios were generally lower than model predictions by 30% (Figure. 2.2).

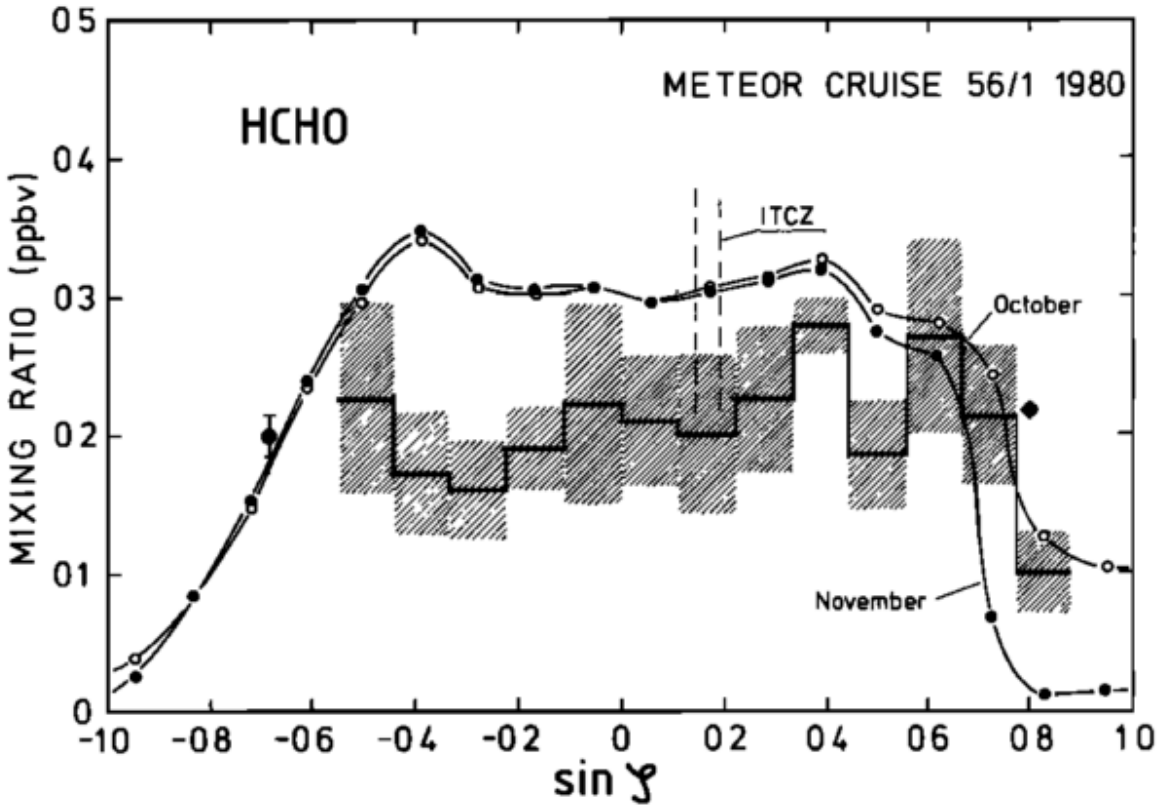

Figure 2.2 Latitudinal means of the HCHO mixing ratio measured over the Atlantic during the F/S Meteor cruise. The hatched area represents the ±1σ variation of the means. A modeled latitudinal distribution calculated by the Atomic Energy Research Establishment 2D model is also shown. The distinct symbols represent additional means of measurement data from an Irish coastline (diamond) and New Zealand (large solid circle). (Image taken from Lowe and Schmidt, 1983)

Similarly, Jacob et al. (1996) attempted to accurately model observations during the TRACE-A study across the tropical South Atlantic Basin. Calculated HCHO concentrations in the tropical South Atlantic averaged 410 pptv, an overestimate of observed concentrations by a factor of ~3.

More recently, studies have trended towards a severe under prediction of the models. In an attempt to describe observed CH_3O_2H and HCHO mixing ratios, Weller et al. (2000) employed a box model based upon CH_4 and CO photooxidation in the MBL of the subtropical Atlantic Ocean (28° N-24° N). The model under predicted measured HCHO

mixing ratios by nearly a factor of 2, even upon modification of reaction rates. Predicted values only reached 330 pptv, with observations at 580 pptv ± 160. Due to a lack of observational data, neither Weller et al. (2002) nor Ayers et al. (1997) considered the production of HCHO by oxidation of NMHCs.

Model estimates of HCHO in the free troposphere also have a history of under prediction. As part of TROPOZ II, a series of 149 aircraft measurements of the HCHO mixing ratio were made between 0 and 10 km from 70° N-60° S of the Atlantic Ocean during winter 1991 (Arlander et al., 1995). A vertical decrease of mixing ratio was observed at all latitudes, with broad latitudinal maxima between 30° N and 30° S. Measured mixing ratios between 6 and 10 km reached values of 110 pptv, a factor of nearly two times what a 2-D model including NMHC and methane oxidation predicted. Furthermore, HCHO estimates based upon methane oxidation alone under predicted HCHO concentrations at all altitudes.

Jaegle et al., (2000) compared results of a point model with HCHO measurements for altitudes of 8-12 km during the subsonic assessment ozone and nitrogen oxide experiment (SONEX) aircraft campaign over the North Atlantic in October-November 1997. Model evaluations were low by a factor of ~2-3, with maximum observed HCHO concentrations reaching 270 pptv (Figure 2.3). Finally, Heikes et al. (2001) reported HCHO concentrations that were 1.4 times larger than model estimates at a height of 8 km above the ocean.

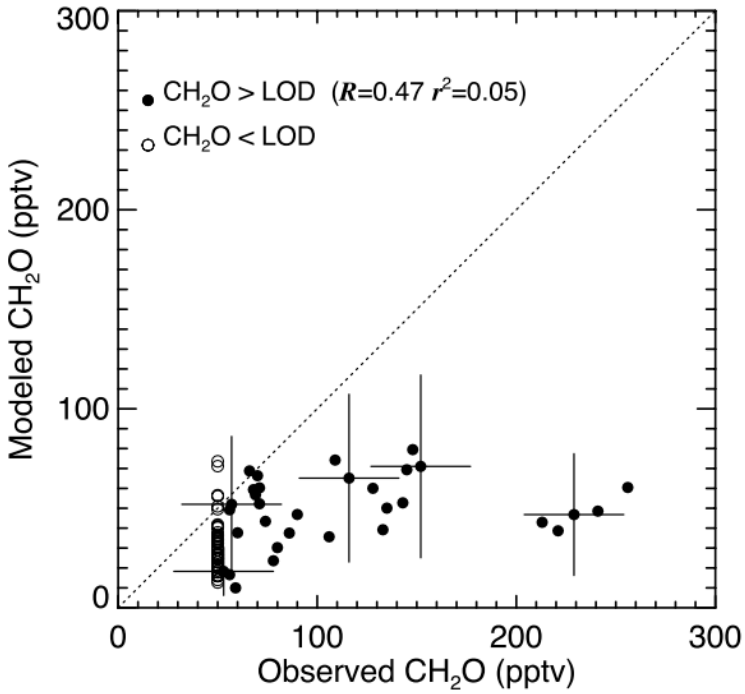

Figure 2.3 Comparison of observed concentrations of HCHO with model calculations using observations of OH, acetone, CH_3OOH, HCHO photolysis frequency, temperature, and assuming diel steady state for HCHO. Observations below the limit of detection (<50 pptv) are shown by open circles, with observations above LOD shown by solid circles. (Image taken from Jaegle et al., 1999)

Discrepancy Possibilities

A number of hypotheses have been proposed to explain under prediction of measured HCHO levels. Recently, the importance of NMHCs in the production of formaldehyde has been examined more closely. An estimate by Cox (1999) using NMHC measurements at Cape Grim indicated that they could account for 20% of the HCHO budget in the remote marine boundary layer. Ladstätter-Weiβenmayer et al. (2003) attributed the discrepancy between their model and observations over the Mediterranean Sea to a lack of terpene chemistry. However, results from Sabolis et al. (2011) suggested that contribution of ocean-derived terpenes was likely not a large source of HCHO in the MBL. While isoprene concentrations are only expected to be elevated in coastal regions, Yokouchi et al., (1999) showed that concentrations around 10 pptv can occur over the remote ocean. Indeed, very

large discrepancies (up to a factor of 30 for isoprene) in reported marine NMHC emission rates estimates exist (Luo and Yu, 2010). The overall lack of NMHC data over the ocean makes its inclusion in chemical modeling difficult. For this reason, further research assessing the impact of these compounds on HCHO budgets is needed.

Other possible sources of uncertainty in HCHO budgets include halogen and heterogenous chemistry. Chatfield (1994) and Lelieveld and Crutzen (1990), presented results from modeling studies that indicated heterogeneous chemistry in aerosols and droplets could provide a sink for HCHO. Wagner et al. (2002) presented a range of possible reactions involving oxidation of methane by halogen species that could act as a source of additional HCHO. However, calculations with the Model of Chemistry Considering Aerosols indicated that halogen and aerosol chemistry have no significant impact on HCHO concentrations in. remote marine regions (Wagner et al., 2002).

As will be discussed in chapter 3 of this paper, the surface of the ocean has been proposed as a possible HCHO source. Measurements of HCHO in surface seawater have been reported, but clearly indicate a net flux from the atmosphere to the ocean (Zhou and Mopper, 1997). Research investigating the role of air mass exchange between the free troposphere and the marine boundary layer has also failed to explain discrepancies. Measurements from Arlander et al. (1995) indicated a decrease in HCHO concentration with altitude, largely in agreement with chemical models. For this reason, mixing from the free troposphere to the MBL is thought to decrease HCHO concentrations near the surface. However, back trajectory studies have indicated that long-range transport of polluted air masses may cause isolated instances of elevated HCHO levels in the free troposphere, which upon mixing with the MBL, could act to increase concentrations (Lelieveld et al., 2002; Ladstätter-Weiβenmayer et al., 2003). A recent airborne campaign covering an area between the Mediterranean Sea up to the subpolar regions north of Norway revealed homogenous distribution of HCHO, except in areas over the Mediterranean (Klippel et al., 2011). Such observations seem to contradict the polluted air mass hypothesis.

The observed differences in the magnitude of diurnal variations of HCHO concentrations are also a point of uncertainty in MBL chemistry. During the day, production

of HCHO by oxidation of methane and NMHCs is thought to be in balance with photochemical removal processes, dry deposition, and entrainment. At night, the only active processes are dry deposition and entrainment, thereby reducing the overall HCHO concentration. Because of this, it is expected that HCHO will follow a distinct diurnal cycle, with maximum values occurring in the early afternoon (Lowe and Schmidt, 1983). However, observations of HCHO by Weller et al. (2000) over the Atlantic did not feature such diurnal cycling. While it is possible that dynamical processes may mask diurnal cycles, it is clear that the overall understanding of HCHO production and destruction is poorly understood. At this point, none of the proposed processes have succeeded in explaining discrepancies between models and observations. We hypothesize a new formation mechanism for HCHO featuring the carbon cycling between the ocean and atmosphere systems, followed by photolysis of organic matter in the atmosphere. The theoretical basis of this hypothesis is addressed in the following chapters.

CHAPTER 3

Composition of the Surface Ocean and the Clean Marine Boundary Layer

3.1 Organic Matter in the Ocean

Marine organic matter is most commonly classified within one of two categories (i.e., dissolved and particulate) determined by simple filtration procedures. Organic matter from seawater that is retained on filters with pore sizes ranging 0.1-1 μm is defined as particulate organic matter (POM), while the fraction of organic matter that passes through is termed dissolved organic matter (DOM). DOM is both a major reactant and product of biogeochemical processes, while serving as a carbon and energy source for biota and various organisms. According to Sharp (1973), the vast majority of organic matter in the ocean exists in the dissolved fraction (>97%). Despite contributing such a large fraction of matter to the overall carbon pool, DOM is still poorly characterized. It is generally described as a complex mixture of aromatic and aliphatic hydrocarbon structures that have attached amide, carboxyl, hydroxyl, and ketone functional groups (Lenheer et al., 2003). However, DOM composition, as well as its concentration and chemistry are all highly variable, depending on source mechanisms, temperature, pH, and other environmental characteristics.

While the simple size delineation between POM and DOM is useful, there are two additional distinctions to be made. First, is the fact that organic matter is not cleanly separated between DOM and POM, but rather occurs in a size continuum ranging between the two phases (Sharp, 1973). Dissolved colloids are considered to be the bridge between the

DOM and POM pools. These gel-like structures can spontaneously assemble, forming polymer particles that are in a reversible physical equilibrium with DOM (Chin et al., 1998.) Included within this class of organic matter are transparent exopolymeric particles (TEP).

Second, is the classification of organic matter based upon its optical properties (e.g., absorbance and fluorescence). Chromophoric dissolved organic matter (CDOM) is the fraction of DOM that absorbs solar radiation, and can undergo a plethora of chemical reactions upon irradiation (de Bruyn et al., 2011). Further discussion of these two distinctions within the OM pool (i.e., TEP and CDOM) is warranted, as they have been shown to have unique transformation mechanisms and are an important component of the clean marine aerosol fraction.

3.2 Transparent Exopolymer Particles (TEP)

Existing within the continuum from dissolved to particulate organic matter, TEP are transparent, sticky particles formed by the coagulation of DOM released into the water as phytoplankton exudates and/or byproducts of bacterial growth (Verdugo et al., 2004). TEP are among the most abundant of all exopolymeric gel substances (EPS) in the marine environment. The exact chemical makeup of TEP are not currently well defined. However, it has been shown that they are rich in sulfated deoxy-sugars, proteins, lipids, nucleic acids, and a range of other acidic polysaccharides (Passow, 2002b). As indicated by the name, TEP are not visible to the naked eye. Nevertheless, they can be detected through a staining method with Alcian Blue, a cationic copper pthalocyanine dye that complexes the carboxyl (-COO-) and half-ester sulfate reactive groups of polysaccharides (Ortega-Retuerta, 2008).

TEP are crucial to the carbon cycling of both the surface and deep oceans. The high abundance and stickiness of TEP allows them to facilitate the aggregation of solid, non-sticky particles, thereby increasing the sedimentation rate of carbon in the form of marine snow (Engel et al., 2004; Thornton, 2002). However, as not all TEP sink, they are also an important surface-active component of the ocean environment (Azetsu-Scott and Passow, 2004). We focus upon the surface-active properties of TEP and how they affect the marine boundary layer above.

3.2.1 Determination of TEP

TEP are operationally defined as particles retained on polycarbonate filters that are stainable with Alcian Blue dye. There are currently two methods for quantitation of TEP: microscopic and colorimetric. Both methods require a staining process (Passow, 2002b). The microscopic determination of TEP allows the quantitation of both number and sizes of TEP, from which their total surface area and volume can then be estimated. Samples are first prepared by filtration through 0.2 or 0.4 μm polycarbonate filters, and then stained with Alcian Blue (Passow, 2002b). Samples are then transferred to slides and TEP are counted and sized either manually or semi-automatically using an image analysis system (Mari and Kiorboe, 1996). The encased volume can then be estimated using the assumption that stained particles represent the cross section of spherical particles. The size distributions of TEP follow a power law distribution:

$$\frac{dN}{dl} = a^{-b}$$

where N represents the number of TEP, and l the length of the TEP (Passow and Alldredge, 1994).

In the colorimetric method, the TEP are stained in the same way as in the microscopic method. However, the samples are then placed in 80% sulfuric acid to allow dissolution of the stained particles, which are then quantified using spectrophotometry (Passow and Alldtedge, 1995b). The amount of dye bound to TEP is standardized using Gum Xanthan, allowing TEP concentrations to be expressed in μg Gum Xanthan equivalent per liter (Passow and Alldredge, 1995).

Both the colorimetric and microscopic methods have advantages and disadvantages, and the decision of which method to use depends on the sample and what information the experimenter desires to learn. Microscopic enumeration yields better results when the size distribution of TEP is important. However, this method is time consuming, and the various odd shapes of TEP means that assumptions based on the volume calculations are prone to

error (Passow, 2002b). Conversely, while the colorimetric method is faster, it gives no information pertaining to the size distribution of the particles (Passow, 2002b).

3.2.2 Properties of TEP

Chemical

While the exact chemical composition of TEP is unknown, it is generally understood that it varies based upon the biological source and the aggregation conditions (Passow, 2002b). Because they can be stained with Alcian Blue, TEP are by definition composed largely of acidic polysaccharides (Passow, 2002b). Upon addition of glucosidase, TEP disappear, indicating that they also consist largely of sugars (Long and Azam, 1995). Indeed, studies have also shown TEP are composed primarily of sulfated deoxy sugars, like fucose, rhamnose, arabinose, and galactose. They also have been found to contain proteins, lipids, and nucleic acids (Passow, 2002b). While measurements of the carbon content of TEP indicate they are predominantly composed of water, colorimetric determinations suggest their carbon content is at the same range as phytoplankton, making them a significant part of the marine carbon pool (Mari, 1999; Engel and Passow, 2001).

Physical

Because TEP are gels, they are highly flexible and sticky. Due to their high fraction of sulfate ester groups, TEP particles exhibit stickiness coefficients (a value based upon aggregation rate) generally 2-4 orders of magnitude higher than most other particles (Passow, 2002b). Such properties make TEP hotspots for microbial organisms, housing live and dead plankton, bacteria, and various mineral particles (Cunliffe et al., 2012). Furthermore, because of their low density, some TEP ascend and accumulate at the surface, making them important in the rate of gas exchange at the air-sea interface (Azetsu-Scott and Passow, 2004).

TEP can generally be described using polymer gel theory (Chin et al., 1998). Briefly, the polymer network entraps seawater, which is in thermodynamic equilibrium with the surrounding seawater (Passow, 2002b). Gels can then undergo reversible transitions between

condensed and hydrated phases, depending on environmental factors like pH, temperature, pressure, and ion density (Tanaka, 1981).

3.2.3 Generation of TEP

Phytoplankton were traditionally considered to be the main source of TEP in marine ecosystems, either through a two-step biotic/abiotic process involving aggregation of dissolved organic matter precursors and nanogels excreted during exponential growth, or through direct formation during sloughing and lysis of senescent cells (Kiorboe and Hansen, 1993; Schuster and Herndl, 1995; Grossart and Simon, 1997; Passow and Wassman, 1994; Hong, et al., 1997; Passow, 2000). In addition to phytoplankton, macroalgae and zooplankton have been reported as secondary sources of TEP (Ortega-Retuerta 2010; Passow, 2002a).

Released DOM polymers coagulate via hydrophobic and electrostatic bonding to form submicron aggregates (Passow, 2002b) and submicron gels via gelation and annealing (Chin et al., 1998). Upon further congealing driven by surface coagulation onto bubbles, laminar and turbulent shear, and adsorption onto particles (Passow, 2002b), larger aggregates are formed, which eventually grow into TEP (Kepkay, 2000). The formation of TEP from fibrillar DOM precursors acts as a bridge between the dissolved and particulate pools of organic matter (Passow, 2002b). Studies show that only 10% polysaccharides within a water column exist as nanogels, with an even smaller fraction of polysaccharides existing as TEP (Chin et al., 1998). For this reason, TEP are believed to replenish rapidly (Passow, 2002b).

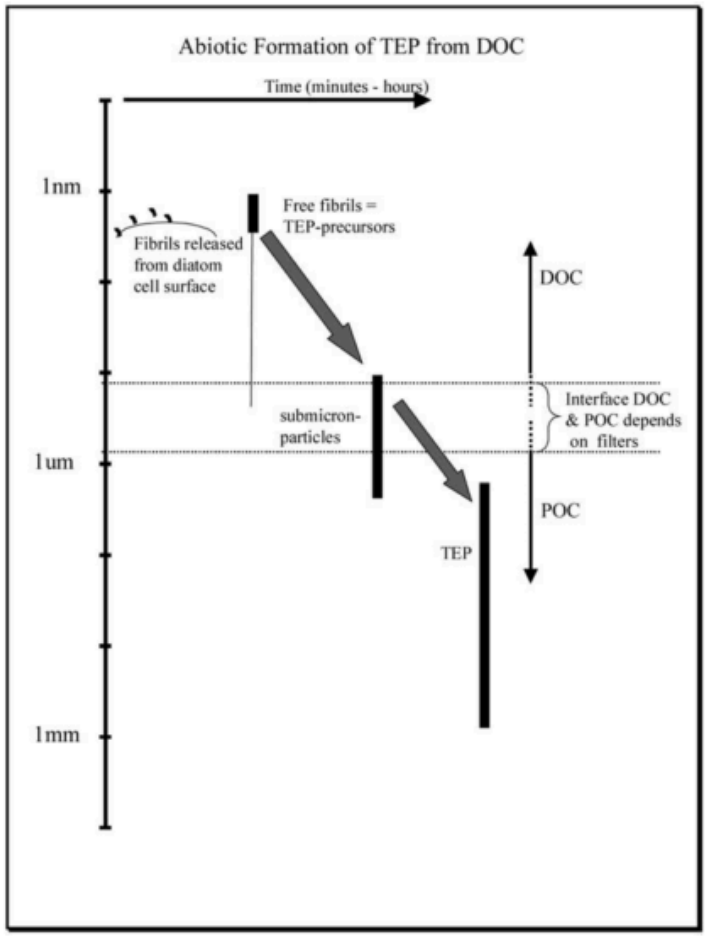

Figure 3.0 Illustration of the abiotic formation of TEP from DOC. TEP exists on a continuum of size ranges from colloidal to particulate. Fibrillar precursors are only a few nanometers wide, but are up to several hundred nm long. Upon gelation into submicron particles, TEP precursors then undergo annealing and aggregation to form TEP. (Image from Passow, 2002)

Recently, the role of bacteria in TEP formation has gained increased attention, as they have been shown to directly release large amounts of polysaccharides and TEP exopolymers (up to 25% of the respired carbon) (Stoderegger and Herndl, 1998). Bacteria have also been found to indirectly stimulate the release of TEP by phytoplankton, as bacteria are more efficient nutrient assimilators, causing the phytoplankton to become nutrient limited (Kirchman, 1994; Cotner and Biddanda, 2002; Guerrini et al., 1998). Finally, bacteria may

enhance the assembly of TEP precursors by increasing collision frequency through Brownian motion (Johnson and Kepkay, 1992).

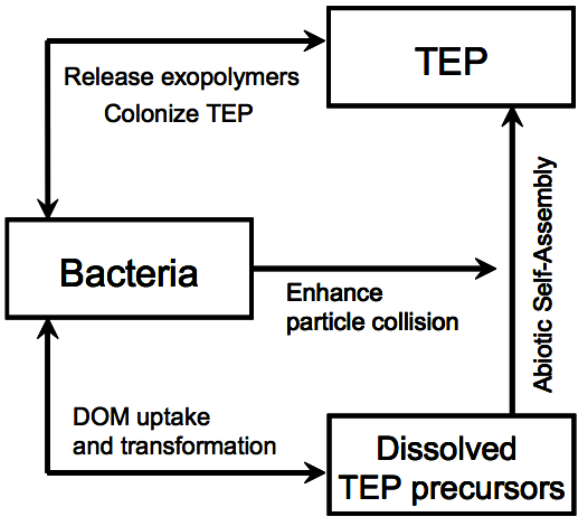

Figure 3.1 Hypothesized pathways relating bacteria and TEP in marine environments. (Image taken from Ortega-Retuerta, 2008)

Studies differ on whether formation is driven mainly from phytoplankton (Hong et al., 1997; Passow, 2002a; Passow and Alldredge, 1994) or bacterial activity (Ortega-Retuerta et al., 2010; Passow, 2002a; Stoderegger and Herndl, 1998, 1999). One difficulty in assessing the relative impact of phytoplankton vs. bacteria on TEP concentrations is the task of separating the two contributors. Attempts to relate plankton production based on chl-*a* abundance to TEP concentrations can be misleading, as plankton are still a source of TEP during cell lysis and senescence when chl-*a*. values are dropping (Passow, 2002b). Despite these uncertainties, it is clear that phytoplankton and bacteria both play large roles in TEP generation. Their relative contributions will likely be found to depend on culture taxonomy, location, temperature, nutrients, and a variety of environmental characteristics.

3.2.4 Reactivity of TEP

To date, only two studies have examined the effects of UV radiation on microgels (Orellana and Verdugo, 2003; Ortega-Retuerta et al., 2009). Ortega-Retuerta et al., (2009) experimentally determined the effects of visible and ultraviolet (UVB) radiation on the degradation and assembly of TEP. Results showed that UVB range light caused significant TEP photolysis, with loss rates from 27 to 34% per day. Interestingly, dissolved polysaccharides did not increase, indicating the TEP was transformed into a different compound (Ortega-Retuerta et al., 2009). Additionally, no TEP were formed under UVB, indicating UVB can block the assembly of DOM to form TEP (Orellana and Verdugo, 2003). This experiment confirmed that although TEP are transparent in the visible range, they exhibit significant absorption in the UV range (Ortega-Retuerta et al., 2009). Further experimentation regarding the products of TEP photolysis remains to be conducted.

3.3 Chromophoric Dissolved Organic Matter

Chromophoric dissolved organic matter (CDOM) (also referred to as gelbstoff or gilvin) is a ubiquitous component of DOM that is light absorbing. A recent review of CDOM Nelson and Siegel (2013) defined it as "material that passes through a submicron filter (usually 0.2-0.4 μ m) and absorbs light in the solar radiation bands as found at the Earth's surface (280-700 nm)." Studies of light absorption on open ocean samples during the US CO2/CLIVAR Repeat Hydrography show that CDOM is a substantial component of the marine environment, in part due to the fact that it is biologically refractory (Nelson and Siegal, 2013). CDOM is the most important factor controlling UV and visible light penetration into the open ocean, making it a critical factor in photobiology, microorganism productivity, and color-based remote sensing of the ocean (Siegel et al., 2002).

3.3.1 Sources CDOM

In coastal regions, sources of CDOM include river runoff, sewage, phytoplankton, zooplankton, bacteria, and sediments (Chen and Gardner, 2004). Sources of CDOM in the

open ocean are less known, and according to remote sensing and field studies, any terrestrial-origin CDOM is mostly removed in the coastal zone (Mannino et al., 2008). Currently, the consensus is that photoreaction of fatty acids, sugars, amino acids, phytoplankton exudates (Harvey et al., 1983), zooplankton feeding and defecation (Urban-Rich et al., 2006), and bacterial feeding of plankton detritus (Rochelle-Newall and Fisher, 2002), are all possible sources for CDOM in the remote ocean.

While direct production of CDOM by phytoplankton has been observed in certain species (Vernet and Whitehead, 1996), recent studies have also shown that microbial degradation of organic matter is responsible for the majority of CDOM production, as evidenced by the decoupling of CDOM and chl-*a* concentration (Nelson et al., 1998). Experiments using mesocosms (Rochelle-Newall et al., 1999; Ortega-Retuerta et al., 2009), microbial cultures (Nelson et al., 2004), and field data (Nelson et al., 1998) corroborate the hypothesis that the degradation of organic matter can lead to CDOM production. Recent work in estuaries shows a linkage between fluorescence properties of DOM and of POM (Osburn et al., 2012). In addition to the secondary biological mechanism, direct release of CDOM by zooplankton (Steinberg et al., 2004), dinoflagellates (Vernet and Whitehead 1996), and macroalgae (Shank et al., 2010) has been observed.

According to Nelson and Siegel (2013), the seasonal cycle of CDOM can be explained in three parts: 1) the formation of subsurface CDOM below the mixed layer during the summer through biological production, 2) the decrease of CDOM in the mixed layer during the summer and fall through photobleaching and 3) homogenization of CDOM during convective mixing in winter, which restarts the seasonal cycle. These three processes, heterotrophic production, photobleaching, and convective mixing, drive the seasonal patterns in surface CDOM. While subsurface ocean cycling of CDOM is on a centennial scale, surface ocean CDOM cycling is believed to be on the order of tens to 100s of days (Nelson et al., 1998, 2007; Siegel et al., 2002). Nelson et al. (2004) saw rapid CDOM decline in culture experiments, indicating that a fraction of CDOM is labile (rather than refractory) and has a short 10-day timescale turnover. Some of this semi-labile CDOM produced near the surface

is able to escape degradation and is transported downward by mixing or subduction (Nelson and Siegel, 2013).

3.3.2 Measurement and Characterization of CDOM

Spectroscopic analyses, including ultraviolet-visible absorption spectroscopy (UV-vis spec) and fluorescence spectroscopy are currently the two main techniques for analyzing the origin and composition of CDOM. Determination through UV-vis spectroscopy involves the characterization of the absorption coefficient as an index of CDOM abundance as well as the spectral slope parameter as it correlates to chemical composition parameters (Nelson and Siegel, 2013). Spectral slopes measured in the 300-700 nm range have been shown to correlate positively with CDOM bleaching and negatively with age (Nelson et al., 2007). Within the UVB range, spectral slopes have been found to be quantitatively linked to DOC abundance (Fichot and Benner, 2011) and molecular weight distribution (Helms et al., 2008). In terms of fluorescence spectroscopy, the main method used to characterize composition is excitation-emission matrix spectroscopy (Coble, 1996).

Attempts to characterize the composition of CDOM involving nuclear magnetic resonance (NMR) have been employed, but are poor at resolving between DOM and CDOM (Kujawinski et al, 2004, 2009; Repeta et al., 2004). Hernes and Benner (2003) found that terrestrial lignin phenols are present in oceanic CDOM in low concentrations. Near the coastal transition zone, terrestrial humic and fulvic acids are present in large quantities (Carder et al., 1989). Spectrofluorometric analysis has recently identified aromatic amino acids as a component of the CDOM pool in the surface ocean (Murphy et al., 2008; Yamashita and Tanoue, 2008; Jorgensen et al., 2011). Certain blooms of dinoflagellates have been shown to contribute large amounts of mycosporine-like amino acids, which are used as photoprotection against UV radiation (Nelson and Siegel, 2013). The remainder of CDOM is loosely classified as marine humic material.

3.3.3 Reactivity of CDOM

CDOM's spectroscopic absorption of light is unusual in that the UV-visible absorption spectrum declines smoothly with increasing wavelength and typically does not contain discrete absorption peaks (Nelson and Siegel, 2013). Furthermore, it has been shown that CDOM fractionation may result in fractional absorption spectra that cannot be recombined to reproduce the original spectrum (Goldstone et al., 2004; Nelson and Siegel, 2013).

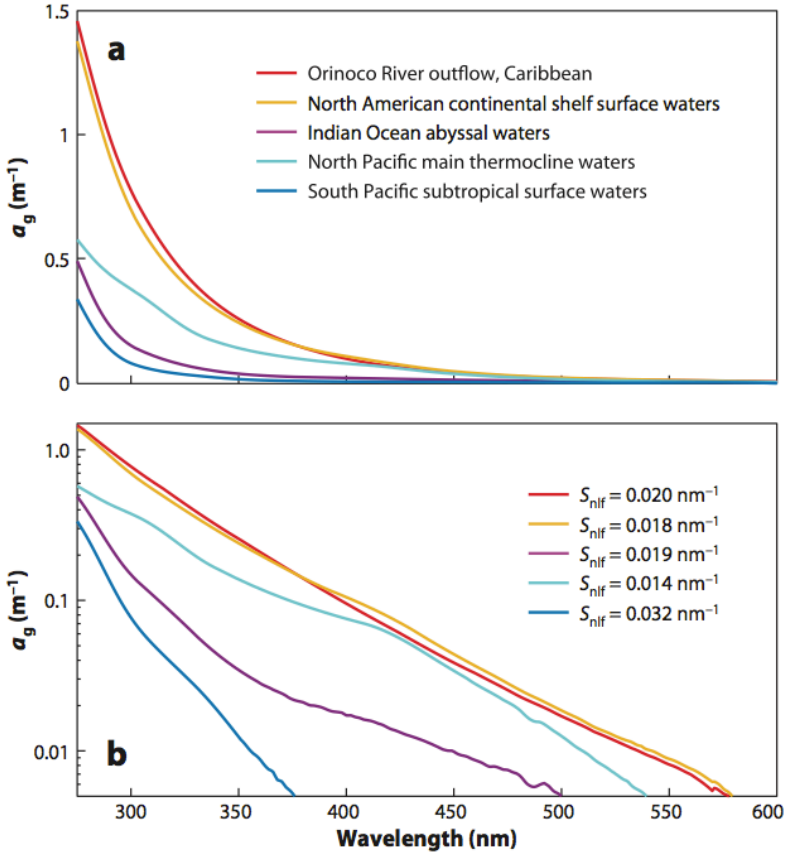

Figure 3.2 a) Absorption spectra (a_g) of CDOM from different environments. Clearly, the origin of CDOM plays a part in its absorption spectra. However, in all cases, it is most reactive in the near UV to UVA regions of the spectrum. b) Estimates of the exponential slope parameter for each location using nonlinear fitting (S_{nlf}) over the wavelength interval 320-400 nm. (Image taken from Nelson and Siegel, 2013)

The reaction of CDOM begins with the absorption of solar radiation, which leads to the formation of a singlet excited state species (DOM*) that then decays through a number of photochemical pathways (de Bruyn et al., 2011). One such pathway is the degradation of organic compounds into smaller molecules (Kieber et al., 1989; Mopper et al., 1991), which involves a loss in absorbance known as photobleaching (Skoog et al., 1996). A second process involves the sunlight-mediated transformation of organic compounds into humic-like substances, known as photohumification (Kieber et al., 1997). The third known process, photomineralization, leads to the formation of inorganic compounds such as carbon monoxide, dioxide, or dissolved inorganic carbon (Valentine and Zepp, 1993; Miller and Zepp, 1995). Each of these pathways alters the availability of CDOM as a bacterial substrate, with overall contribution of reaction pathways depending on a variety of intrinsic properties and chemical characteristics (Reche et al., 1998).

Results from laboratory studies by Mopper and Stahovec (1986) first indicated that low molecular weight carbonyl compounds (e.g., formaldehyde, acetaldehyde, acetone and glyoxal) could be produced by the photobleaching of biologically refractory organic matter. Filtered seawater was irradiated with intense UV light at 254 nm for several minutes, resulting in relatively high concentrations of carbonyl compounds (10-20 μM). While the wavelengths used were not environmentally relevant, the results suggested for the first time that the photochemical production of carbonyl compounds in seawater was feasible.

Following the work of Mopper and Stahovec, Kieber et al. (1990) and Mopper et al. (1991) both presented new rates of photochemical production of carbonyl compounds (i.e., formaldehyde, acetaldehyde, acetone, glyoxal, etc.) in a wide variety of natural waters. Mopper et al. collected seawater samples from the Sargasso Sea, Gulf Stream, Windward Passage, and Orinoco estuary and irradiated them for 4 hours with natural sunlight. The results corroborated the findings of Mopper and Stahovec, in that LMW compounds could be photochemically produced.

Similarly, Kieber et al. (1990) irradiated seawater samples for 50 hours using a 450-W medium pressure arc lamp and saw nearly identical action spectra for the production of all carbonyl compounds studied. No production was found above 320 nm, leading the authors to

believe that the range of wavelengths responsible for photoproduction was confined predominantly to the UV-B region (Kieber et al., 1990). Similar action spectra were obtained for photobleaching of absorbance as for photoproduction (Figure 3.3). The observed loss in absorbance was attributed to the photodegradation of the humic substances, implying a linear relationship between production rates and initial absorbance at 300nm.

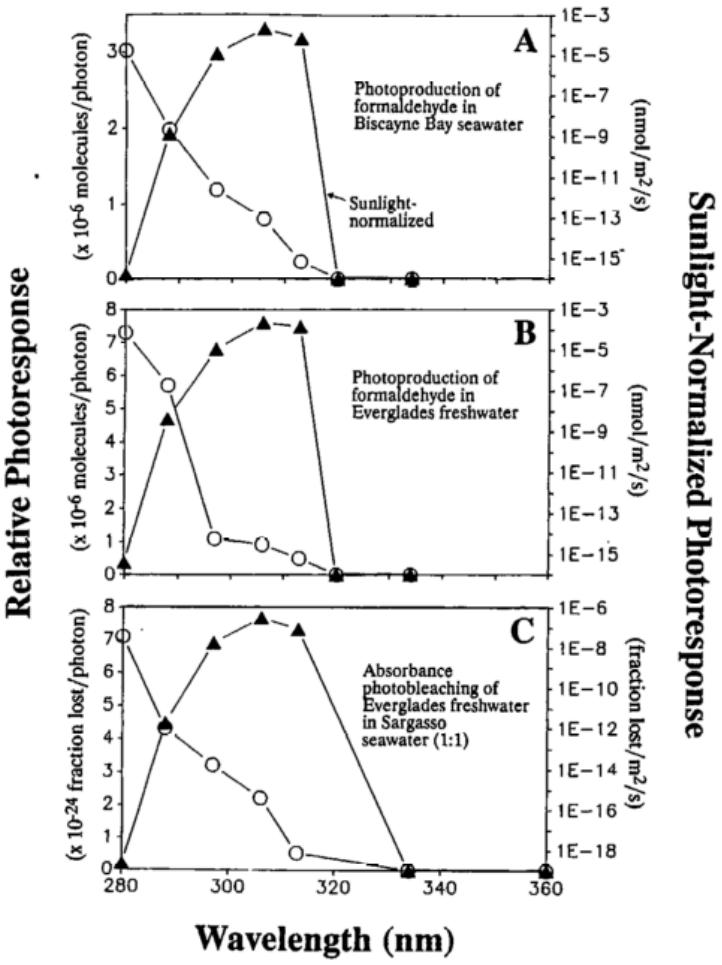

Figure 3.3 Action spectra (O) for photoproduction of HCHO (A and B) and photobleaching of absorbance (C), expressed as relative response per incident photo vs. irradiation wavelength. Action spectra (triangles) normalized to downward solar spectral irradiance incident at the sea surface. (Image taken from Kieber et al., 1990)

De Bruyn et al., (2011) reported production rates of acetone, acetaldehyde, and formaldehyde measured in coastal waters on the west coast of USA. Irradiation experiments were carried out with a 300 W ozone-free Xenon lamp. Over the course of three hours, production rates for formaldehyde increased, reaching a maximum of 240 nmol/L. For comparison, the authors repeated the experiment using a solar simulator to assess the importance of wavelengths below 300 nm. They discovered that quantum yields were higher in the solar simulator by a factor of 1.2 for formaldehyde, suggesting 20% of its production was from sub-300 nm wavelengths.

Steady-state photochemical experiments using molecular probes were also carried out in De Bruyn's experiment. Upon addition of oxygen and nitrate (a known OH radical producer) (Arnold et al, 2004), the production of formaldehyde increased by a factor of two, indicating that formaldehyde production proceeded predominantly via OH/O_2 pathway. This was again in contrast to Kieber's results, which showed no dependence upon oxygen and a production method driven by direct photolysis. It is worth noting that Kieber's light source included the more energetic light with wavelengths below 300nm, whereas De Bruyn's published results were from experiments with a light source that had a cutoff at 300nm, thereby possibly reducing the contribution of direct photolysis. More studies are needed to determine which pathway is the direct contributor to formaldehyde production.

3.4 Sea Surface Microlayer

The sea surface microlayer (SML) exists as the boundary between the atmosphere and ocean that covers roughly 70% of the Earth's surface (Wurl et al., 2011). Despite being only 1-1000 μm thick, the SML is a region of richly varying physicochemical properties and biological productivity, distinct from the bulk waters below it (Cunliffe et al., 2012). Additionally, the air-sea interfacial solution has high concentrations of trace metals, microorganisms, and dissolved and particulate organic matter, including carbohydrates, proteins, and lipids (Sieburth et al., 1976; Williams et al., 1986; Calace et al., 2007; Gasparovic et al., 2007). Several macroscopic properties of the ocean are impacted by the presence of the SML, such as wave damping, microwave backscatter, gas transfer, and

bubble mediated aerosol formation (Cosovic, 2005). The unique position and ubiquity of the SML at the air-sea interface makes it an important intermediate between the hydrosphere and atmosphere in terms of biogeochemical and climate related processes (Cunliffe et al., 2012). Despite having been studied for almost a century, an appreciation of the SML's role in such global-scale cycles is only recently emerging (Cunliffe et al., 2011).

3.4.1 Physical Structure of the SML

Early descriptions of the surface microlayer visualized it as a distinct entity with a stratified structure, comprised of an upper lipid layer containing highly surface-active molecules (such as fatty acids, long-chain alcohols, and lipids) overlying a protein-polysaccharide layer extending into the subsurface waters (Cunliffe et al., 2011). This was known as the "wet-dry" stratified model of the SML (Hardy, 1982; Hermansson, 1990; Norkrans, 1980). Since then, the view of the microlayer has been drastically revised. A newer model proposed by Sieburth (1983) highlighted the unstratified, and disorganized nature of the SML, describing it as a "highly hydrated loose gel of tangled macromolecules and colloids", produced from dissolved organic matter.

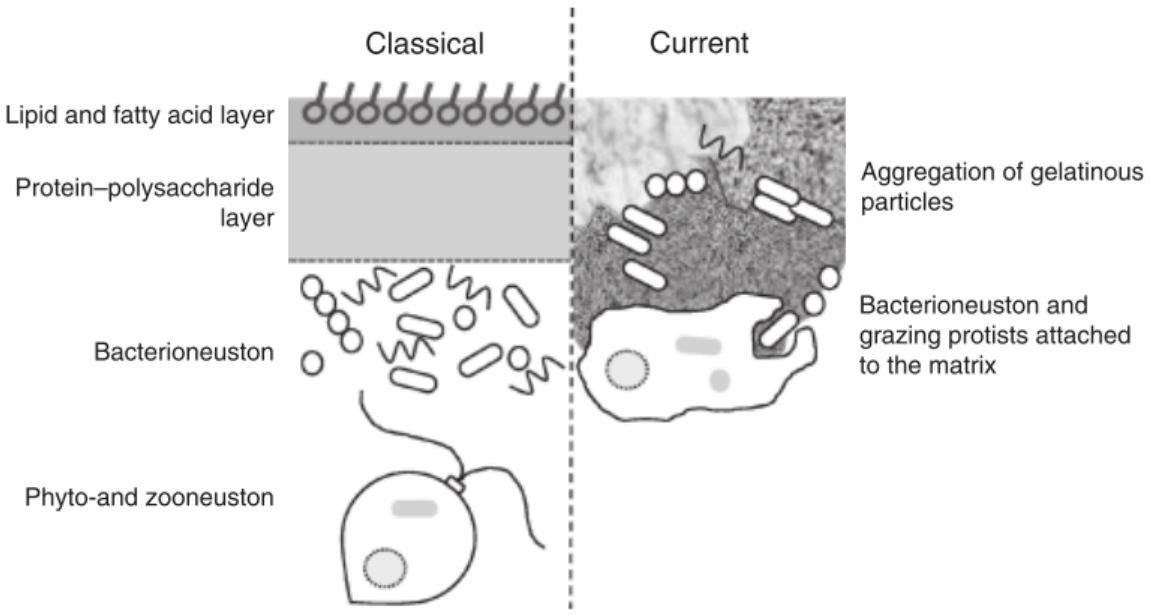

Figure 3.4 Classical and revised model of the structure of the sea surface microlayer. The classical model features a distinct, two layer entity consisting of an upper hydrophobic lipid layer and a lower hydrophilic protein-polysaccharide layer. Bacterioneuston and plankton exists below the surface. The current model exhibits a gelatinous film with a heterologous matrix enriched with TEP and various forms of organic matter. (Image taken from Cunliffe et al., 2011)

Research in the past 30 years has since verified Sieburth's hypothesis. Studies show that carbohydrates and polysaccharides are an important component of the SML (Cunliffe et al., 2009; Wurl et al., 2011). Indeed, Wurl and Holmes (2008) identified a high concentration of transparent exopolymer particles (TEP) collected from seawater samples gathered around Singapore. Similarly, TEP were also found to be concentrated in SML samples collected from open leads within the Arctic pack ice (Gao et al., 2012). Azetuso-Scott and Passow (2004) showed the importance of TEP in microlayer formation by demonstrating that ascending TEP are able to aggregate with latex spheres that mimicked solid particles.

The molecular properties of the SML allow surface-active chemical species to be adsorbed at the air-water interface (Cosovic, 2005). As a result, a general characteristic of microlayers is that many of their various components occur at higher concentrations than in the water below (Cunliffe et al., 2011, 2012). A number of studies have quantified so-called

enrichment factors, defined as the concentration of a specific constituent in the microlayer divided by its concentration in subsurface water (Cunliffe et al., 2011). Most results imply that surface-active substances, (i.e., total dissolved carbohydrates, CDOM, DOM, and TEP) are significantly enriched by factors of up to 3 at winds speeds below 9.6 m/s (Williams et al., 1986; Wurl and Holmes, 2008; Wurl et al., 2009). In fact, Zhou and Mopper (1997) showed that exposing seawater surface samples to sunlight resulted in higher yields of carbonyl compounds than the bulk seawater samples by a factor of 1.1-25, suggesting the enrichment of such surface-active compounds.

Whereas enrichment has been shown to occur over a range of globally average wind speeds, lingering questions remain about whether biologically active or oligotrophic waters are most beneficial for enrichment. Surface enrichments in the SML have been found to be slightly higher in oligotrophic waters than in eutrophic (EF=2.8 vs EF=1.8) waters (Wurl et al., 2011). While the mechanism behind preferential SML enrichment of oligotrophic waters over eutrophic coastal regions is not fully understood, early indications point to the larger role of bacteria in the open ocean as one possible reason (Wurl et al., 2011).

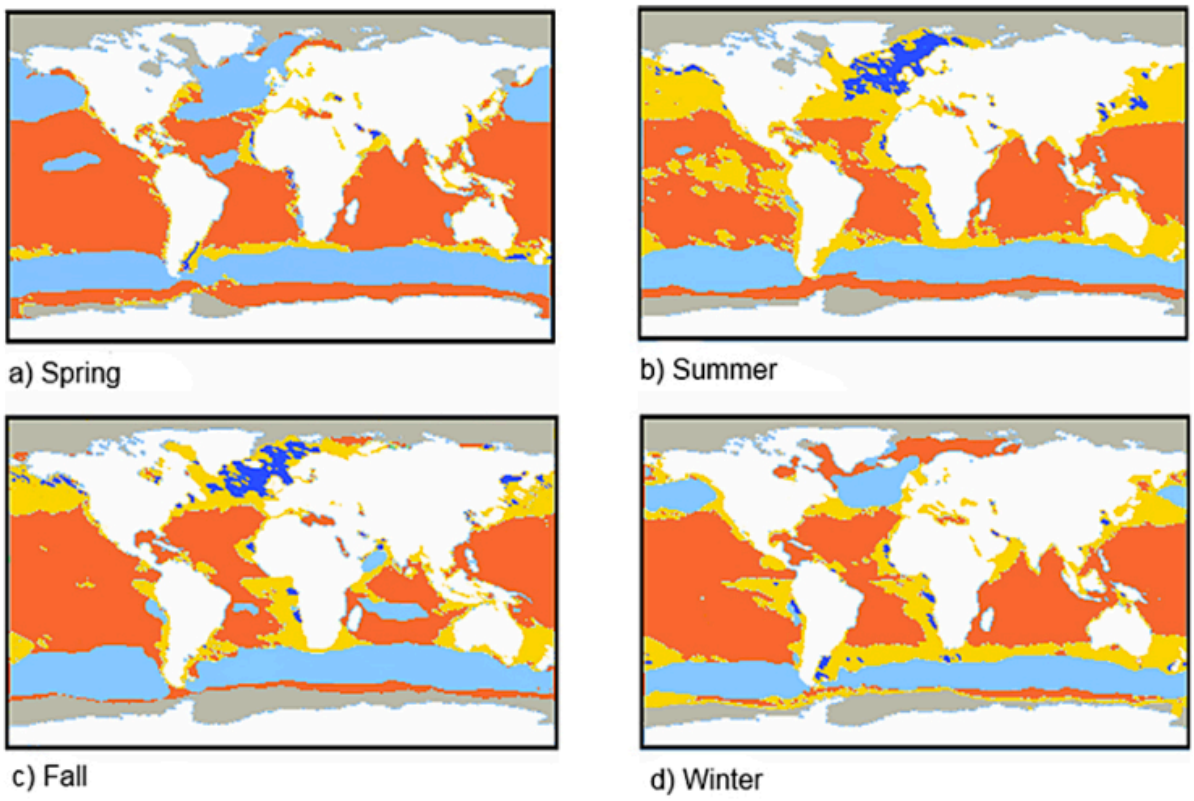

Figure 3.5 Global maps of mean concentrations of surfactants in the SML and their enrichment factors for a) spring b) summer c) fall and d) winter. Note that although open areas are more enriched, their overall concentration of organic matter is lower than in coastal regions. Red: 320 =- 66 µg Teq L^{-1}, EF > 2; yellow: 502 +- 107 µg Teq L^{-1}, 2 > EF > 1.5; dark blue: 663 +- 77 µg Teq L^{-1}, 1.5 > EF > 1.0; light blue: no enrichment. (Image taken from Wurl et al., 2011)

3.4.2 Ecology

The physicochemical properties of the SML make it a unique habitat in that it is both an ideal and at times harsh ecosystem for various microbial organisms (Cunliffe et al., 2011). On one hand, the accumulation of organic and inorganic matter at the SML makes it a favorable environment for microbial growth (Cosovic, 2005). On the other hand, organisms in the SML are exposed to high levels of toxic substances, sunlight intensity, and UV-B radiation (Cosovic, 2005).

Naumann first described any organism present within the surface microlayer as part of the neuston (Naumann, 1917). Analyses show that phyto-, zoo-, and bacterioneuston all have distinct species compositions in the microlayer compared with the bulk water below (Cunliffe et al., 2012; Franklin et al., 2005; Cunliffe et al., 2009). Bacterioneuston communities are formed from recruitment of bulk water organisms (Agogue et al., 2005) and are more aggregated than in subsurface water (Cunliffe and Murrell, 2010). Phytoneuston have been shown to be enriched in the SML (Hardy and Apts, 1984; Joux et al., 2006) and also have different structures from those in bulk water. Studies of both phytoneuston and bacterioneuston show that microorganisms within the SML are likely associated with buoyant microgels such as TEP. In addition to bacteria and plankton, Joux et al. (2006) also showed that virus-like particles are enriched in the SML.

The trophic interactions in aquatic environments are exemplified by a complex microbial loop in which protists prey on bacterial and archaeal cells, and are in turn preyed upon by larger organisms (e.g., copepods) (Cunliffe et al., 2011). This microbial food web in the SML has a strong impact on biogeochemical processes (Cunliffe et al., 2011). Surface microlayer samples collected from the Atlantic Ocean and Mediterranean Sea have indicated higher rates of bacterial respiration than subsurface water (Reinthaler et al., 2008). Azam (1998) showed that the degradation of POM to DOM was driven by enhanced microbial extracellular enzyme activity in microlayers. The conclusion is that not only are POM and microgels enriched and formed in the SML, but they are also broken down by microbial activity (Cunliffe et al., 2012). Cunliffe et al. (2012) cites the need for future studies to examine the microbial POM and DOM cycling in the SML.

3.4.3 Stability of the SML

The presence of organic films and surface tension are thought to contribute to the physical stability of the SML. Wurl et al. (2009, 2011) demonstrated that the SML exists above the global average wind speed of 6.6 m/s, and can persist up to speeds of 10 m/s (Carlson, 1983; Reinthaler et al., 2008). Upon the disruption of the SML by breaking waves, dissolved and particulate material is scavenged by rising bubble plumes (Wurl et al., 2011),

aiding in further gel aggregation at the surface. This bubble scavenging is believed to be a key process in the cycling of surface-active material in the upper ocean (Cunliffe et al., 2012).

Relatively few studies have been conducted to assess the time required for reformation of the SML. However, current published data indicate that reformation is a rapid process, usually occurring in less than one minute (Cunliffe et al., 2012). Van-Vleet and Williams (1983) removed SML samples in a laboratory tank using a slider and studied its subsequent reformation. Based on their observations, the authors estimated that recovery occurred in less than 20 seconds. Kuznetsova and Lee (2001) also observed rapid re-establishment of the SML based on enzyme activity measurements after vigorously mixing subsurface coastal waters and leaving them to settle.

3.4.4 Gas Exchange with the Marine Boundary Layer

The aquatic environment can act as both a source and a sink for trace gases, including carbon dioxide, carbon monoxide, methane, nitrous oxide, halocarbons, and various sulfur-containing gases (Cunliffe et al, 2011). Exchange with the atmosphere is influenced by both the physicochemical and microbiological nature of the SML (Cunliffe et al., 2011). In terms of physicochemistry, surface films act to reduce gas transfer velocities at the air-sea interface through the dampening of capillary waves (Broecker et al., 1978; Goldman et al., 1988). Increasing concentrations of soluble and insoluble surfactants have been shown to decrease the gas transfer velocity, with the soluble surfactants being more effective over a wider range of wind speeds (Salter et al., 2011). Laboratory experiments with natural plankton exudates have resulted in a suppression of the transfer velocity ranging from 5-50% (Frew et al., 1990; Goldman et al., 1988) with values of 60-90% for synthetic soluble surfactants (Frew, 2005). While lab studies effectively demonstrate the role of synthetic and natural surfactants on gas exchange, in situ quantification of the suppression of gas transfer velocity by natural surfactants remains a challenge (Cunliffe et al., 2012). At the very least, observations of phytoplankton blooms suggests that the amount and nature of the stabilizing compounds

depend on the biomass, primary production of the plankton, its taxonomic state, and the degradation and dispersion of surfactants (Cosovic, 2005).

There have only been limited studies that investigated the microbial impact on air-sea gas exchange. Calleja et al., (2005) showed that the difference in atmospheric and oceanic CO_2 partial pressures was dependent upon the microbial metabolism at the surface layer. Net autotrophic metabolism created a CO_2 demand and subsequent uptake at some locations, while net heterotrophy led to CO_2 supersaturation and subsequent emission in other locations (Calleja et al., 2005). The role of bacterioneuston in air-sea gas exchange has been studied in-situ through the use of free-floating gas exchange boxes (Conrad and Seiler, 1988) and in laboratory settings (Upstill-Goddard et al., 2003). The accepted conclusion from these studies is that bacterioneuston are involved in the cycling of some climatically active trace gases and potentially act as both a source and a sink.

Our review on the organic matter present within oceanic waters is highlighted by several key facts: 1) organic matter exists within a continuum ranging from dissolved to particulate, with gel-like substances bridging the gap between the size classes. 2) Classification of organic matter can be determined by size (TEP) or by reactivity (CDOM). 3) CDOM has been shown to produce formaldehyde upon photooxidation. While TEP has also been shown to undergo photolysis, the resulting products of such transformations are unknown. 4) CDOM and TEP in the open ocean are currently thought to be mainly generated through biotic processes involving phytoplankton and bacteria. 5) The sea-surface microlayer is a ubiquitous boundary between the ocean and atmosphere, and contains high concentrations of organic matter, including CDOM and TEP. While all of these facts naturally point to the presence of a formaldehyde source in the SML, its solubility in water seems to preclude the possibility of the ocean acting as a source for atmospheric formaldehyde. The question remains if oceanic formaldehyde precursors can partition into the atmosphere, thereby acting as a source of tropospheric HCHO.

3.5 Marine Organic Aerosol Fluxes and Production Mechanisms

Sea spray aerosol (SSA) consists of an in-air suspension of particles that are directly produced at the sea surface (de Leeuw et al., 2011). Such aerosols consist of a mixture of sea-salt, sulfates, and organics (de Leeuw, 2011). The radii of SSA can vary from roughly 10 nm to several millimeters, with residence times ranging from seconds to minutes (de Leeuw et al., 2011). In regions removed from anthropogenic or other continental sources, SSA dominates the mass concentration of marine aerosols (de Leeuw, 2011).

Sea-salt is thought to be the major component of SSA over regions where wind speeds are high (O'Dowd et al., 1997). Global emissions estimates of sea salt based upon chemical transport models, climate models, and various parameterizations of sea spray source functions range between 2000-10000 Tg/yr for particles less than 20 μm in size (de Leeuw et al., 2011). A large portion of this variation is due to the differences in wind speeds used in calculations.

While it has been known for quite some time that organic substances can be incorporated in the submicron fraction of SSA (Blanchard, 1964), only recently have studies been conducted to quantify and better characterize the link between size and chemical composition of such aerosols (de Leeuw et al., 2011).

Depending on their formation mechanism, marine organic aerosols can be divided into one of two classes: primary and secondary. Primary marine organic aerosols are formed at the sea surface by breaking waves, through bubble bursting, and by tearing of wave crests (de Leeuw et al., 2011). Upon the breaking of a wave, air becomes entrained into the water column and is then dispersed into a burst of bubbles. The bubbles then rise to the surface, scavenging organic material along the way. As a bubble sits at the surface of the ocean, water is filtered off of it, leaving a thin film of organic material. When the bubble bursts, this organic film disintegrates into film droplets, which are ejected at a wide distribution of angles into the atmosphere (de Leeuw et al., 2011). Each bubble can produce up to 1000 film droplets, depending on the size of the bubble. After bursting of the bubble, a vertical cylindrical jet forms in the middle of the cavity left by the bubble. This jet drop may break up into smaller jet drops, which are subsequently ejected into the atmosphere as well. In addition

to the bursting of bubbles, spume droplets can be formed by the tearing of wave crests when wind speeds exceed 10 m/s (Monahan et al., 1983).

Secondary organic aerosols are formed upon the oxidation of volatile organic compounds. Examples of SOA precursors include dimethyl sulfide (DMS), aliphatic amines, isoprene, and monoterpenes (Bates et al., 1992; Bonsang et al., 1992; Yassaa et al., 2008; Gantt and Meskhidze, 2012). The production mechanism for secondary organic aerosols can proceed through one of two ways: 1) The nucleation of stable clusters around 0.5-1nm in size, which then grow to larger sizes via condensation processes and 2) heterogenous reactions and aqueous phase oxidation of dissolved gases in existing aerosol particles (O'Dowd, 2007). This remainder of this section focuses upon the characteristics of primary marine organic aerosols.

3.5.1 Primary Marine Organic Aerosols Characteristics

Aerosol Mass Concentrations

A large amount of research has been carried out with the purpose of defining the organic aerosol concentration in the remote marine regions. The earliest studies date back to the 1960s, when Blachard (1964) utilized the surface-active nature of organics to separate them from sea-salt. Following on Blachard's work, Barger and Garrett (1970) collected sea spray aerosol from the Hawaiian coast on glass fiber filters and determined the concentration of chloroform extractable organic material to be between 0.6 and 5.7 μ g/m^3. Hoffman and Duce (1974) used the hot persulfate-induced organic material oxidation method to measure organic aerosol concentration in Bermuda, with results ranging from 0.15 to 0.47 μ g/m^3. Studies since then have been in general agreement with Hoffman and Duce's values, indicating an average marine organic aerosol concentration around 0.5 ±0.4 μ g C/m^3 (Gantt et al., 2013).

Recent studies have also shown that the contribution of organic matter in marine aerosols can be quite large under certain scenarios. Measurements of organic aerosol concentrations in the marine boundary layer of the north Atlantic Ocean showed

concentrations up to 3.8 μ g/m^3 during high biological activity ([chl-*a*] >1.0 mg m^{-3})(Ovadnevaite et al., 2011). Additional long-term measurements at Mace Head Ireland and Amsterdam Island in the South Indian Ocean found that organic aerosol concentrations followed a strong seasonal cycle, with highest levels occurring during biologically active seasons (Yoon et al., 2007; Sciare et al., 2009).

In the past several years, knowledge of the contribution of organic species to SSA has extended into particle sizes smaller than previously expected (de Leeuw et al., 2011). Despite their overall low bulk concentration, organic aerosols have been found to make up a large fraction of the mass concentration in accumulation mode sized aerosols. Barker and Zeitlin (1972) and Hoffman and Duce (1977) first showed that as aerosol diameter size decreases, the fraction of the sea spray aerosol that is composed of organics increases. Subsequent studies worked to further elucidate the role of organics in the composition of marine aerosols. Oppo et al. (1999) quantified the volume of an organic film surrounding a marine aerosol in relation to the total aerosol volume as a means of developing a spray drop absorption model.

Recent reports have reinforced the belief that organics play an important part in the composition of submicron sized sea spray aerosols. A series of field experiments conducted at Mace Head, Ireland showed that the organic mass fraction of accumulation mode aerosol particles over the North Atlantic Ocean increases with biological productivity (up to 60% during summer) and decreases during periods of low biological productivity (<20% during winter)(O'Dowd et al., 2004). Rinaldi et al., (2010) and Miyazaki et al. (2010) showed further proof that marine organics become larger contributors to aerosol mass as size decreases and biological productivity increases.

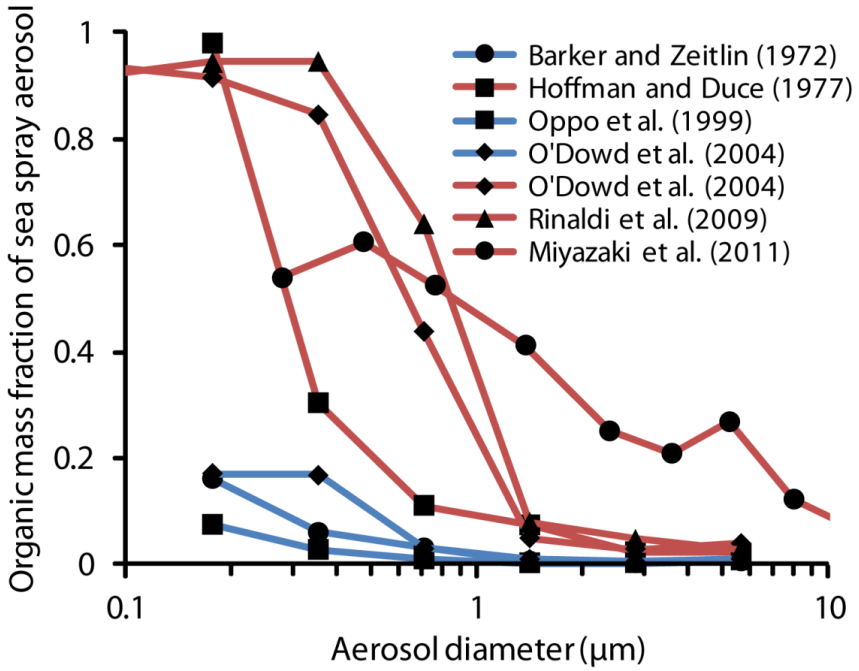

Figure 3.6 Size-resolved organic mass fraction of sea spray aerosol measured in remote marine regions. Blue lines: low biological activity; Red lines: high biological activity. (Image taken from Gantt et al., 2013)

Laboratory experiments have presented a range of values for the size resolved organic mass fraction of sea spray aerosols. The variety of conditions that can be altered in each experiment (salinity, water temperature, bubble production mechanism, surfactants, etc.) makes direct comparison of such studies difficult. Chamber studies were conducted by Keene et al. (2007) and Fachini et al. (2008) in an attempt to determine the size-resolved mass fraction of organic material in SSA particles. Using natural seawater from an oligotrophic region, Keene et al. reported that particles with 0.06 μm diameters had organic mass fractions of up to 80%, decreasing to 40-50% for particles with diameters near 0.6 μm (Keene et al., 2007). Similar to Keene's results, Facchini et al. found a strong dependence of the organic mass fraction and enrichment factor on particle size. While SSA particles greater than 0.5 μm in size contained mainly inorganic sea salt mass (~90%), particles with radii

less than 0.25 μm consisted predominantly of organic matter (~77%), of which a large fraction was water-insoluble (94% ± 4% of total carbon).

Not all laboratory studies agree with such large organic fractions in the submicron size range. Modini et al. (2010) used a volatility hygroscopicity tandem differential mobility analyzer to show that the organic volume fraction of aerosols produced from bubble bursting of seawater was 8% ±6% for aerosols with diameters between 71 and 77nm. Such a value corresponds to an organic mass fraction of less than 40%. Other laboratory studies have reported similar organic mass fractions of <40% (Sellegri et al., 2008; Fuentes et al., 2010, 2011). The various bubbling methods and water compositions likely have large effects on the bubbles produced, and thus the resulting aerosols. For this reason, further studies are needed in order to better determine to size dependence on the organic aerosol mass fraction.

Composition

It should be no surprise that aerosols consist of the very organic matter that is enriched in the SML. Field studies by Bigg and Leck (2001, 2008) using transmission electron microscopy indicated that marine aerosol particles smaller than 0.1 μm mainly consist of organic matter. Similarly, aerosol particles in the Arctic marine boundary layer with dry radii less than 0.025 μm were found to be composed of organic matter, while slightly larger particles (>0.05 μm) consisted of fragments of diatoms and bacteria. In 2002, Leck et al. sampled the microlayer of open water between ice floes in the Arctic and again reported the presence of organic matter in aerosols smaller than 0.025 μm. Subsequent studies have shown that aerosol particles between 50-200 nm are composed of fragmented aggregates, microcolloids, and exopolymer secretions, all major components of the SML.

CHAPTER 4

Experimental Method Development and Results

4.1 GC/MS Theory of Operation

Gas chromatography/Mass Spectrometry (GC/MS) is an invaluable instrument for the identification and quantitation of organic compounds. Through the pairing of two individual analytical techniques, GC/MS achieves precise separation of compounds followed by accurate identification of eluents. As mass spectrometry requires gas-phase analytes, it is ideally equipped to sample volatile compounds. While a range of GC/MS analysis techniques exist, we focus now on a brief overview of the system used in our lab.

4.1.1 Gas Chromatograph

The key components of a gas chromatograph are the gas supply and flow controllers, injection port, analyte detector, oven, column, and data system. The basic principle of operation for GC is straightforward. Analysis begins with the injection of a liquid or vapor sample through a heated inlet. After volatilization, the molecules of the sample are moved by a carrier gas (mobile phase) through the column (stationary phase) at different speeds, depending on their interactions with the stationary phase. Elution rate is contingent upon a variety of parameters including column choice, compound structure, column temperature, and flow rate (Rood, 2007). As the compounds exit the column, they are passed through a detector, which quantifies the amount of substance based upon an electrical signal. Numerous

GC detectors exist, including thermal conductivity, flame ionization, nitrogen-phosphorus, and flame photometric (Sparkman, 2011). We use a mass spectrometer, which allows advanced detection of samples (see section 4.1.2).

When developing a GC method, there are two desired effects that should be considered: 1) adequate separation of compounds and 2) concentration of each compound into a small, narrow band as it exits the column. As mentioned before, the nature of a compound's elution depends upon an assortment of parameters. One such choice is the type of column used in analysis (Rood, 2007).

The most commonly employed column in GC/MS research is the capillary column. Capillary columns are composed of a fused silica tube with an outer protective polyimide coating and an inner stationary phase, and can have inner diameters as small as 50 μm (Rood, 2007). The three types of stationary phases for capillary columns are polysiloxanes, arlyene-modified polysiloxanes, and polyethelyne glycols (Rood, 2007). Polysiloxane phases are characterized by their alternating silicone and oxygen linear backbone and contain two functional groups attached to each silicone (Rood, 2007). The type and amount of functional groups determine the stationary phase properties. The four most common groups include methyl, cyanopropyl, trifluoropropyl and phenyl.

Each type of stationary phase has its own advantages and drawbacks based upon its interactions with the compound of interest. The two most important column interactions involve phase selectivity and column polarity, as they both determine the degree of separation of compounds (Rood, 2007). Using a column and solvent that have similar polarity is crucial to analysis, as immiscibility between the two causes column overloading and irregular compound elution. Following the suggestion by Ho (2004), we chose a 5% phenylmethylpolysiloxane column, which features slightly higher polarity due to the phenyl content, allowing for the analysis of semi-polar compounds. The column has an inner diameter of .25 mm, a general-purpose size for GC/MS analysis. Finally, the 0.25 μm film thickness allows for excellent retention of active compounds, leading to high resolution during MS analysis.

Two other method parameters that have an effect on the separation of compounds are the choice of carrier gas, and the temperature ramp method. Common carrier gases used in GC analysis are nitrogen, helium and hydrogen, with helium being the most common for capillary columns (Rood, 2007). It is important that the gas be pure and free of any contaminants, as any impurities will be detected by the mass spectrometer, causing interference during analysis. When setting the temperature ramping method, it is helpful to set the beginning temperature slightly below the boiling point of the solvent (~10° C). Doing so ensures the condensation of the solvent at the head of the column. If the analyte has a boiling point higher than the solvent, it will remain dissolved in the condensed solvent. As the temperature continues to increase, the solvent gradually evaporates. Once all the solvent has evaporated, the compound of interest is finally volatilized and passes through the column in a focused, narrow band. Keeping in mind that higher temperatures cause compounds to elute faster, one must decide on a temperature ramp method that gives both good separation of compounds, and elutes each compound in a timely fashion.

A final consideration in method development is the injector type and injection method used. Of the available injector types, vaporization injectors are the most common, and include split, splitless, and direct (Rood, 2007). Briefly, a split injector splits the sample into two unequal portions by use of an additional purge line. The two parameters that can be altered are the temperature of the injector and the split ratio. The temperature should be hot enough to ensure instant vaporization of the entire sample, but not so hot as to cause degradation of thermally unstable compounds (Rood, 2007). Additionally, if the chosen solvent undergoes massive expansion upon rapid volatilization, large solvent fronts, peak tailing, and carryover problems can occur. Conversely, an injection temperature that is too low may cause incomplete or slow vaporization of the sample, resulting in broad or tailing peaks, especially for semi-volatile compounds (Rood, 2007).

The split ratio is the volume of carrier gas entering the column versus the volume leaving via the split line (Rood, 2007). Selection of a split ratio is determined by the amount of sample that needs to be introduced to the column. Low split ratios introduce a greater amount of sample onto the column, and vice versa. For large sample injections, a large split

flow is preferable, as this reduces the chance of column overloading. If the sample concentration is very small, low split ratios are recommended. Additional effects caused by the split ratio include the amount of time the sample has in the injection port and the discrimination of the injector. When put together, all of the previously mentioned considerations must be balanced to create a robust method for compound detection. Tailoring the method to produce the accurate and precise results requires a strong knowledge of both the theory of GC/MS, and the chemical characteristics of the compound. Table 4.0 gives a description of our resulting method.

4.1.2 Mass Spectrometer

After elution from the GC, the gas compound enters the mass spectrometer where it is immediately ionized. Depending on the energy of the ionization source, the ions can undergo further fragmentation into ions with smaller mass (Sparkman, 2011). A number of ionization techniques exist, including electron capture negative ionization (ECNI), field ionization (FI), and atmospheric pressure chemical ionization (APCI) (Sparkman, 2011). The two most common methods are electron ionization and chemical ionization. The latter of these two methods is sometimes called 'soft ionization' in that it is not as energetic, and therefore does not produce fragmentation of the compound, but rather produces a single positively charged molecular ion (Sparkman, 2011). The amount of fragmentation that occurs is key, as the resulting spectrum provides insight into the structure of the compound of interest.

After ionization, the compound is then accelerated into a mass/charge (m/z) analyzer, which separates the ions based upon their mass to charge ratio. The three main types of m/z analyzers include quadrupole mass filter (QMF), quadrupole ion trap (QIT), and time-of-flight (TOF). Our lab's mass spectrometer is equipped with a QIT, which consists of three hyperbolic stainless steel electrodes. These electrodes form a cavity in which the ions are held for a fixed period of time, called the 'ion-time.' The ion-time is determined by an algorithm called the automatic gain control (AGC), which is based upon the concentration of analyte present (Sparkman, 2011). The ions are stored in stable, 3D concentric orbitals using an RF voltage emitted from the ring electrode (Sparkman, 2011). As the amplitude of the RF

voltage on the ring electrode is increased, certain ion trajectories become destabilized and are ejected towards the two end caps. Emitted ions then enter a high-energy dynode where they are accelerated into an electron multiplier for detection.

The data resulting from this process are known as "mass spectra." The mass spectra x and y axes represent the m/z value of an ion and its abundance at a given time step, respectively. Using a chromatogram, one can plot the amount of analyte as a function of time; this display is constructed from consecutively recorded mass spectra, and is called the total ion current chromatogram (Sparkman, 2011). Through analysis of the chromatogram, an accurate qualitative and quantitative assessment of the compound can be attained.

4.2 History of Formaldehyde Detection Techniques

The detection of trace concentrations of formaldehyde is complicated by the reactivity and ubiquity of the compound. Early attempts to directly quantify HCHO involved spectroscopic and colorimetric methods. These techniques required extremely specific experiment parameters, long reaction times, and had poor detection limits. As detection technology became more advanced, the use of indirect detection by GC/MS and high performance liquid chromatography (HPLC) became the standard approach to HCHO quantitation. A brief overview of these methods is now presented.

Early gas chromatograph and ion chromatography (IC) methods involved the direct analysis of formaldehyde samples. Techniques typically included the use of an adsorbent for collection (e.g., charcoal), a solvent for extraction, and gas chromatography-flame ionization (FID) or photo-ionization for detection (Chien and Yin, 2009). Kim et al. (1980) used charcoal impregnated with an oxidizing agent to collect formaldehyde. After oxidization of formaldehyde to formate, it was desorbed using a hydrogen peroxide solvent and analyzed by IC using an anion separator column. Kamens and Jefferies (1978) injected 2 ml air samples on a porapak Q precolumn. While lighter hydrocarbons passed through the column, formaldehyde was retained and directed to a porapak Q analytical column. After conversion to methane, original formaldehyde content was detected by FID.

As HPLC and GC/MS technology advanced, so too did the methods for detection of low molecular weight aldehydes. In recent years, derivatization techniques have offered a much faster and more reliable method than previous direct measurement schemes. Since its inception, more than 1500 articles have reported the use of derivatization in analysis of carbonyls (Vogel et al., 2002). Advantages of this technique include greater stabilization of aldehydes, enhanced sensitivity due to specification of aldehydes, and a reduction of background interferences (Man, 2005).

A reliable method for the detection of formaldehyde became available through the use of derivatization with 2,4-dinitrophenylhydrazone (DNPH) followed by HPLC analysis. The derivatization reaction of aldehydes with DNPH involved a two-step nucleophilic addition. Upon formation of the derivatized hydrazine, analysis was achieved through detection of UV absorption after separation by HPLC (Man, 2005). Early methods of DNPH analysis involved the use of an impinger that contained solution used to collect air samples (Kuntz et al., 1980). Since then, a cartridge approach has been adopted in which DNPH coated solid sorbents trap aldehydes, allowing subsequent analysis by reverse phase HPLC with UV detection at 340 nm (Beasley et al, 1980).

Ho and Yu (2002) first demonstrated the feasibility of a new approach for the detection of formaldehyde using derivatization by 0-(2,3,4,5,6-pentafluorobenzyl)-hydroxylamine (PFBHA), resulting in a derivative that was thermostable and could therefore be used with thermal desorption and GC/MS analysis. This method showed several advantages over the traditional DNPH HPLC approach. First, the use of GC provided better separation for derivatives of carbonyl compounds similar to formaldehyde. Second, the detection limits were much better. Third, the tandem use of the MS allowed identification of unknown compounds, thereby reducing a large amount of uncertainty caused by aldehyde interference.

However, PFBHA did have its drawbacks. At flow rates above 20 ml/min, sampling efficiency dropped rapidly (Ho and Yu, 2004). While this could be remedied by increasing the amount of PFBHA on the sorbent, it proved impractical due to the fact that the excess PFBHA reagent eluted between the derivatives of formaldehyde and other carbonyls on a GC

column of nonpolar stationary phase (Ho and Yu, 2004). As a result, increased reagent amounts saturated the mass spectrometer detector and caused a loss in peak resolution.

In 2004, Ho and Yu (2004) developed an augmented approach to formaldehyde detection method that involved the collection of carbonyls onto 2,3,4,5,6-pentafluorophenyl hydrazine (PFPH) coated solid sorbent followed by thermal desorption and GC/MS analysis. The reaction scheme of PFPH with aldehydes is shown in figure 4.0. In comparison with both PFBHA and DNPH methods with HPLC, the detection limits of PFPH were lower, detected more compounds, and had better peak separation (Ho and Yu, 2004). Since then, most work in formaldehyde detection has been to improve upon this method (Man, 2005). Briefly, calibration of the method involved preparation of a PFPH-hexane solution in which a specific amount of liquid formaldehyde was injected and left to react. A glass sampling tube packed with Tenax TA adsorbant was then spiked with 2 μl of the PFPH-hexane-formaldehyde solution and analyzed via GC/MS after extraction via thermal desorption.

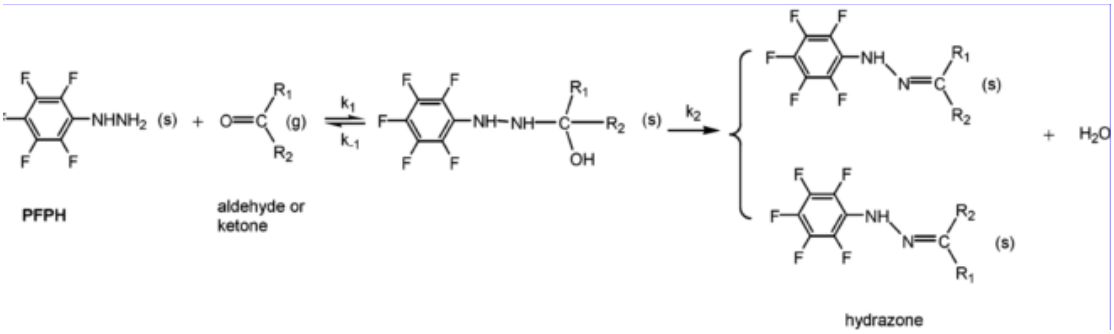

Figure 4.0 Derivatization reaction of gaseous carbonyls with PFPH (s, surface; g, gaseous state). (Image taken from Ho and Yu, 2004)

4.3 Experimental Setup

The goal of this experiment was to create a reliable method for the detection of trace concentrations of formaldehyde that was compatible with the equipment in our lab.

Furthermore, the method needed to be compatible with our marine aerosol generation/aging apparatus to test the validity of the hypothesis that primary marine organic aerosols can photolyze into formaldehyde (see Chapter 5). Our detection method followed the general outline presented by Ho and Yu (2004), but was customized in several key ways to address our purposes.

4.3.1 Sampling Tube Preparation

Sampling tubes were constructed from 5" Pyrex glass desorption tubes (CDS Analytical, PA) packed with 200 mg of 60/80 Tenax TA. Each sampling tube was soaked in PFPH (Sigma Aldrich, MO). Following Ho and Yu (2004), 510 nmol of PFPH was used for every 50 mg of Tenax, resulting in a total of 2040 nmol. The PFPH solution was prepared by weighing 4.0 milligrams of PFPH and dissolving it in 5 ml of 97% hexane (Sigma Aldrich, MO).

The tube was then placed in a 10 ml graduated cylinder and soaked with 500 μl of the PFPH-hexane solution for three minutes. The tube was then transferred to the conditioning stand of a Model 10 Single Tube Conditioner (CDS Analytical, PA) with the Tenax side of the tube facing inwards. A heating sleeve set to 60 C° was placed over the tube to aid in the drying of excess solvent, while high purity nitrogen gas was passed through the desorption tube at a flow rate of 50 ml/min. After three minutes, the heating sleeve was removed and the tube was further dried with nitrogen for three more minutes.

4.3.2 Preparation and Analysis of Vapor Calibration Standards

A stock solution of 2% formaldehyde were prepared by diluting 37% formaldehyde (Sigma Aldrich, MO) in Acetonitrile. From this stock solution, 10 ml standard solutions at concentrations of 25, 50, 75, 100 nmol/μl were made. The choice of dilution solvent for the formaldehyde solutions presented a challenge. Following Ho and Yu (2004), hexane was used in early attempts. However, as hexane is immiscible with formalin, homogenous solutions were not attainable. This led to a lack of precision in our calibration, as the amount

of sampled formaldehyde varied considerably between runs. In an attempt to create a homogenously mixed solution, we next tried methanol. The greater polarity of methanol allowed the complete dissolution of formalin into the solution. However, the relative non-polarity of the stationary phase of our GC column led to poor peak shapes as methanol was eluted irregularly.

Upon the realization that hexane and methanol would not work as dilution solvents, we began a more extensive search for a viable solvent. Before beginning the search, we decided on several important characteristics that the solvent would need to exhibit. First, the solvent would need a boiling point below 100° C, so that it would vaporize at a temperature that ensured the thermal stability of formaldehyde. Furthermore, with a boiling point lower than that of formaldehyde (and its PFPH-derivative) we could employ a solvent effect, thereby creating a sharper GC/MS peak. Next, the solvent needed to thoroughly and evenly dissolve formalin. As stated earlier, this meant the solvent needed to be relatively polar. However, as shown with methanol, a highly polar solvent was useful in dissolving formalin but led to peak irregularities upon interaction with the less polar GC column. Therefore, we opted to use only solvents that had a relative polarity (WRT water) that was between 0.2 and 0.5. Finally, we wanted to use a solvent that would not expand greatly upon volatilization, thereby avoiding column overload and backflash. This was achieved by looking for solvents that had an overall larger molecular weight. Table 4.0 shows the results of our investigation.

Table 4.0: Characteristics of various organic solvents. Green indicates a trait that is favorable, orange means borderline, and red means unfavorable.

Solvent	Formula	MW (g)	Boiling Point	Relative Polarity	Solubility in Water g/100g
t-butyl alcohol	$C_4H_{10}O$	74.12	82.2	0.389	M
acetonitrile	C_2H_3N	41.05	81.6	0.46	M
2-propanol	C_3H_8O	60.1	82.4	0.546	M
heptane	C_7H_{16}	100.2	98	0.012	0.0003
di-n-butylphthalate	$C_{16}H_{22}O_4$	273.34	340	0.272	0.0011
pentane	C_5H_{12}	72.5	36.1	0.009	0.0014
hexane	C_6H_{14}	86.18	69	0.009	0.0039
cyclohexane	C_6H_{12}	84.16	80.7	0.006	0.005

Table 4.0 Continued

p-xylene	C_8H_{10}	106.17	138.3	0.074	0.02
toluene	C_7H_8	92.14	110.6	0.099	0.05
chlorobenzene	C_6H_5Cl	112.56	132	0.188	0.05
ethyl benzoate	$C_9H_{10}O_2$	150.17	213	0.228	0.07
carbon tetrachloride	CCl_4	153.82	76.7	0.052	0.08
1-octanol	$C_8H_{18}O$	130.23	194.4	0.537	0.096
anisole	C_7H_8O	108.14	153.7	0.198	0.1
N,N-dimethylaniline	$C_8H_{11}N$	121.18	194.2	0.179	0.14
1-heptanol	$C_7H_{16}O$	116.2	176.4	0.549	0.17
benzene	C_6H_6	78.11	80.1	0.111	0.18
carbon disulfide	CS_2	76.139	46.3	0.065	0.2
benzonitrile	C_7H_5N	103.12	205	0.333	0.2
dimethylphthalate	$C_{10}H_{10}O_4$	194.18	283.8	0.309	0.43
1,1-dichloroethane	$C_2H_4Cl_2$	98.96	57.3	0.269	0.5
1-hexanol	$C_6H_{14}O$	102.17	158	0.559	0.59
chloroform	$CHCl_3$	119.38	61.2	0.259	0.8
2-butanone	C_4H_8O	72.11	79.6	0.327	0.87
methylene chloride	CH_2Cl_2	84.93	39.8	0.309	1.32
1-pentanol	$C_5H_{12}O$	88.15	138	0.568	2.2
cyclohexanone	$C_6H_{10}O$	98.15	155.6	0.281	2.3
ethyl acetoacetate	$C_6H_{10}O_3$	130.14	180.4	0.577	2.9
3-pentanone	$C_5H_{12}O$	86.13	101.7	0.265	3.4
aniline	C_6H_7N	93.13	184.4	0.42	3.4
benzyl alcohol	C_7H_8O	108.14	205.4	0.608	3.5
cyclohexanol	$C_6H_{12}O$	100.16	161.1	0.509	4.2
2-pentanone	$C_5H_{10}O$	86.13	102.3	0.321	4.3
2-pentanol	$C_5H_{12}O$	88.15	119	0.488	4.5
methyl t-butyl ether (MTBE)	$C_5H_{12}O$	88.15	55.2	0.124	4.8
3-pentanol	$C_5H_{12}O$	88.15	115.3	0.463	5.1
1-butanol	$C_4H_{10}O$	74.12	117.6	0.586	7.7
ethyl acetate	$C_4H_8O_2$	88.11	77	0.228	8.7
acetyl acetone	$C_5H_8O_2$	100.12	140.4	0.571	16
2-butanol	$C_4H_{10}O$	74.12	99.5	0.506	18.1
methyl acetate	$C_3H_6O_2$	74.08	56.9	0.253	24.4
1,2-dichloroethane	$C_2H_4Cl_2$	106.12	83.5	0.327	25.6
tetrahydrofuran(THF)	C_4H_8O	72.12	66	0.207	30
diethylamine	$C_4H_{11}N$	73.14	56.3	0.145	M

Table 4.0 Continued

dioxane	$C_4H_8O_2$	88.11	101.1	0.164	M
dimethoxyethane (glyme)	$C_4H_{10}O_2$	90.12	85	0.231	M
diglyme	$C_6H_{14}O_3$	134.17	162	0.244	M
pyridine	C_5H_5N	7910	115.5	0.302	M
acetone (Not good for column)	C_3H_6O	57.08	56.2	0.355	M
dimethylformamide (DMF)	C_3H_7NO	3.09	153	0.386	M
dimethylsulfoxide (DMSO)	C_2H_6OS	78.13	189	0.444	M
1-propanol	C_3H_8O	60.1	97	0.617	M
acetic acid	$C_2H_4O_2$	60.05	118	0.648	M
2-aminoethanol	C_2H_7NO	61.08	170.9	0.651	M
ethanol	C_2H_6O	46.07	78.5	0.654	M
diethylene glycol	$C_4H_{10}O_3$	106.12	245	0.713	M
methanol	CH_4O	32.04	64.6	0.762	M
ethylene glycol	$C_2H_6O_2$	62.07	197	0.79	M
glycerin	$C_3H_8O_3$	92.09	290	0.812	M
water, heavy	D_2O	18	101.3	0.991	M
water	H_2O	18	100	1	M

Table 4.0 shows that acetonitrile fit within our constraints. With a molecular weight of 41 g, it expands to a lesser degree than methanol. While having a large degree of solubility with water (a large component of formalin), it was also only moderately polar. Finally, with a boiling point of 80 degrees, we were able to easily volatilize it without risking the stability of formaldehyde.

Previous experiments with the PFPH method used liquid standards for calibration (Ho and Yu, 2004). As our experiment will involve the detection of gaseous formaldehyde, the use of vapor standards is preferred. While the preparation of standard concentrations of nonreactive gases and vapors is relatively straightforward, it is considerably more difficult for formaldehyde (Ho, 1985). Experimentation to determine the best method for vapor standard preparation proved to be time consuming. Initially, we attempted direct injection of

a pre-derivatized solution of HCHO-PFPH-hexane onto a heated desorption tube with a purging flow rate of nitrogen gas at 50 ml/min. Incomplete volatilization and inefficient trapping of the solution rendered this method unsatisfactory. A second method involved the injection of the HCHO-hexane solution into a 1L Teflon bag that was gently heated to aid in volatilization. Using a vacuum pump, the air within the bag was sampled through the PFPH-soaked desorption tube. Due to diffusion through the bag as well as absorption and condensational wall losses, this method also yielded poor precision. A viable vapor preparation method was finally attained with the use of a 250 ml glass-sampling bulb, as described below.

The PFPH soaked desorption tube was placed in-line with a 250 ml glass sampling bulb. A 1 μl sample of formaldehyde-acetonitrile solution was injected through a septa on the top of the glass-sampling bulb. At room temperatures, formaldehyde polymerizes into a white powder known as paraformaldehyde. Above temperatures of 120° C, it decomposes into methanol and carbon monoxide. To ensure volatilization of formaldehyde, but not decomposition, the sampling bulb was placed inside of a water bath regulated by a Kitchen Kettle Steamer (Presto). Doing so allowed the solution to volatilize at a stable 90° C. A continuous flow of nitrogen at 50 ml/min was passed through the bulb, which carried the evaporated sample onto the PFPH soaked desorption tube. After 7 minutes of sampling, the desorption tube was inserted into the thermal desorption attachment of a CDS-8000 sample concentrator unit (CDS Analytical, PA). Figure 4.1 shows the vapor standard generation setup.

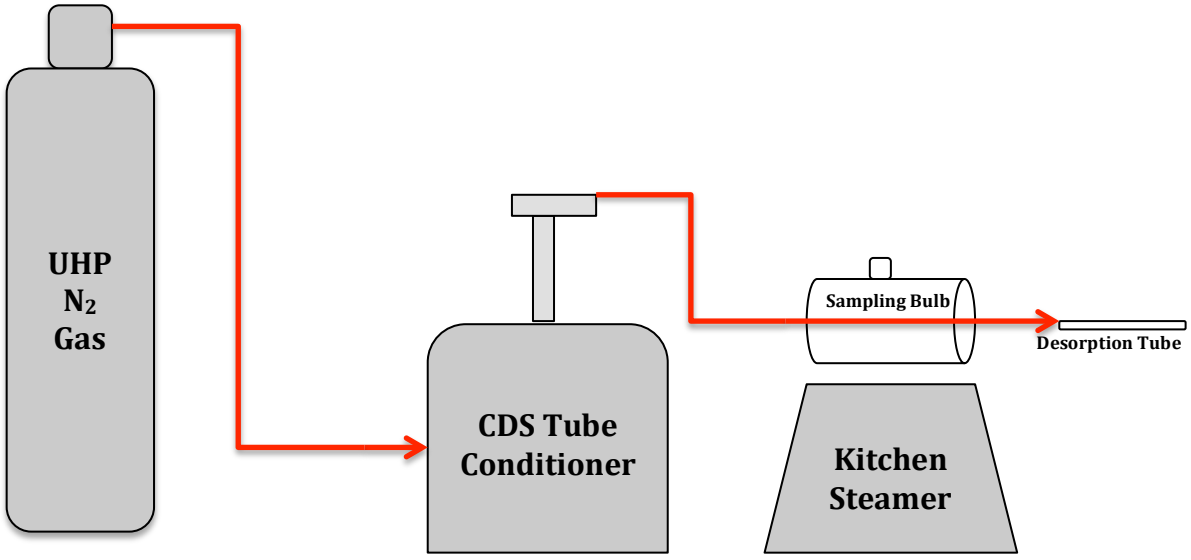

Figure 4.1 Experimental setup of the HCHO vapor standard preparation technique.

Table 4.0 shows the instrument parameters for the CDS 8000 and the 450 GC/220 MS. The vessel rest temperature of the CDS unit was initially held at 55° C. When sampling began, the purge temperature of the vessel ramped to 275° C and was held for 15 minutes to allow complete desorption of all compounds from the desorption tube. After extraction of the sample from the desorption tube, eluted compounds were trapped on a Vocarb 3000 (K Trap) within the CDS-8000. The desorb preheat of the Vocarb trap was set to 250° C to focus the sample, and was then ramped up and held at a final temperature of 275° C for ten minutes. Helium gas carried the desorbed sample to a Varian 45-GC/220-MS through a transfer valve line held at 250° C.

Table 4.1 Analytical Method Parameters for the Detection of Formaldehyde

CDS 8000 Concentration Unit	
Vessel Rest	55° C
Vessel Purge	15 min hold at 275° C
Desorb Preheat	250° C

Table 4.1 Continued

Trap Desorb	10 min hold at 275° C
Trap Bake	10 min hold at 290° C
Valve Oven	275° C
GC Transfer Line	250° C
450 GC	
Injector Temperature	250° C
Split Ratio	Initial Off 0.75-30.75 min 20:1 30.75 min off
Column Type	VF-5ms 30x0.25 mm ID 0.25 μm DF
Column Pressure	8 PSI
Column Oven	4 min hold at 50° C 7° C/min to 100° C 8° C/min to 250° C 2 min hold at 250 C
220 MS	
Acquisition Method	0-13.00 min: DELAY 13-31.89 min: Full Scan (50-350 m/z)

Upon transfer to the GC/MS, the sample was sent through an injection port set at 250° C. The first 0.75 minutes of the analyses was splitless. At 0.75 minutes, the split ratio was set to 20:1, and was reset to splitless at the end of the sample analysis. The column used for separation of compounds was a VF-5ms with a 30x0.25 mm inner diameter and a film thickness of 0.25 μm. The column head pressure was set to 8.0 PSI for the entire analysis. The temperature program began with a four minute hold at 50° C, followed by an increase to 100° C at 7.0° C/min, and a final ramp to 250° C at 8.0° C/min where the temperature was then held for two minutes. A solvent delay time of 12.75 minute was used to allow elution of the PFPH reagent before the mass spec detector was turned on. Analysis was carried out in full scan mode from 50-350 m/z. Figure 4.2 shows the CDS thermal desorbing unit and GC/MS analysis systems.

Figure 4.2 After collection and derivatization on a 5" Tenax-packed desorption tube, the sample is desorbed using a CDS 8000 Preconcentrator and then analyzed with a 450 GC/220 MS.

4.3.3 Instrument Calibration

A four-point calibration curve was constructed using external standard quantitation. This was done by injecting a 1 μ l volume of the calibration standard (liquid acetonitrile-formaldehyde solution) in triplicate at four different concentrations into the glass-sampling bulb and completing the analysis process. Ion-abundances were measured for quantitative ions (210, 155, 182, 210, 211) and a curve was generated using a simple least squares regression model. As previously mentioned, using acetonitrile as a solvent for formaldehyde samples caused interference. To remedy this problem, repeated runs of acetonitrile 'solvent blanks' were analyzed. The average area of the resulting solvent blanks was then subtracted from each formaldehyde-spiked standard run:

$$Y_{HCHO} = Y_{total} - Yavg_{acetonitrile}$$

Y_{total} is the total peak area caused by the calibration standard injection, $Yavg_{acetonitrile}$ is the average peak area of injections with only acetonitrile (with PFPH interference already subtracted), and Y_{HCHO} is then the corrected peak area for an injection caused only by formaldehyde. The relative standard deviation ($\%RSD_{conc.}$) for triplicate injections at each concentration level was then calculated to test the precision of the method:

$$\%RSD_{conc.} = \frac{S}{Yavg_{HCHOconc.}} * 100$$

S is the standard deviation of the peak areas at a certain concentration level, $Yavg_{HCHOconc,}$ is the average peak area caused by formaldehyde (Y_{HCHO}) of all replicate injections at one concentration level. After identification of the target analyte's peak area, the response factor (RF) of the instrument was calculated by dividing the corrected peak area caused by HCHO at a given concentration ($Y_{HCHOconc}$) by the concentration of HCHO (X_{HCHO}; nmol/250 ml):

$$Response\ Factor\ (RF) = \frac{Y_{HCHOconc}}{X_{HCHO}}$$

The mean of the response factors for each injection over all concentrations (RF_{avg}) was then used to calculate the percent relative standard deviation of the response factor ($RF\%RSD$):

$$RF\%RSD = \frac{S_{RF}}{RF_{avg}} * 100$$

where S_{RF} is the standard deviation of the response factors.

Examination of results to determine the statistical significance and robustness of the linear fit were carried out by analysis of variance (ANOVA). The F-test was calculated by taking the ratio of the explained variance to the unexplained variance of the least squares regression, and assessed the significance of the relationship between the dependent variable and the set of independent variables. The P-value was calculated to determine the probability that the observed data occurred as a result of the null hypothesis (i.e., that there was no relationship between the dependent and independent variables). Verification of the linearity of the analytical method was achieved by calculating the coefficient of determination (R^2):

$$R^2 = 1 - \frac{SS_{err}}{SS_{tot}}$$

in which SS_{err} is the sum of squares of residuals (i.e., unexplained variance) and is calculated using the estimated peak area as modeled by the linear fit (Y_{calc}):

$$SS_{err} = \sum (Y_{HCHO} - Y_{calc})^2$$

SS_{tot} is the total sum of squares, defined as:

$$SS_{err} = \sum (Y_{HCHO} - Yavg_{HCHO})^2$$

where $Yavg_{HCHO}$ is the average peak area caused by HCHO over all concentration levels. The coefficient of determination ranges from 0 to 1, and is the proportion of variation in the data explained by the regression model. A value of 0 indicates a complete lack of fit, and 1 indicates a perfect fit. Further assessment of the calibration curve was performed by calculating the percent difference between any one injection's resulting peak area caused by formaldehyde and the expected peak area given by the linear regression:

$$\%\ Difference = \frac{Y_{HCHO} - Y_{calc}}{Y_{calc}} * 100$$

Finally, the minimum detection limit (in nmol/250 ml) was calculated by taking the sum of the y-intercept of the regression fit (b) plus 3 times the standard deviation (σ_{pfph}) of the PFPH blank sample runs:

$$Y_{MDL} = b + 3\sigma_{pfph}$$

This value was used to calculate the concentration from the origin-forced regression equation. We then converted this into a mixing ratio in PPBV by assuming a sampled air volume of 24 liters (i.e., 4-h of sampling at 0.1 l/min). While our calibration ran at 50 ml/min, further runs showed no discernable difference between collection efficiency at 100 ml/min.

4.4 Results and Discussion

4.4.1 GC/MS Characteristics of the PFPH-HCHO Derivative

The HCHO hydrazine eluted at 13.24 minutes. Since PFPH can derivatize a variety of carbonyls, additional peaks representing these compounds were also visible after the HCHO elution. An example electron ionization mass spectrum of the PFPH-HCHO derivative is given in figure 4.3. A number of ion fragments are present as a result of the moiety C_6F_5NH caused by the derivatizing agent (Ho and Yu, 2004). The base peak ion fragment (also the molecular ion) was 210 m/z and the three most abundant ion fragments used for quantitation were 155, 182, and 211 m/z.

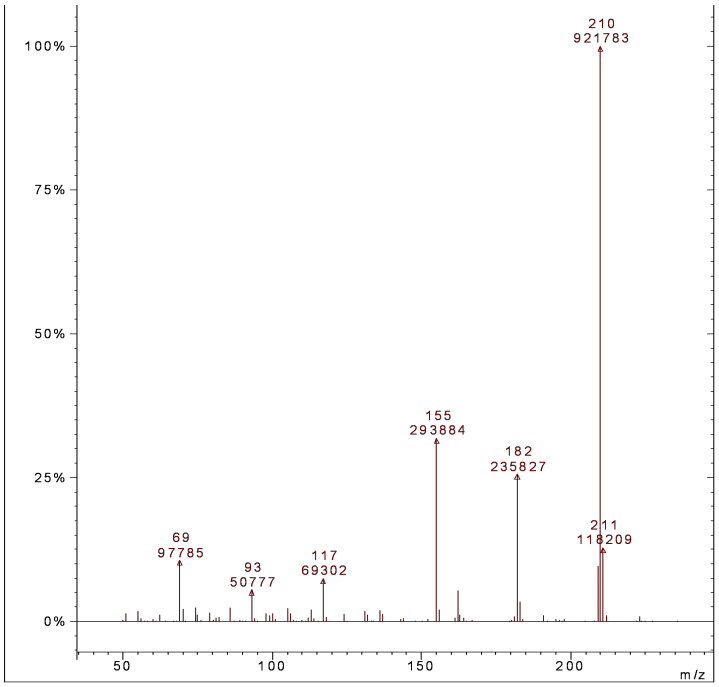

Figure 4.3 Typical ionization spectrum of the derivatized formaldehyde sample. The 210 m/z ion represents the molecular ion of the HCHO-PFPH derivative, with ions 69,155,182, 210, and 211 acting as quantitation ions.

4.4.2 Calibration Curve

Table 4.2 Precision and accuracy of calibration at various concentrations (nmol/250 ml).

Concentration Level (nmol/250 ml)	$\%RSD_{conc}$	Avg. %Difference from Y_{calc}
6.25	1.40%	4.14%
12.5	4.85%	8.72%
25.0	6.82%	12.9%
50.0	2.17%	3.68%
Total Avg.	3.78%	7.37%

Calculated calibration statistics showing the analytical precision and accuracy of our method are given in table 4.1. The average $\%RSD_{conc}$ for the replicate injections at each concentration level (~4%) indicates an acceptable level of method precision. The % difference at each concentration level is indicative of the random error caused by background interference. Our overall average % difference of ~7% shows the accuracy of the method. Finally, the average relative standard deviation of the instrument's response factor (RF%RSD) to the formaldehyde injections over all concentrations was 17.74%, below the accepted limit of 26% that is required to assume linearity of the calibration method. The constructed calibration curve is shown in figure 4.4, with an additional trend line that is forced through the origin.

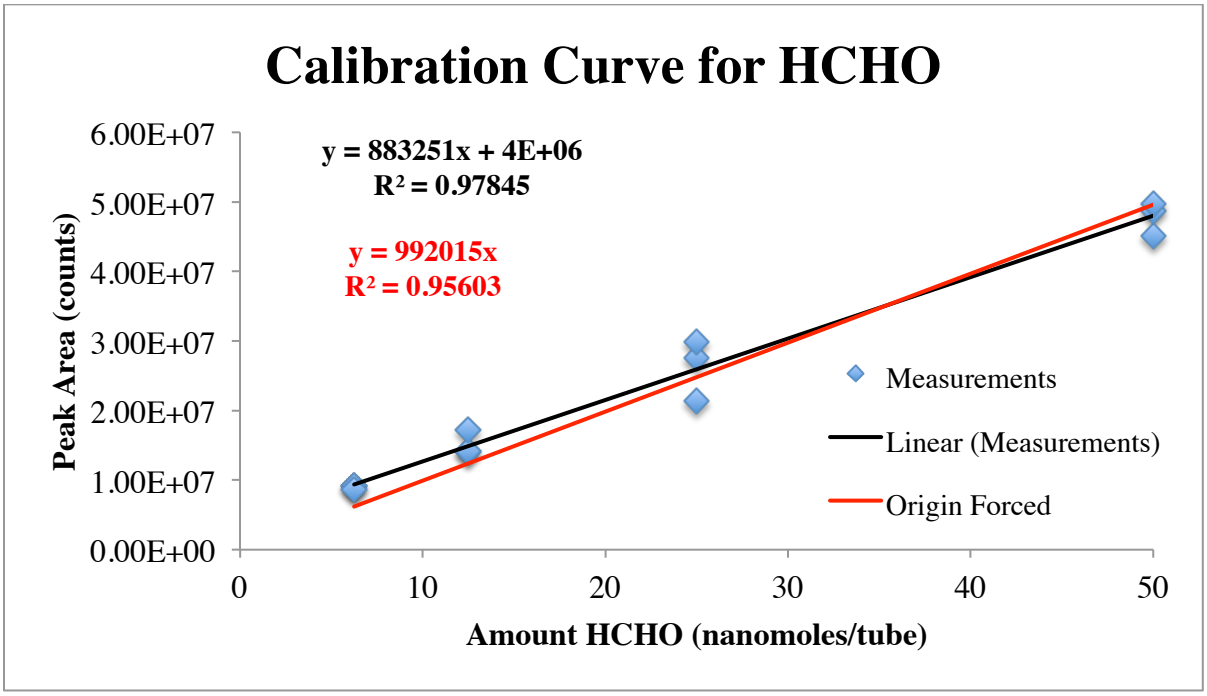

Figure 4.4 Calibration curve for 6.25-50 nm of HCHO using 1.0 µl injections. The black trendline follows a simple least squares fit. The red line indicates a forced-origin linear fit.

Regression statistics are shown in table 4.2. The coefficient of determination for the least squares fit was R^2=0.978. This indicates that the regression accurately represents the data. Table 4.2 gives the results from the ANOVA calculation. The result from the F-test indicates that a large fraction of the variance can be explained using the least squares regression. The p-level shows that there is a low probability that the observed relationship between the dependent and independent variables was completely by chance.

Table 4.3 Regression statistics for the least squares fit of the data.

Regression Statistics	
MDL (nmol/250 ml)	4.92
MDL (ppbv)[a]	5.01
R^2	0.978
Standard Error	2.40×10^5
F-test	454
p-level	1.10×10^{-9}
Response (y) = $3.85 \times 10^6 + 8.83 \times 10^5$ * Concentration (x)	

[a]Assuming a sampled air volume of 24 L (i.e., 4 hour sampling at 0.1 L/min).

4.4.3 Minimum Detection Limit

The minimum detection limit of our method is determined by the size and uncertainty of the signal produced by the hexane-PFPH solution in blank samples. While time did not permit for extensive experimentation of the desorption tube preparation method, simple tests in which tubes were soaked in smaller amounts of the hexane-PFPH solution resulted in a decrease in blank signal size. Ho (2004), cites the use of 100 microliters aliquots of hexane-PFPH solution when preparing the desorption tubes. Decreasing the amount of hexane-PFPH solution from 500 microliters to 100 µl in our method would likely allow for a lower MDL. The MDL of 0.26 ppbv (assuming a sampled air volume of 24 L at 0.1 L/min) cited in Ho (2004) is ~20 times lower than our method. However, it is possible that this is due to the calibration method used in Ho (2004), in which PFPH-hexane solutions were spiked with

liquid samples of formaldehyde and then left to react before injecting 2 microliters of the resulting hexane-PFPH-HCHO solution onto the desorption tube. It is unclear if the blank signal size used to calculate the MDL in Ho (2004) was taken from the calibration blank (2 µl of hexane-PFPH solution) or the sample blanks (100 µl of hexane-PFPH solution). Since the size of the blank signal is related to the amount of hexane-PFPH solution used, it would make sense that if a calibration were performed using the former method, it would produce a lower MDL than the latter method. Regardless, it is imperative that future attempts to lower the MDL of our method by decreasing the amount of hexane-PFPH solution be consistent with the preparation methods used in test samples.

Aside from decreasing the amount of solution used to soak the desorption tubes, another possible way of lowering size of blank signals involves the removal of contaminants from the PFPH powder. Man (2005) purified samples by extracting acidic aqueous solutions of PFPH from dichloromethane. Purified PFPH was recovered as a white precipitation by neutralizing the solution with NaOH. Experiments showed that purification of PFPH drastically reduced the amount of signal caused by the resulting hexane-PFPH solution (Man, 2005).

Finally, the MDL can be lowered by decreasing the uncertainty of the signal size in replicate blank samples. Ho (2004) used desorption tubes that allowed the Tenax to be removed, conditioned, and pre-soaked with hexane-PFPH solution. This meant the application of hexane-PFPH solution was highly precise and featured little variability. Our desorption tubes do not allow for the removal of the Tenax that is held in place by glass wool inserts. For this reason, the hexane–PFPH solution is simply inserted into the top of the tube and allowed to soak through the glass wool onto the Tenax. There is no definitive way of ensuring the same amount of solution soaks onto the Tenax from one run to the next, meaning the variability of the signal size between blank runs fluctuates. To remedy this problem, desorption tubes should be prepared by using a needle syringe to inject the hexane-PFPH solution directly onto the Tenax packed within the desorption tube, thereby reducing the random error caused by the glass wool.

CHAPTER 5

Future Work and Discussion

5.1 Aerosol Generation/Reaction Chamber

With our formaldehyde detection method successfully developed and calibrated, the next step is to use it in conjunction with our aerosol generation/reaction chamber to test our hypothesis. The apparatus that will be used for these experiments was built and tested during the same time period that the formaldehyde detection method was developed. This section first gives a brief description of the experimental setup and methods. We then discuss the viability of our experimental method in terms of its ability to produce a certain theoretical amount of formaldehyde, and compare this production to the discrepancies found between models and observations.

5.2 Experimental Method

The aerosol generation/aging chamber consists of a 9 liter Pyrex bottle filled with 6 liters of autoclaved North Carolina coastal seawater that has been enriched with phytoplankton strains of *Emiliania Huxleyi*. Hydrocarbon free air is then bubbled through a glass frit placed 8" inches below the water surface. Previous studies have shown that such aerosol-generation techniques can create particles characteristic of oceanic sea spray (Fuentes et al., 2010a). Resulting aerosol-enriched air is then vented through stainless steel tubing into a second 9 Liter Pyrex bottle that acts as an aerosol aging chamber. Six 9W Ushio Midrange UVB (306nm) lights, located in a closed container outside the residence chamber, act as the driving force for photolysis. At the end of the mixed-flow reaction system, aerosols are

passed through a Nafion dryer, and removed through a HEPA filter. Resulting filtered air is then sampled by the desorption tube, and tested for formaldehyde per the methods described in chapter four. Figure 5.0 shows the completed setup.

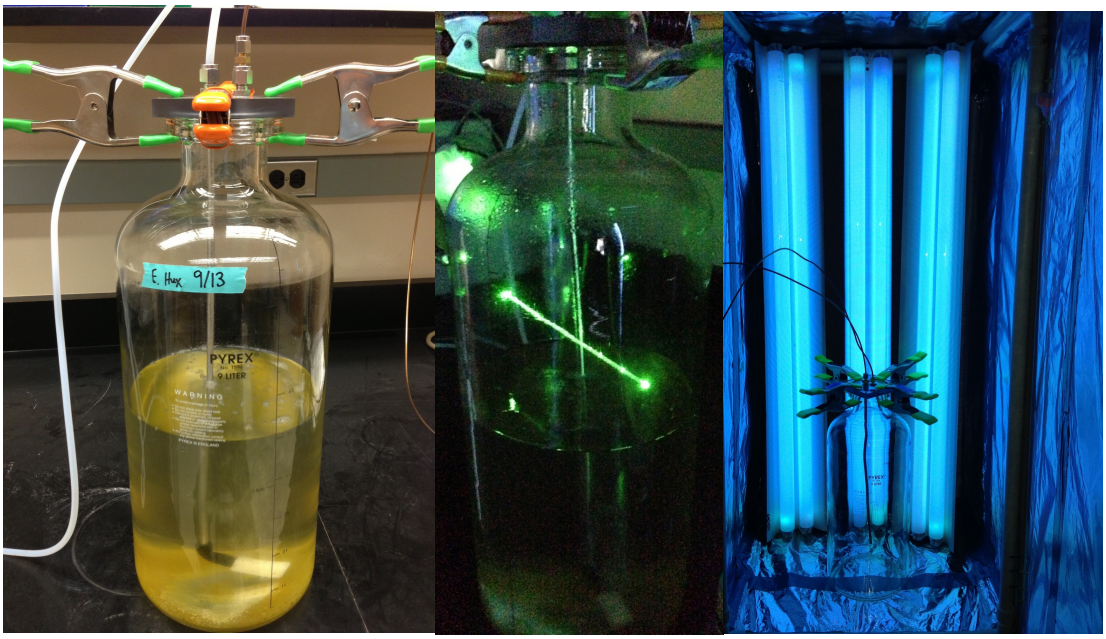

Figure 5.0 Aerosol generation/reaction apparatus. Left: aerosols are generated in a 9 liter Pyrex bottle filled with 6 liters of *Emiliana Huxleyi* using a glass bubbler and ultra-pure nitrogen at a flow rate of 0.1 l/m. Middle: a laser aids shows that aerosols are indeed being formed. Right: aerosols from the generation chamber are transferred to the reaction chamber, surrounded by six 9W Ushio Midrange UVB lights. After an average residence time of 90 minutes, air is then flowed through a Tenax packed desorption tube and then analyzed.

Collaborative work between Meskhidze's and Petters' labs involving measurements of sea spray hygroscopicity parameter, κ through cloud condensation nuclei-activation spectra or size-resolved hygroscopicity tandem differential mobility analyzer-derived growth factor pdfs will allow for quantification of HCHO production rates relative to aerosol number concentration, size distribution, and bulk organic content. Additional experiments will be performed to quantify the concentration of CDOM and TEP in our plankton cultures (see

sections 3.2.1 and 3.3.2). This will allow us to create a formaldehyde production estimate based upon known TEP/CDOM amounts. Finally, by introducing ozone to the aerosol chamber at various concentrations and by experimentation with different light sources and wavelengths (306 and 350nm) when irradiating produced aerosols, we will assess the relative contributions of photolysis and radical oxidation on formaldehyde production.

5.3 Viability of experiment

We now present a discussion of the theoretical amount of formaldehyde that our experimental setup can produce based upon values used in literature. Fuentes et al. (2010a) tested a range of bubble and sea spray aerosol generators in terms of the characteristics of produced aerosols for each method. Table 3 shows the size distribution characteristics of aerosols obtained from artificial seawater samples bubbled with an aquarium diffuser. We assume a total number concentration of sea spray aerosol of 3000/cm^3, per Gantt (2010) and Sellegri (2006). From this data, we calculated the theoretical aerosol number concentration our apparatus will produce in each mode.

Table 5.0 Calculated aerosol generation statistics.

Mode	D_{pg} (m)	σ_g	N_{tot} (#/m^3)
Mode 1	3.70E-08	1.8	1.89E+09
Mode 2	8.70E-08	1.7	1.05E+09
Mode 3	2.86E-07	1.4	4.50E+07

$\rho_{sea\ salt}$	Calculated M_{tot}	Organic Fraction	Flow Rate
2165000 g/m^3	5.43E-6 g/m^3	60%	0.1 l/min

Using the calculated aerosol number concentration and the data from table 5.0, we calculated the aerosol size distribution for all three modes:

$$n_N(D_p) = \frac{dN}{dD_p} = \frac{N}{(2\pi)^{\frac{1}{2}} D_p \ln \sigma_g} \exp\left(-\frac{(\ln D_p - \ln D_{pg})^2}{2\, ln^2 \sigma_g}\right)$$

From this data we then calculated the total number of aerosols produced in each size bin per m^3 for all three modes using:

$$N = \int_0^{\infty} n_N\left(D_p\right) dD_p = \sum_{j=1}^{N_{bins}} n_N(D_{p,j})\Delta D_{p,j}$$

Figure 5.1 shows the theoretical aerosol lognormal number distribution created by our aerosol generation/aging apparatus.

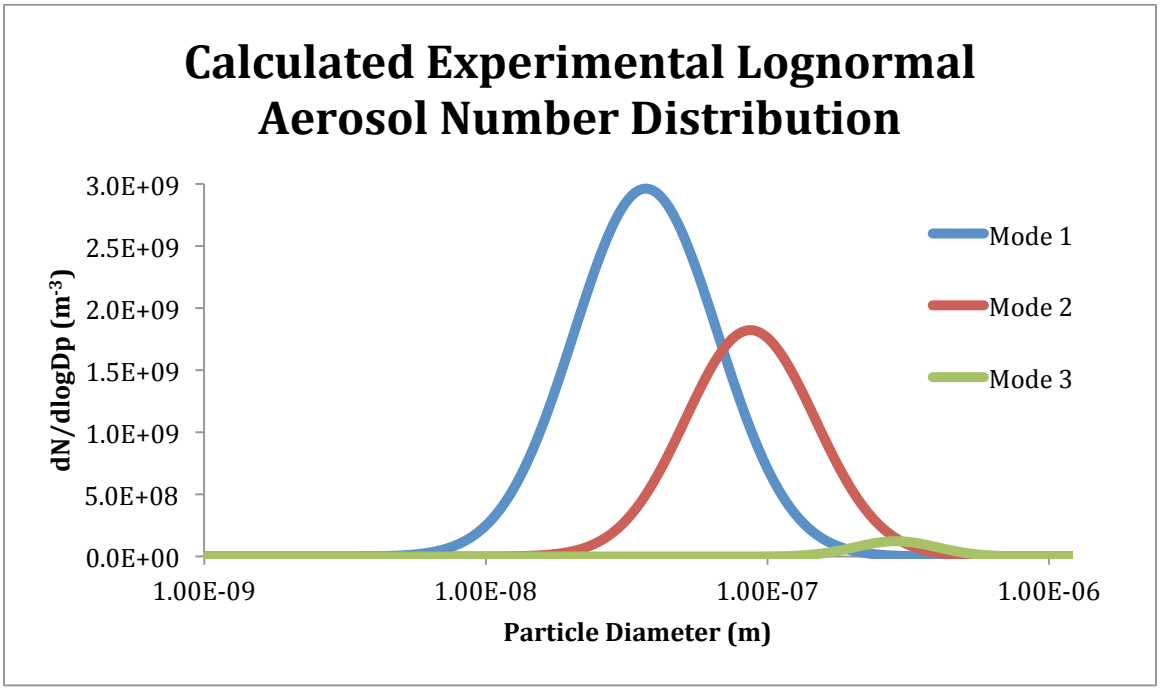

Figure 5.1 Calculated experimental lognormal aerosol number distribution. Mode 1 peaks at 60 nm, mode 2 peaks at 100 nanometers, and mode 3 peaks at 400 nanometers.

Assuming a density of sea salt ($\rho_{\text{sea salt}}$) of 2.18×10^6 grams/m^3, we calculated the total mass of marine aerosols (M_{tot}) for each mode:

$$M_{tot} = \int_0^{\infty} \frac{\pi}{6} \rho_{sea\ salt}\, D^3 n_N(D_p)\, dD_p = \sum_{j=1}^{N_{bins}} n_N(D_{p,j})\, \Delta D_{p,j} \frac{\pi}{6} D_p \rho_{sea\ salt}$$

The results of these calculations are given in table 5.0, along with the total aerosol concentration mass per meter cubed produced using our apparatus.

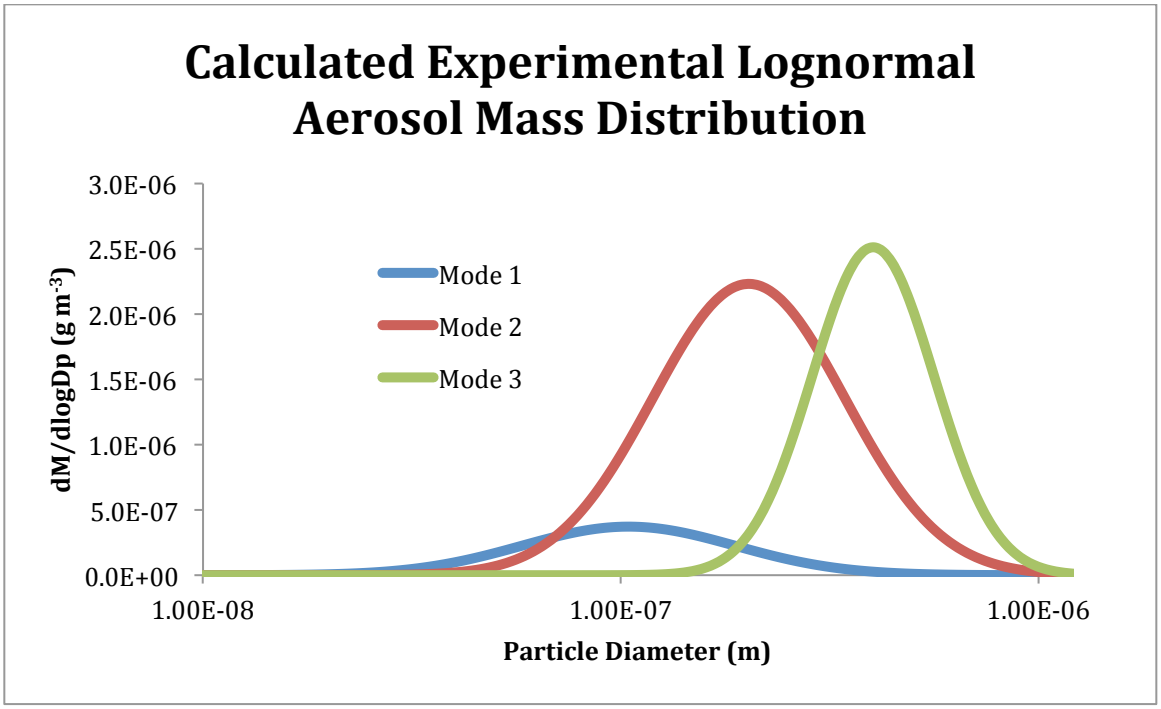

Figure 5.2 Calculated experimental aerosol mass distribution. Despite mode 1 having the largest amount of particles, it clearly contains the least amount of mass. In contrast, mode 3 features the smallest amount of particles, but makes up a majority of the total mass.

The flow rate (α) between the aerosol generator and reaction chamber is set to 100 ml/min. The total mass in grams that is exposed to photolysis (M_{photo}) over a given time period (t) is then:

$$M_{photo} = \alpha\, t\, M_{tot}$$

Since our aerosol generation chamber is filled with biologically active waters, we assume an aerosol organic mass fraction of 60% (Rinaldi et al., 2010). We can then calculate the total amount of organic mass ($M_{organic}$) that will be exposed within the reaction chamber:

$$M_{organic} = 0.60 * M_{photo}$$

We then assume a baseline formaldehyde production yield of 0.16% based upon Grannas et al. (2004), who reported photolysis rates of different concentrations of organic matter in arctic snowpacks. By varying the experiment time (t) and % yield of $M_{organic}$ that photolyzes into formaldehyde (δ), we can produce a simple model showing the theoretical production of formaldehyde (M_{HCHO}) in grams:

$$M_{HCHO} = \delta * M_{organic}$$

Figure 5.3 shows the amount of formaldehyde produced over time based upon yield of HCHO from organic aerosols. It is evident that the % yield will have a large impact on the viability of the hypothesis. If the HCHO yield is similar to values seen by Grannas et al., it is unlikely that this method will have any discernible impact on the ambient formaldehyde concentration. Furthermore, at such concentrations, the detection of formaldehyde will prove difficult as they are near the MDL of our method. While increasing the flow rate would increase the amount of aerosols exposed to photolysis in the reaction chamber, thus making a greater theoretical amount of formaldehyde, Ho and Yu (2004) showed that at flow rates greater than 100 ml/min, the collection efficiency of Tenax is greatly reduced. Future experiments will need to augment the GC/MS method for lower detection limits or the aerosol generation/reaction apparatus to allow greater amounts of aerosols into the reaction chamber without changing the flow rate.

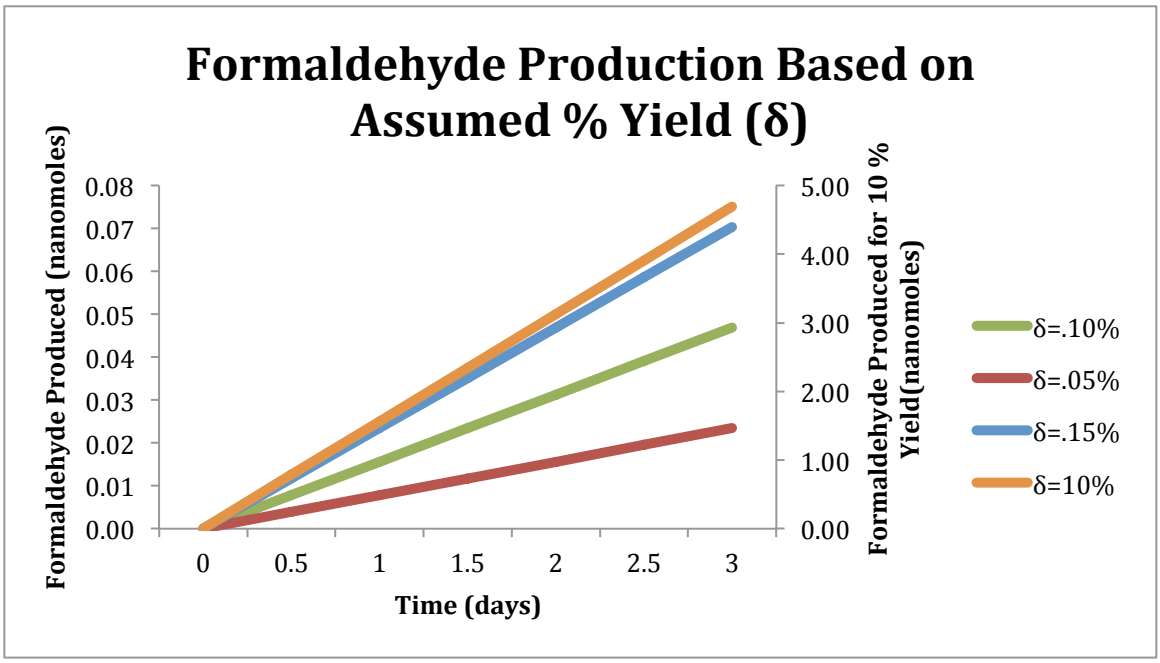

Figure 5.3 Formaldehyde production based on assumed % yield (δ) and time of experiment (in days). The 10% yield is represented on the right side y-axis.

Recall that the difference between formaldehyde observations and predicted concentrations is roughly on the order of 200 pptv (~8.0 nmol/m^3). If we do not include restrictions on the amount of aerosols exposed to UV radiation due to the nature of our experiment, we see that the production of aerosols through bubbling yields 3.3 µg/m^3 of organics. This value is similar to the highest ever reported organic concentration of 3.8 µg/m^3 over biologically active waters (Ovadnevaite et al., 2011). Taking Ovadnevaite's number of 3.8 µg/m^3 and using the HCHO yield of 0.16%, only a concentration of 0.20 nm/m^3/hr of HCHO is produced (~5 pptv/hr). This value is a factor of ~40 times smaller than observed differences between models and observations (~200 pptv). Such a small source of formaldehyde is unlikely to explain these discrepancies.

It is worth noting that different types of organic carbon have different reactivities to light, thereby adding some uncertainty to our calculation. De Bruyn et al. (2011) found that

the concentration of CDOM was not alone sufficient in determining the amount of HCHO photolytically produced. Various factors can change the characteristics of CDOM, including age, temperature, source, and size. The dissolved matter studied by Grannas et al. (2004), from which we derived our hypothetical HCHO yield, may exhibit different characteristics from that of oceanic organic matter. For example, analyses by Grannas showed the organic carbon composition used in their experiments had large amounts of lignin phenols, typical of tree debris (Grannas et al., 2004). Such detritus is not thought to be a significant component of the sea surface microlayer. However, Grannas also found that mono and diacids similar to those by zooplankton and phytoplankton were dominant in their terrestrial samples. Another possible difference can be attributed to the age of the DOM of interest. Grannas sampled snow that was representative of the entire previous year's accumulation. Accompanying organic matter could very well have already been degraded, leading to a lower formaldehyde yield during studies.

If we assume a higher % yield due to differences in the organic matter, the proposed production mechanism successfully explains the model/observation discrepancy. Again, taking Ovadnevaite's atmospheric organic mass concentration measurement of 3.8 $\mu g/m^3$ and instead assuming a 10% organic-to-HCHO yield, as much as 12.6 $nmol/m^3/hr$ (~310 pptv/hr) of HCHO can be formed. The uncertainties in DOM characterization described above make the determination of an HCHO yield for aerosolized organic matter difficult. It is likely that the actual yield of aerosolized organic matter to HCHO varies depending on a number of environmental and chemical characteristics. For this reason, the experiment will be important in determining the reactive nature and potential of DOM as an HCHO source in the marine boundary layer.

5.4 Conclusions

This study explored the possibility of the existence of a previously unknown source of atmospheric formaldehyde over the remote marine regions. We first discussed the importance and sensitivity of the hydrocarbon oxidation cycle over the oceans. We then presented an extensive review of the various in-situ measurements and modeling studies of

formaldehyde carried out over the oceans in the past 30 years, making note of the recent trend for models to under predict observed values. We reviewed research that described enrichment of DOM, POM, and TEP in the sea surface microlayer and saw that the nature of dissolved organic matter and transparent exopolymer particles allows them to transform through photolysis. Studies in the 1990s showed that irradiation of seawater samples produced formaldehyde, with increasing production values positively correlated with CDOM concentrations. Finally, we discussed recent studies of primary marine aerosols in terms of their organic mass fraction. While much work remains to be done, early results indicate that over biologically active regions, upwards of 60% of the aerosol mass fraction can be made up of organic matter in the smallest submicron size range. We proposed that the emitted primary marine organic aerosol could be photolyzed to produce formaldehyde.

To test this hypothesis, work was done to create an aerosol generation/aging chamber and a formaldehyde detection method that could be used to detect the amount of formaldehyde produced. While developing the method, we became aware of several difficulties inherent within detection of trace amounts of formaldehyde. First, HCHO is an extremely reactive compound, and requires derivatization into a more stable compound before analysis via GC/MS. Second, the derivatization technique calls for the preparation of gaseous formaldehyde standards at nanomolar concentrations. This meant we were required to prepare diluted stock solutions of formaldehyde in an organic solvent. Acetonitrile was chosen as the dilution solvent due to its favorable boiling temperature and miscibility with formalin. Through careful handling of data, we were able to prepare a statistically robust method for the detection of formaldehyde down to 6 nmol/250 ml.

Upon completion of our theoretical formaldehyde production calculations, there remain two obstacles that are evident. First, it is still unknown if marine organic aerosol will be a viable source of formaldehyde over marine regions. The critical factor in determining the contribution of this method will be the % yield of aerosolized organic matter that photolyzes into formaldehyde. Second, testing this hypothesis will require augmentation of our current experimental setup, as the detection limit of our method may be below the range of formaldehyde that will be produced in our apparatus over short periods of time.

Further experimentation to test SML-MBL interactions is needed. The possibility that the SML can become supersaturated with HCHO, thereby acting as a source rather than a sink to the atmosphere warrants attention. Experiments irradiating phytoplankton cultures with UV-B light and bubbling the waters could present an alternative method for HCHO to escape the ocean surface. Additionally, other important carbonyl compounds that can be detected using our GC/MS method need to be examined. Acetaldehyde and glyoxal are two compounds that have uncertainties similar to those of HCHO. Furthermore, acetaldehyde is a known formaldehyde precursor, and glyoxal has been shown to be a viable source secondary organic aerosol. Experiments investigating the role of carbon in the SML as a formation mechanism for these compounds could be valuable. Finally, future work will focus on lowering the detection limit of the method and increasing the amount of aerosols produced without sacrificing the sensitivity of our detection method.

REFERENCES

Agogue, H., E. O. Casamayor, M. Bourrain, I. Obernosterer, F. Joux, G. J. Herndl, and P. Lebaron (2005), A survey on bacteria inhabiting the sea surface microlayer of coastal ecosystems, *FEMS Microbiol. Ecol.*, *54*, 269-280.

Albrecht, B. A. (1989), Aerosols, cloud microphysics, and fractional cloudiness, *Science*, *245*, 1227–1230.

Arlander, D. W., D. Bruning, U. Schmidt, and D. H. Ehhalt (1995), The tropospheric distribution for formaldehyde during TROPOZ II, *J. Atmos Chem.*, *22*, 251-268.

Arlander, D. W., D. R. Cronn, J. C. Farmer, F. A. Menzia, and H. H. Westberg (1990), Gaseous oxygenated hydrocarbons in the remote marine troposphere, *J. Geophys. Res.*, *95*, 16391-16403.

Ayers, G. P., R. W. Gillett, H. Granek, C. de Serves, and R. A. Cox (1997), Formaldehyde production in clean marine air, *Geophys. Res. Lett.*, *24*, 401-404.

Azam, F. (1998), Microbial control of oceanic carbon flux: the plot thickens, *Science*, *280*, 694-696.

Azetsu-Scott, K., and U. Passow (2004), Ascending marine particles: significance of transparent exopolymer particles (TEP) in the upper ocean, *Limnol Oceanogr.*, *49*, 741-748.

Barger, W. R., and W. D. Garrett (1970), Surface active organic material in the marine atmosphere, *Geophys. Res.*, *75*, 4561-4566.

Barker, D. R. and H. Zeitlin (1972), Metal-ion concentrations in sea-surface microlayer and size separated atmospheric aerosol samples in Hawaii, *J. Geophys. Res., 77,* 5076-5086.

Bates, T. S., J. A. Calhoun, and P. K.Quinn (1992), Variations in the concentration ratio of methane-sulfonate to sulfate in marine aerosol particles over the South Pacific Ocean, *J. Geophys. Res., 97*, 9859-9865.

Beasley, R. K., C. E. Hoffmann, M. L. Ruepell, and J. W. Worley (1980), Sampling of formaldehyde in air with coated solid sorbent and determination by high performance liquid chromatography, *Anal. Chem., 52*, 1110-1114.

Bigg, E. K. and C. Leck (2001), Cloud-active particles over the central Arctic Ocean, *J. Geophys*. *Res*., *106*, 32155-32166, *doi*:*10.1029/1999JD901152*.

Bigg, E. K. and C. Leck (2008), The composition of fragments of bubbles bursting at the ocean surface, *J. Geophys. Res., 113*, D11209, doi:10.1029/2007JD009078.

Blanchard, D. C. (1964), Sea-to-air transport of surface active material, Science, 146, 396-397, doi:10.1126/science.146.3642.396.

Blough, N. V., and R. Delvecchio (2002), Chromophoric DOM in the coastal environment,

Bonsang, B., C. Polle, and G. Lambert (1992), Evidence for marine production of isoprene, Geophys. *Res. Lett., 19,* 1129-1132.

Brasseur, G. P., J. J. Orlando, and G. S. Tyndall (1999), *Atmospheric chemistry and global change*, 1st ed., Oxford University Press, USA.

Broecker, H. C., J. Petermann, and W. Siems (1978), The influence of wind on CO2-exchange in a wind-wave tunnel, including the effects of monolayers, *J. Mar. Res.*, *36*, 595-610.

Burrows, J. P., E. Holzle, A. P. H. Goede, H. Visser, and W. Fricke (1995), SCIAMACHY – scanning imaging absorption spectrometer for atmospheric chartography, *Acta. Astronaut.*, *35*, 445-451.

Calace, N., T., Catrambone, B. M. Petronio, and M. Pietroletti (2007), Fulvic acids in microlayer waters of the Gerlache Inlet Sea (Antarctica): their distribution in dissolved and particulate phases, *Water Res.*, *41*, 152-158.

Calleja, M. L., C. M. Duarte, N. Navarro, and S. Agusti (2005), Control of air-sea CO2 disequilibria in the subtropical NE Atlantic by planktonic metabolism under the ocean skin, *Geophys. Res. Lett.*, *32*, L08606.

Calvert, J. G. (1980), The homogenous chemistry of formaldehyde generation and destruction within the atmosphere, *Rep. FAA-EE-80-20*, 153-190.

Carder, K. L., R. G. Steward, G. R. Harvey, and P. B. Ortner (1989), Marine humic and fulvic acids: their effects on remote sensing of ocean chlorophyll, *Limnol. Oceanogr.*, *34*, 68-81.

Carlier, P., H. Hannachi, and G. Mouvier (1986), The chemistry of carbonyl compounds in the atmosphere, *Atmos. Environ.*, *20*, 2079-2099.

Carlson, D. J. (1983), Dissolved organic materials in surface microlayers: temporal and spatial variability and relation to sea state, *Limnol. Oceanogr.*, *28*, 415-431.

Charlson, R. J., J. E. Lovelock, M. O. Andreae, and S. G. Warren (1987), Oceanic phytoplankton, atmospheric sulfur, cloud albedo and climate, *Nature*, *326*, 655-661.

Chatfield, R. B. (1994), Anomalous HNO3/NOx ratio of remote tropospheric air: Conversion of nitric acid to formic acid and NOx, *Geophys. Res. Lett.*, *21*, 2705-2708.

Chen, R. F., G. B. Gardner (2004), High resolution measurements of chromophoric dissolved organic matter in the Mississippi and Atchafalaya River plume regions, *Mar. Chem.*, *89*, 103-125.

Chien, Y., and K. Yin (2009), Simultaneous determination of airborne carbonyls and aromatic hydrocarbons using mixed sorbent collection and thermal desorption chromatography/mass spectrometric analysis, *J. Environ. Monit.*, *11*, 1013-1019.

Chin, W. C., M. V. Orellana, and P. Verdugo (1998), Spontaneous assembly of marine dissolved organic matter into polymer gels, *Nature*, *391*, 568-572.

Coble, P. G. (1996), Characterization of marine and terrestrial DOM in seawater using excitation-emission matrix spectroscopy, *Mar. Chem.*, *51*, 325-346.

Conrad, R. and W. Seiler (1988), Influence of the surface microlayer on the flux of nonconservative trace gases (CO, H2, CH4, N2O) across the ocean-atmosphere interface, *J. Atmos. Chem.*, *6*, 83-94.

Conrad, R., and W. Seiler (1980), Photoxidative production and microbial consumption of carbon monoxide in seawater, *FEMS Microb. Lett.*, *9*, 61-64.

Cosovic, B. (2005), Surface-Active properties of the sea surface microlayer and consequences for pollution in the Mediterranean Sea, *Hdb Env. Chem.*, *5*, 269-296.

Cotner, J. B., and B. A. Biddanda (2002), Small players, large role: Microbial influence on biogeochemical processes at pelagic aquatic ecosystems, *Ecosystems*, *5*, 105-121.

Cox, R. A. (1999), Ozone and peroxy radical budgets in the marine boundary layer: Modeling the effect of NOx, *J. Geophys. Res.*, *104*, 8047-8056.

Cunliffe, M., R. C Upstill-Goddard, and J. C. Murrell (2011), Microbiology of aquatic surface microlayers, *FEMS Microbiol. Rev., 35*, 233-246.

Cunliffe, M., A. Engel, S. Frka, B. Gasparovic, C. Guitar, J. C. Murrell, M. Salter, C. Stolle,R. Upstill-Goddard, and O. Wurl (2012), Sea surface microlayers: A unified physicochemical and biological perspective of the air-ocean interface, *Prog. Oceanogr.*, doi: http://dx.doi.org/10.1016/j.pocean.2012.08.004.

Cunliffe, M., and J. C. Murrell (2010), Eukarya 18S rRNA gene diversity in the sea surface microlayer: insights on the structure of the neustonic microbial loop, *ISME J*, *4*, 455-458.

Cunliffe, M., M. Salter, P. J. Mann, A. S. Whitely, R. C. Upstill-Goddard, and J. C. Murrell (2009), Dissolved organic carbon and bacterial populations in the gelatinous surface microlayer of a Nowregian fjord mesocosm, *FEMS Microbiol. Lett, 299*, 248-254.

de Bruyn, J. W., D. C. Clark, L. Pagel, and C. Takehara (2011), Photochemical Production of formaldehyde, acetaldehyde, and acetone from chromophoric dissolved organic matter in coastal waters, *J. Photochem. Photobiol.*, *226*, 16-22.

De Leeuw, G., E. L. Andreas, M. D. Anguelova, C. W. Fairall, E. R. Lewis, C. O'Dowd, M. Schulz, and S. E. Schwartz (2011), Production Flux of Sea Spray Aerosol, *Rev. Geophys.*, *49*, RG2001, DOI:10.1029/2010RG000349.

Derwent, R. G., (1982) Two-dimensional model studies of the impact of aircraft exhaust emissions on tropospheric ozone, *Atmos. Environ.*, *16*, 1997-2007.

Engel, A., and U. Passow (2001), Carbon and nitrogen content of transparent exopolymer particles (TEP) in relation to their Alcian Blue absorption, *Mar. Ecol. Progr. Ser.*, *219*, 1-10.

Engel, A., S. Thoms, U. Riebesell, E. Rochelle-Newall, and I. Zondervan (2004), Polysaccharide aggregation as a potential sink of marine dissolved organic carbon, *Nature*, *428*, 929-932.

Facchini, M. C., M. Rinaldi, S. Decesari, C. Carbone, E. Finessi, M. Mircea, S. Fuzzi, D. Ceburnis, R. Flanagan, D. Nilsson, G. de Leeuw, M. Martino, J. Woeltjen, and C. D. O'Dowd (2008), Primary sub-micron marine aerosol dominated by insoluble organic colloids and aggregates, *Geophys*. *Res*. *Lett*., *35*, L17814, doi:10.1029/2008GL03421.

Ferek, R. J., and M. O. Andreae (1984), Photochemical production of carbonyl sulphide in marine surface waters, *Nature*, *307*, 148-150.

Fichot, C., and R. Benner (2011), A novel method to estimate DOC from CDOM absorption coefficients in coastal waters, *Geophys. Res. Lett.*, *38*, L03610.

Franklin, M. P., I. R. McDonald, D. G. Bourne, N. J. Owens, R. C. Upstill-Goddard, and J. C. Murrell (2005), Bacterial diversity in the bacterineuston (sea surface microlayer): the bacterioneuston through the looking glass, *Environ. Microbiol.*, *7*, 723-736.

Frew, N. M. (2005), The role of organic films in air-sea gas exchange, *The Sea Surface and Global Change,* Cambridge University Press, Cambridge, UK.

Frew, N. M., and R. K. Nelson (1992), Scaling of marine microlayer film surface pressure-area isotherms using chemical attributes, *J. Geophys. Res.*, *97*, 5291-5300.

Frew, N. M., J. C. Goldman, M. R. Dennett, and A. S. Johnson (1990), Impact of phytoplankton-generated surfactants on air-sea gas-exchange, *J. Geophys. Res-Oceans*, *95*, 3337-3352.

Frka, S., Z. Kosarac, and B. Cosovic (2009), Characterization and seasonal variations of surface active substances in the natural sea surface microlayers of the coastal middle Adriatic stations, *Estuar. Coast Shelf S.*, *85*, 555-564.

Fuentes, E., H. Coe, D. Green, and G. McFiggans (2011), On the impacts of phytoplankton-derived organic matter on the properties of the primary marine aerosol – Part 2: Composition, hygroscopicity and cloud condensation activity, *Atmos. Chem. Phys.*, *11*, 2585-2602, doi:10.5194/acp-11-2585-2011.

Fuentes, E., H. Coe, D. Green, G. de Leeuw, and G. McFiggans (2010a), Laboratory-generated primary marine aerosol via bubble-bursting and atomization, *Atmos. Meas. Tech., 3*, 141-162.

Fuentes, E., H. Coe, D. Green, G. de Leeuw, and G. McFiggans (2010b), On the impacts of phytoplankton-derived organic matter on the properties of the primary marine aerosol – Part 1: Source fluxes, *Atmos. Chem. Phys.*, *10*, 9295-9317, doi:10.5194/acp-10-9295-2010.

Gantt, B. and N. Meskhidze (2012), The physical and chemical characteristics of marine organic aerosols: a review, *Atmos. Chem. Phys. Discuss.*, *12*, 21779-21813.

Gantt, B. N. Meskhidze, and A. G. Carlton (2010), The contribution of marine organics to the air quality of the western United States, *Atmos. Chem. Phys.*, *10*, 7415-7423.

Gao, Q., C. Leck, C. Rauschenberg, and P. A. Matrai (2012), On the chemical dynamics of extracellular polysaccharides in the high Arctic surface microlayer, *Ocean Sci. Disc.*, *9*, 215-259.

Gasparovic, B., M. Pavsic, B. Cosovic, and A. Saliot (2007), Organic matter characterization in the sea surface microlayers in the subarctic Norwegian fjords region, *Mar. Chem.*, *105*, 1-14.

Goldman, J. C., M. R. Dennet, and N. M. Frew (1988), Surfactant effects on air-sea gas exchange under turbulent conditions, *Deep-Sea Res.*, *35*, 1953-1970.

Goldstone, J. V., R. Del Vecchio, N. V. Blough, and B. M. Voelker (2004), A multicomponent model of chromophoric dissolved organic matter photobleaching, *J. Photochem. Photobiol.*, *80*, 52-60.

Grannas, A. M., P. B. Shepson, and T. R. Filley (2004), Photochemistry and nature of organic matter in Arctic and Antarctic snow, *Global Biogeochem. Cyc.*, *18*, GB1006, doi:10.1029/2003GB002133.

Grossart, H. P., and M. Simon (1997), Formation of macroscopic organic aggregates (lake snow) in a large lake: The significance of transparent exopolymer particles, phytoplankton, and zooplankton, *Limnology and Oceanography*, *42*, 1651-1659.

Guerrini, F., A. Mazzotti, L. Boni, R. Pistocchi (1998), Bacterial-algal interactions in polysaccharide production, *Aquat. Microb. Ecol.*, *15*, 247-253.

Hadamczik, L. (1947), Bericht uber untersuchungen des formaldehydgehaltes der luft, Ph.D. thesis, Univ. of Kiel, Federal Republic of Germany.

Hanst, P. L., J. W. Spence, and E. O. Edney (1980), Carbon monoxide production in photooxidation of organic molecules in the air, *Atmos. Environ.*, *14*, 1077-1088.

Hardy, J. T. (1982), The sea-surface microlayer- biology, chemistry, and anthropogenic enrichment, *Prog. Oceanogro.*, *11*, 307-328.

Hardy, J. T., and C. W. Apts (1984), The sea-surface microlayer: phytoneuston productivity and effects of atmospheric particulate matter, *Mar. Biol.*, *82*, 293-300.

Harvey, G. R., D. A. Boran, L. A. Chesal, and J. M. Tokar (1983), The structure of marine fulvic and humic acids, *Mar. Chem.*, *12*, 119-132.

Heikes, B. G. (1992), Formaldehyde and hydroperoxides at Mauna Loa observatory, *J. Geophys. Res.*, *97*, 18001-18013.

Heikes, B., J. Snow, P. Egli, D. O'Sullivan, J. Crawford, J. Olson, G. Chen, D. David, N. Blake, and D. Blake (2001), Formaldehyde over the central Pacific during PEM-Tropics B, *J. Geophys. Res., 106*, 32717-32731.

Heikes, B., M. Lee, D. Jacob, R. Talbot, J. Bradshaw, H. Singh, D. Blake, B. Anderson, H. Fuelberg, and A. M. Thompson (1996), Ozone, hydroperoxides, oxides of nitrogen, and hydrocarbon budgets in the marine boundary layer over the South Atlantic, *J. Geophys. Res.*, *101*, 24221-24234.

Helms, J. R., A. Stubbins, J. C. Ritchie, E. C. Minor, D. J. Kieber, and K. Mopper (2008), Absorption spectral slopes and slope ratios as indicators of molecular weight, source, and photobleaching of chromophoric dissolved organic matter, *Limnol. Oceanogr.*, *53*, 955-969.

Hermansson, M. (1990), The dynamics of dissolved and particulate organic material in surface microlayers, *The Biology of Particles in Aquatic Systems,* 1st ed), 145-149. CRC Press, Boca Raton, FL.

Hernes, P. J., and R. Benner (2003), Photochemical and microbial degradation of dissolved lignin phenols: implications for the fate of terrigenous organic matter in marine systems, *J. Geophys. Res.*, *108*, 3291.

Ho, S. S. H., and J. Yu (2002), Feasibility of collection and analysis of airborne carbonyls by on-sorbent derivatization and thermal desorption, *Anal. Chem.*, *74*, 1232-1240.

Ho, S. S. H., and J. Yu (2004), Determination of airborne carbonyls: comparison of a thermal desorption/GC method with the standard DNPH/HPLC method, *Environ. Sci. Technol.*, *38*, 862-870.

Hoffman, E. J. and R. Duce (1974), The organic carbon content of marine aerosols collected on Bermuda, *J. Geophys. Res*., *79*, 4474-4477.

Hong, Y., W. O. Smith, A. M. White (1997), Studies on transparent exopolymer particles (TEP) produced in the Ross Sea (Antarctica) and by Phaeocystis antarctica, *J. Phycol*, *33*, 368-376.

Hong, Y., W. O. Smith, and A. M. White (1997), Studies on transparent exopolymer particles (TEP) produced in the Ross Sea (Antarctica) and by *Phaeocystis Antarctica* (Prymnesiophyceae), *Journal of Phycology*, *33*, 368-376.

Jacob, D. J., B. G. Heikes, S. M. Fan, J. A. Logan, D. L. Mauzerall, J. D. Bradshaw, H. B. Singh, G. L. Gregory, R. W. Talbot, D. R. Blake, and G. W. Sachse (1996), Origin of ozone and NOx in the tropical troposphere: A photochemical analysis of aircraft observations over the South Atlantic basin, *J. Geophys. Res.*, *101*, 24235-24250.

Jaegle, L. (2000), Photochemistry of HOx in the upper troposphere at northern midlatitudes, *J. Geophys. Res.*, *105*, 3877-3892.

Johnson, B. D., and P. E. Kepkay (1992), Colloid transport and bacterial utilization of ocean Doc, *Deep-Sea Res.*, *39*, 855-869.

Jorgensen, L., C. A. Stedmon, T. Tragh, S. Markager, M. Middleboe, and M. Sondergaard (2011), Global trends in the fluorescence characteristics and distribution of marine dissolved organic matter, *Mar. Chem.*, *126*, 139-148.

Joux, F., H. Agogue, I. Obernosterer, C. Dupuy, T. Reinthaler, G. J. Herndl, P. Lebaron (2006), Microbial community structure in the sea surface microlayer at two contrasting coastal sites in the northwestern Mediterranean sea, *Aqua. Microbial. Ecol.*, *42*, 91-104.

Kamens, R. M., and H. E. Jefferies (1978), A critical review of ambient air aldehyde measurement methods and analysis of Houston aldehyde data, University of North Carolina, Rep. No. HAOS-10: 75.

Keene, W. C., H. Maring, J. R. Maben, D. J. Kieber, A. A. P. Pszenny, E. E. Dahl, M. A. Izaguirre, A. J. Davis, M. S. Long, X. L. Zhou, L. Smoydzin, and R. Sander (2007), Chemical and physical characteristics of nascent aerosols produced by bursting bubbles at a model air-sea interface, *J. Geophys. Res.*, *112*, D21202, doi:10.1029/2007JD008464.

Kepkay, P. E. (2000), Colloids in the ocean cycle, in: The Handbook of Environmental Chemistry, 5, D Marine Chemistr. Edited by: Wangersky, P., 35-36, Springer, Berlin, 2000. 14127.

Kieber, D. J., J. McDaniel, and K. Mopper (1989), Photochemical source of biological substrates in seawater: implications for carbon cycling, *Nature*, *341*, 637-639.

Kieber, R. J., L. H. Hydro, and P. J. Seaton (1997), Photoxidation of triglycerides and fatty acids in seawater: Implication toward the formation of marine humic substances, *Limnol. Oceanogr.*, *42*, 1454-1462.

Kieber, R. J., X. Zhou, and K. Mopper (1990), Formation of carbonyl compounds from UV-induced photodegradation of humic substances in natural waters: Fate of riverine carbon in the sea, *Limnol. Oceanogr.*, *35*, 1503-1515.

Kim, W.S., A. L. Geraci, and R. E. Kupel (1980), Solid sorbent tube sampling and ion chromatographic analysis of formaldehyde, *Am. Ind. Hyg. Assoc. J.*, *41*, 334-339.

Kiorboe, T., and J. L. S. Hansen (1993), Phytoplankton aggregate formation: Observations of patterns and mechanisms of cell sticking and the significance of exopolymeric material, *Journal of Plankton Research*, *15*, 993-1018.

Kirchman, D. L. (1994), The uptake of inorganic nutrients by heterotrophic bacteria, *Microb. Ecol.*, *28*, 255-271.

Kormann, R., H. Fisher, M. de Reus, M. Lawrence, Ch. Bruhl, R. von Kuhlmann, R. Holzinger, J. Williams, J. Lelieveld, C. Warneke, J. de Gouw, J. Heland, H. Ziereis, and H. Schalger (2003), Formaldehyde over the eastern Mediterranean during MINOS: Comparison of airborne in-situ measurements with 3D-model results, *Atmos. Chem. Phys.*, *3*, 851-861, doi: 10.5194/acpd-3-1303-2003

Kozarac, Z., B. Cosovica, D. Mobiusb, and M. Dobrica (2000), Interaction of polysaccharides with lipid monolayers, *J. Coll. Interf. Sci.*, *226*, 210-217.

Kozarac, Z., D. Risovic, S. Frka, and D. Mobius (2005), Reflection of light from the air/water interface covered with sea-surface microlayers, *Mar. Chem.*, *96*, 99-113.

Kuntz, R, W. Laumenman, G. Nami, and L. A. Hull (1980), Rapid determination of aldehydes in air analysis, *Anal. Lett.*, *13*, 1409-1415.

Kuznetsova, M. and C. Lee (2001), Enhanced extracellular enzymatic peptide hydrolysis in the sea-surface microlayer, *Mar. Chem.*, *73*, 319-332.

Ladstätter-Weiβenmayer, A., J. Heland, R. Kormann, R. von Kuhlmann, M. G. Lawrence, K. Meyer-Arnek, A. Richter, F. Wittrock, H. Ziereis, and J. P. Burrows (2003), Transport and build-up of tropospheric trace gases during the MINOS campaign: comparison of GOME, in situ aircraft measurements and MATCH-MPIC data, *Atmos. Chem. Phys.*, *3*, 1887-1902, doi:10.5194/acp-3-1887-2003.

Ladstätter-Weiβenmayer, A., M. Kanakidou, J. Meyer-Arnek, E. V. Dermitzaki, A. Richter, M. Vrekoussis, F. Wittrock, and J. P. Burrows (2007), Pollution events over the East Mediterranean: Synergistics use of GOME, ground-based and sonde observations and models, *Atmos. Environ.*, *41*, 7261-7273.

Leck, C., M. Norman, E. K. Bigg, and R. Hillamo (2002), Chemical composition and sources of the high Arctic aerosol relevant for fog and cloud formation, *J. Geophys*. *Res*., *107*, D12, 4135, doi:10.1029/2001JD001463.

Lelieveld, J., H. Berresheim, S. Bormann, P. J. Crutzen, F. J. Dentener, H. Fischer, J. Feichter, P. J. Flateu, J. Heland, R. Holzinger, R. Korrmann, M. G. Lawrence, Z. Levin, K. M. Markowitz, N. Mihalopoulos, A. Minikin, V. Ramanathan, M. de Reus, G. J. Roelofs, H. A. Scheeren, J. Sclare, H. Schlager, M. Schultz, P. Siegmund, B. Steil, E. G. Stephanou, P. Stier, M. Traub, C. Warneke, J. Williams, and H. Ziereis (2002), Global air pollution crossroads over the Mediterranean, *Science*, *298*, 794-799.

Lelieveld, J., and P. J. Crutzen (1990), Influences of cloud photochemical processes on tropospheric ozone, *Nature*, *343*, 227-233.

Levy, H. (1971), Normal atmosphere: large radical and formaldehyde concentrations predicted, *Science*, *173*, 141-143.

Lightfoot, P. D., R. A. Cox, J. N. Crowly, M. Destriau, G. D. Hayman, M. E. Jenkin, G. K. Moortgat, and F. Zabel (1992), Organic peroxy radicals: kinetics, spectroscopy and tropospheric chemistry, *Atmos. Environ.*, *26A*, 1805-1961.

Logan, J. A., M. J. Prather, S. C. Wofsy, and M. B. McElroy (1981), Tropospheric chemistry: A global perspective, *J. Geophys. Res.*, *86*, 7210-7254.

Long, R. A., and F. Azam (1996) Abundant protein-containing particles in the sea, *Aq. Microb. Ecol., 10*, 213-221.

Lovelock, J.E., and L. Margulis (1974), Atmospheric homeostasis by and for biosphere-gaia hypothesis, *Tellus*, *26*, 2-10.

Lowe, D. C., and U. Schmidt (1983), Formaldehyde (HCHO) measurements in the nonurban atmosphere, *J. Geophys. Res.*, *88*, 844-910.

Luo, G. and F. Yu (2010), A numerical evaluation of global oceanic emissions of a-pinene and isoprene, *Atmos. Chem. Phys.*, *10*, 2007-2015.

Mackay, G. I., D. R. Karecki, and H. I. Schiff (1996), Tunable diode laser absorption measurements of H2O2 and HCHO during the mauna Loa Observatory photochemistry experiment, *J. Geophys. Res.*, *101*, 14721-14728.

Man, L. K. (2005) Determination of airborne carbonyl compouns by a thermal desorption GC/MS method: development and application of a vapour coating technique, M.S. thesis, Hong Kong University of Science and Technology, Hong Kong.

Mannino, A., M. E. Russ, and S. Hooker (2008), Algorithm development and validation for satellite-derived distributions of DOC and CDOM in the U.S. Middle Atlantic Bight, *J. Geophys. Res.*, *113*, C07051.

Mari, X. (1999), Carbon content and C : N ratio of transparent exopolymeric particles (TEP) produced by bubbling exudates of diatoms, *Mar. Ecol. Prog. Ser.*, *183*, 59-71.

Mari, X., and T. Kiorboe (1996) Abundance, size distribution and bacterial colonization of transparent exopolymeric particles (TEP) during spring in Kattegat, *J. Plankton Res.*, *18*, 969-986.

Mazurek, Z. A., i. J. S. Pogorzelsk, t. K. Boniewicz-Szmy (2008), Evolution of natural sea surface film structure as a tool for organic matter dynamics tracing, *J. Mar. Sys.*, *74*, 52-64.

Miller, W. L., and R. G Zepp (1995), Photochemical production of dissolved inorganic carbon from terrestrial organic matter – Significance to the oceanic organic-carbon cycle, *Geophys. Res. Let.*

Miyazaki, Y., K. Kawamura, and M. Sawano (2010), Size distributions and chemicalcharacterization of water-soluble organic aerosols over the Western North Pacific in summer, *J. Geophys. Res.*, *115*, D23210, doi:10.1029/2010JD014439.

Modini, R. L., B. Harris, and Z. D. Ristovski (2010), The organic fraction of bubble-generated, accumulation mode Sea Spray Aerosol (SSA), *Atmos. Chem. Phys.*, *10*, 2867-2877, doi:10.5194/acp-10-2867-2010.

Momzikoff, A., A. Brinis, S. Dallot, G. Gondry, A. Saliot, and P. Lebaron (2004), Field study of the chemical characterization of the upper ocean surface using various samplers, *Limnol. Oceanogr. Meth.*, *2*, 374-386.

Momzikoff, K., R. Santus, and M. Giraud (1983), A study of the photosensitizing properties of seawater, *Mar. Chem.*, *12*, 1-14.

Mopper, K., and W. L. Stahovec (1986), Photochemical production of low molecular weight organic carbonyl compounds in seawater, *Mar. Chem.*, *19*, 305-321.

Mopper, K., X. L. Zhou, R. J. Kieber, D. J. Kieber, R. J. Sikorski, and R. D. Jones (1991) Photochemical degradation of dissolved organic carbon and its impact on the ocean carbon cycle, *Nature*, *353*, 60-62.

Murphy, D. M., D. S. Thomson, and M. J. Mahoney (1998), In situ measurements of organics, meteoritic material, mercury and other elements in aerosols at 5 to 19 kilometers, *Science*, *282*, 1664-1668.

Murphy, K. R., C. A. Stedmon, T. D. Waite, and G. M. Ruiz (2008) Distinguishing between terrestrial and autochthonous organic matter sources in marine environments using fluorescence spectroscopy, *Mar. Chem.*, *108*, 40-58.

Naumann, E. (1917), Beitrage zur kenntnis des teichnanoplanktons, *Biol. Zentbl.*, *37*, 98-106.

Nelson, N. B., and D. A. Siegel (2013), The global distribution and dynamics of chromophoric dissolved organic matter, *Annu. Rev. Mar. Sci.*, *5*, 447-476, DOI:10.1146/annurev-marine-120710-100751.

Nelson, N. B., C. A. Carlson, and D. K. Steinberg (2004), Production of chromophoric dissolved organic matter by Sargasso Sea microbes, *Mar. Chem.*, *89*, 273-287.

Nelson, N. B., D. A. Siegal, and A. F. Michaels (1998), Seasonal dynamics of colored dissolved material in the Sargasso Sea, *Deep-Sea Res.*, *45*, 931-957.

Nelson, N. B., D. A. Siegel, C. A. Carlson, C. M. Swan, W. M. Smethie, and S. Khatiwala (2007), Hydrography of chromophoric dissolved organic matter in the North Atlantic, *Deep-Sea Res. I*, *54*, 710-731.

Neitzert, V., and W. Seiler (1981), Measurement of formaldehyde in clean air, *Geophys. Res. Lett*, *8*, 79-82.

Norkrans, B. (1980), Surface microlayers in aquatic environments, *Advanc. In Microb. Ecol.*

O'Dowd C. D., and G. de Leeuw (2007), Marine aerosol production: a review of the current knowledge, *Phil. Trns. R. Soc. A.*, *365*, 1753-1774.

O'Dowd, C. D., J. A. Lowe, and M. H. Smith (1997), Marine aerosol, sea-salt, and the marine sulphur cycle: A short review, *Atmos. Environ., 31*, 73-80.

O'Dowd, C. D., M. C. Facchini, F. Cavalli, D. Ceburnis, M. Mircea, S. Decesari, S. Fuzzi, Y. J. Yoon, and J. P. Putaud (2004), Biogenically driven organic contribution to marine aerosol, *Nature*, *431*, 676-680, doi:10.1038/nature02959.

Oppo, C., S. Bellandi, N. DegliInnocenti, A. M. Stortini, G. Loglio, E. Schiavuta, and R. Cini (1999), Surfactant components of marine organic matter as agents for biogeochemical fractionation and pollutant transport via marine aerosols, *Mar. Chem., 63*, 235-253.

Orellana, M. V., and P. Verdugo (2003), Ultraviolet radiation blocks the organic carbon exchange between the dissolved phase and the gel phase in the ocean, *Limnol. Oceanogr.*, *48*, 1618-1623.

Ortega-Retuerta, E. (2008), Organic matter distribution and dynamics in marine ecosystems. Field, experimental and remote sensing approaches, Ph.D. thesis, University of Granada, Granada, Spain.

Ortega-Retuerta, E., C. M. Duarte, and I. Reche (2010), Significance of bacterial activity for the distribution and dynamics of transparent exopolymer particles in the Mediterranean Sea, *Microb. Ecol.*, *59*, 808-818.

Ortega-Retuerta, E., U. Passow, C. M. Duarte, and I. Reche (2009), Effects of ultraviolet B radiation on (not so) transparent exopolymer particles, *Biogeosci.*, *6*, 3071-3080.

Ovadnevaite, J., C. O'Dowd, M. Dall'Osto, D. Ceburnis, D. R. Worsnop, and H. Berresheim (2011), Detecting high contributions of primary organic matter to marine aerosol: A case study, *Geophys. Res. Lett., 38*, L02807, doi:10.1029/2010GL046083.

Palmer, P. I., D. J. Jacob, A. M. Fiore, R. V. Martin, K. Chance, and T. P. Kurosu (2003), Mapping isoprene emissions over North American using formaldehyde column observations from space, *J. Geophys. Res.*, *108*, 4180.

Passow, U, and A. L. Alldredge (1994), Distribution, size, and bacterial colonization of transparent exopolymer particles (TEP) in the ocean, *Mar. Ecol. Prog. Ser.*, 185-198.

Passow, U, and A. L. Alldredge (1995), A dye-binding assay for the spectrophotometric measurement of transparent exopolymer particles (TEP), *Limnol. Oceanogr., 40,* 1326-1335.

Passow, U. (2000), Formation of transparent exopolymer particles, TEP from dissolved precursor material, *Mar. Ecol. Prog. Ser.*, 192, 1-11.

Passow, U. (2002a), Production of transparent exopolymer particles (TEP) by phyto and bacterioplankton, Mar. Ecol. Prog. Ser., 236, 1-12.

Passow, U. (2002b), Transparent exopolymer particles (TEP) in aquatic environments, *Prog. Oceanogr.*, *55*, 287-333.

Passow, U., A. L. Alldredge (1994), Distribution, size and bacterial colonization of transparent exopolymer particles (TEP) in the ocean, *Mar Ecol Prog Ser*, *113*, 185-198.

Passow, U., and P. Wassmann (1994), On the trophic fate of *Phaeocystis pouchetii* (Hariot): IV. The formation of marine snow by *P. pouchetii*, *Marine Ecology Progress Series*, *104*, 151-163.

Reche, I., M. L. Pace, and J. J. Cole (1998), Interactions of photobleaching and inorganic nutrients in determining bacterial growth on colored dissolved organic carbon, *Micro. Ecol.*, *36*, 270-280.

Reinthaler, T., E. Sintes, and G. J. Herndl (2008), Dissolved organic matter and bacterial production and respiration in the sea-surface microlayer of the open Atlantic and the western Mediterranean sea, *Limnol. Oceanogr.*, *53*, 122-136.

Richter, A., and J. P. Burrows (2002), Tropospheric NO2 from GOME measurements, *Adv. Space Res.*, *29*, 1673-1683.

Rinaldi, M., S. Decesari, E. Finessi, L. Giulianelli, C. Carbone, S. Fuzzi, C. D. O'Dowd, D. Ceburnis, and M. C. Facchini (2010), Primary and secondary organic marine aerosol and

oceanic biological activity: Recent results and new perspectives for future studies, *Adv. Meteorol.*, *2010*, 310682, doi:10.1155/2010/310682.

Rochelle-Newall, E. J., and T. R. Fisher (2002), Production of chromophoric dissolved organic matter fluorescence in marine and estuarine environmentas: an investigation into the role of phytoplankton, *Mar. Chem.*, *77*, 7-21.

Rochelle-Newell, E., T. R. Fisher, C. Fan, and P. M. Glibert (1999), Dynamics of chromophoric dissolved organic matter and dissolved organic carbon in experimental mesocosms, *Int. J. Remote Sens.*, *20*, 627-641.

Rood, D. (2007), *The troubleshooting and maintenance guide for gas chromatographers*, 4th rev. ed., Wiley-VCH, Weinheim.

Rudolph, J., and D. H. Ehhalt (1981), Measurement of C2-C5 hydrocarbons over the North Atlantic, *J. Geophys. Res.*, *86*, 11959-11964.

Sabolis. A., N. Meskhidze, G. Curci, P. I. Palmer, and B. Gantt (2011), Interpreting elevated space-borne HCHO columns over the Mediterranean Sea using the OMI sensor, *Atmos. Chem. Phys.*, *11*, 12787-12798.

Salter, M. E., R. C. Upstill-Goddard, P. D. Nightingale, S. D. Archer, B. Blomquist, T. Ho, B. Huebert, P. Schlosser, and M. Yang (2011), Impact of an artificial surfactant release on air-sea gas exchange during DOGEE II, *J. Geophys. Res.*, *116*.

Sander, R., and P. J. Crutzen (1996), Model study indicating halogen activation and ozonedestruction in polluted air masses transported to the sea, *J. Geophys. Res.*, *101*, 9121-9138.

Schuster, S., and G. J. Herndl (1995), Formation and significance of transparent exopolymeric particles in the northern Adriatic Sea, *Marine Ecology Progress Series*, *124*, 227-236.

Sciare, J., O. Favez, R. Sarda-Estève, K. Oikonomou, H. Cachier, and V. Kazan (2009), Long-term observations of carbonaceous aerosols in the Austral Ocean atmosphere: Evidence of a biogenic marine organic source, *J. Geophys. Res., 114*, D15302,doi:10.1029/2009JD011998.

Sellegri, K., C. D. O'Dowd, Y, J. Yoon, S. G. Jennings, and G. de Leeuw (2006), Surfactants and submicron sea spray generation, *J. Geophys. Res.*, *111*, D22215.

Sellegri, K., P. Villani, D. Picard, R. Dupuy, C. D. O'Dowd, and P. Laj (2008), Role of the volatile fraction of submicron marine aerosol on its hygroscopic properties, *Atmos*. *Res*., *90*, 2–4, 272–277, doi:10.1016/j.atmosres.2008.04.004.

Shank, G. C., R. G. Zepp, A. Vahatalo, R. Lee, and E. Bartels (2010), Photobleaching kinetics of chromophoric dissolved organic matter derived from mangrove leaf litter and floating Sargassum colonies, *Mar. Chem.*, *119*, 162-171.

Sharp J. H. (1973), Size classes of organic carbon in seawater, *Limnol. Oceanogr.*, *18*, 441-447.

Sieburth, J. M. (1983), *Air-Sea Exchange of Gases and Particles*, Reidel Publishers Co., Hingham, MA.

Sieburth, J. M., P. J. Willis, K. M. Johnson, C. M. Burney, D. M. Lavoie, K. R. Hinga, D. A. Caron, F. W. French III., P. W. Johnson, and P. G. Davis (1976), Dissolved organic matter and heterotrophic miconeuston in the surface microlayers of the North Atlantic, *Science*, *194*, 1415-1418.

Siegel, D. A., S. Maritorena, N. B. Nelson, D. A. Hansell, and M. Lorenzi-Kayser (2002), Global distribution dynamics of colored dissolved and detrital organic materials, *J. Geophys. Res.*, *107*, 3228.

Singh, G. L. Gregory, R. W. Talbot, D. R. Blake, and G. W. Sachse (1996), Origin of ozone and NOx in the tropical troposphere: A photochemical analysis of aircraft observations over the South Atlantic basin, *J. Geophys. Res.*, *101*, 24235-24250.

Singh, H. Y. Chen, A. Staudt, D. Jacob, D. Blake, B. Helkes, and J. Snows (2001), Evidence from the Pacific troposphere for large global sources of oxygenated organic compounds, *Let. Natur.*, *410*, 1078-1081.

Skoog, A., B. Biddanda, and R. Benner (1999), Bacterial utilization of dissolved glucose in the upper water column of the Gulf of Mexico, *Limnol. Oceanogr.*, *44*, 1625-1633.

Skoog, A., M. Wedborg, and E Foelqvist (1996), Photobleaching of fluorescence and the organic carbon concentration in a coastal environment, *Marine Chemistry*, *55*, 333-45.

Sparkman, O. D. (2011), *Gas chromatography and mass spectrometry: a practical guide*, 2nd ed., Elsevier, Boston.

Steinberg, D. K., N. Nelson, C. A. Carlson, and A. C. Prusak (2004), Production of chromophoric dissolved organic matter (CDOM) in the open ocean by zooplankton and the colonial cyanobacteria Trichodesmium spp., *Mar. Ecol. Prog. Ser.*, *267*, 45-56.

Stoderegger, K. E., and G. J. Herndl (1999), Production of exopolymer particles by marine bacterioplankton under contrasting turbulence conditions, *Mar. Ecol. Prog. Ser.*, *189*, 9-16.

Stoderegger, K., G. J. Herndl (1998), Production and release of bacterial capsular material and its subsequent utilization by marine bacterioplankton, *Limnol. Oceanogr.*, *43*, 877-884.

Tanaka, T. (1981), Gels, *Scientific America*, *244*, 124-138.

Thornton, D. C. O. (2002), Diatom aggregation in the sea: mechanisms and ecological implications, *Eur. J. Phycol.*, *37*, 149-161.

Twomey, S. (1977), The influence of pollution on the shortwave albedo of clouds, *J. Atmos. Sci.*, *34*, 1149-1152.

Upstill-Goddard, R. C., T. Frost, G. R. Henry, M. Franklin, J. C. Murrell, and N. J. P. Owens (2003), Bacterioneuston control of air-water methane exchange determined with a laboratory gas exchange tank, *Global Biogeochem Cy.*, *17*, 19.11-19.15.

Urban-Rich, J., J. T. Mccart, D. Fernandez, and J. L. Acuna (2006), Larvaceans and copepods excrete fluorescent dissolved organic matter (FDOM), *J. Exper. Mar. Biol. Ecol.*, *332*, 96-105.

Valentine, R. L., and R. G. Zepp (1993), Formation of carbon monoxide from the photodegradation of terrestrial dissolved organic carbon in natural waters, *Environ. Sci. Tech.*, *27*, 409-412.

Van-vleet, E. S., and P. M. Williams (1983), Surface potential and film pressure measurements in seawater systems, *Limnol. Oceanogr.*, *28*, 401-414.

Verdugo, P., A. L. Alldredge, F. Azam, D. L. Kirchman, U. Passow, and P. H. Santschi (2004), The oceanic gel phase: a bridge in the DOM-POM continuum, *Mar. Chem*, *92*, 67-85.

Vernet, M., and K. Whitehead (1996), Release of ultraviolet-absorbing compounds by the red-tide dinoflagellate Lingulodinium polyedra, *Mar. Biol., 127*, 35-44.

Vogel, M. A. Buldt, and U. Karst (2002), Hydrazine reagents as derivatizing agents in environmental analysis – A critical review, *J. Anal. Chem.*, *366*, 781-791.

Wagner, V., R. von Glasgow, H. Fischer, and P. J. Crutzen (2002), Are CH2O measurements in the marine boundary layer suitable for testing the current understanding of CH4 oxidation?: A model study, *J. Geophys. Res.*, *107*, DOI: 0148-0227/02/2001JD000722

Weller, R., O. Schrems, A. Boddenberg, S. Gab, and M. Gautrois (2000), Meridional distribution of hydroperoxides and formaldehyde in the marine boundary layer of the Atlantic (48° N-35° S) measured during the Albatross campaign, *J. Geophys. Res.*, *105*, 14401-14412.

Williams, P. M., A. F. Carlucci, S. M. Henrichs, E. S. Van Vleet, S. G. Horrigan, F. M. H. Reid, K. J. Robertson (1986), Chemical and microbiological studies of sea-surface films in the Southern Gulf of California and off the West Coast of Baja California, *Mar. Chem.*, *19*, 17-98.

Wurl, O., E. Wurl, L. Miller, K. Johnson, and S. Vagle (2011), Formation and global distribution of sea-surface microlayers, *Biogeosci.*, *8*, 121-135.

Wurl, O., L. Miller, R. Rottgers, and S. Vagle (2009), The distribution and fate of surface-active substances in the sea-surface microlayer and water column, *Mar. Chem.*, *115*, 1-9.

Wurl, O., and M. Holmes (2008), The gelatinous nature of the sea-surface microlayer, *Mar. Chem., 110*, 89-97.

Yamashita, Y. and E. Tanoue (2008), Production of bio-refractory fluorescent dissolved organic matter in the ocean interior, *Nat. Geosci.*, *1*, 579-582.

Yassaa, N., I. Peeken, E. Zöllner, K. Bluhm, S. Arnold, D. Spracklen, and J. Williams (2008), Evidence for marine production of monoterpenes, *Environ. Chem*., *5,* 391-401, doi:10.1071/EN08047.

Yokouchi, Y., H. J. Li, T. Machida, S. Aoki, and H. Akimoto (1999), Isoprene in the marine boundary layer (Southeast Asian Sea, eastern Indian Ocean, and Southern Ocean): Comparison with dimethyl sulfide and bromoform, *J. Geophys. Res.*, *104,* 8067-8076.

Yoon, Y. J., D. Ceburnis, F. Cavalli, O. Jourdan, J. P. Putaud, M. C. Facchini, S. Decesari, S. Fuzzi, K. Sellegri, S. G. Jennings, and C. D. O'Dowd (2007), Seasonal characteristics of the physicochemical properties of North Atlantic marine atmospheric aerosols, *J. Geophys. Res., 112*, D04206, doi:10.1029/2005JD007044.

Zafirou, O. C., J. Alford, M. Herrera, E. T. Peltzer, R. B. Gagosian, and S. C. Liu (1980), Formaldehyde in remote marine air and rain: Flux measurements and estimates, *Geophys. Res. Lett.*, *7*, 341-344.

Zhou, X., and K. Mopper (1997), Photochemical production of low-molecular-weightcarbonyl compounds in seawater and surface microlayer and their air-sea exchange, *Mar. Chem.*, *56*, 201-213.

Zhou, X., Y. Lee, and N. Leonard (1996), Tropospheric formaldehyde concentration at the Mauna Loa Observatory during the Mauna Loa Observatory photochemistry experiment 2, *J. Geophys. Res.*, *101*, 14711-14719.

Zhou, X., Y. N. Lee, L. Newman, X. Chen, and K. Mopper (1997), Tropospheric formaldehyde concentration at the Mauna Loa Observatory during the Mauna Loa Photochemistry Experiment 2, *J. Geophys. Res.*, *101*, 14711-14719.

Zika, R. G., J. W. Moffett, R. G. Petasne, W. J. Cooper, and E. S. Saltzman (1985), Spatial and temporal variations in hydrogen peroxide in Gulf of Mexico waters, *Geochim. Cosmochim. Acta.*, *49*, 1173-1184.